Catalytic combustion in fuel cell: Mechanism on the abrupt change from moderate to accidental scale

ゴー フィー マイン

Catalytic combustion in fuel cell - Mechanism on the abrupt change from moderate to accidental scale-

a dissertation presented

by

NGO PHI MANH

in fulfillment for the degree of

Doctor of Engineering

in

Hydrogen Energy Systems

KYUSHU

UNIVERSITY

Fukuoka, JAPAN

January, 2023

Acknowledgements

I must first acknowledge how fortunate I am to have Prof. Ito Kohei as my supervisor, who helps me in both my academic and social lives. I'm not familiar with fuel cell technology, but after our fruitful discussions and with his encouragement, I felt more confident in completing my study. I also want to thank him for being understanding and patient with me as I went through the paper and desertion revision processes.

I also would like to appreciate Prof. Shiratori Yusuke and Dr.Tu Hoan Phuc, who have introduced me to the Fuel Cell Lab Systems and Prof. Ito Kohei. I believe that was my destiny! Many thanks to Assoc. Prof. Dr. Nakajima Hironori, who gave me valuable lessons about electrochemistry and how to analyze the experimental data. We also have many interesting discussions during the coffee break. Additionally, I also would like to thank Assoc. Prof. Dr. Kitahara Tatsumi who gave me essential recommendations in the lab seminars.

I would also like to thank Mr. Karimata Takahiro, Mrs. Saitou Tomoko, and Mrs. Matsumoto Naoko for their assistance. Thanks to them, the establishment of experimental devices, data collection and analysis, and paper procedures were carried out smoothly. Besides, I am also grateful to the Japan International Cooperation Agency (JICA) for providing funds for my doctoral studies at Kyushu University in Japan.

The last but not least, I would like to thank my family, especially my wife and daughter who always believe in me and constantly encourage me during my study abroad. They were truly my strong anchors for me throughout all my education and life in Japan, especially during the time of the epidemic.

744 Motooka, Nishi-ku, Fukuoka city, Japan

NGO PHI MANH

Table of Contents

List of Tables

List of Figures

Chapter 1

Introduction

1.1. Background

Fossil fuels play an important role in the human being development. Year by year, fossil fuels consumption keeps growing gradually. In the world, US together with China and India are three countries consumed most of fossil fuels. Fossil fuels have an unequal distribution and a limited amount. With the current consumption rate, they will be depleted in decades. Based on a prediction has been done in 2016, coal reserves were predicted to deplete in 114 years, natural gas reserves in 52.8 years, and oil reserves in 50.7 years. [1]. Furthermore, burning enriched-carbon fuels like coal, natural gas, oil emits CO_2, other harmful gases (NO_x, SO_x) and particle matter to environment. Consequently, environmental problems appear such as global warming, acid rain, climate change, air pollution (locally). It is necessary to transition to low-carbon sources for energy like renewable energy, nuclear power.

With high heating value (120 $MJkg^{-1}$ (low heating value), and 142 $MJkg^{-1}$ (high heating value)), hydrogen (H_2) is an energy carrier that can be replaced for other fossil fuels in all energy systems: Heating and power systems, automobile application, portable devices. Hydrogen-based systems are free from CO_2 emission, no air pollution, only water and heat loss emit to environment. Hence, hydrogen is the key alternative fuel for sustainable development of human being in the future. The hydrogen element is the most abundant chemical element on Earth. However, the hydrogen molecule (H_2), as a promising energy carrier, does not exist in large quantities in nature. Thus, H_2 must be produced from variety of sources including fossil fuels (coal, natural gas, oil) and renewable sources (biomass, biogas, electricity from solar, wind, hydropower…). Based on origins, hydrogen gas is classified as brown hydrogen generated from coal, grey hydrogen from natural gas without CO_2 capture system, blue hydrogen from natural gas with CO_2 capture system, and green or clean hydrogen from water electrolysis powered by renewable sources. It is noted that H_2 can be stored at compressed gas, hydride, and liquid forms, although storing requires energy.

Japan, who imported over 90% fuel demand in 2017 [2], is a pioneer in adoption the concept H_2-based society. Their target is to reduce 46% CO_2 emission by 2030 and net zero emission by 2050 [3]. Japan considers that H_2 produced from renewable sources with low price (target 2-3 $\$kg^{-1}$ by 2030 [4]) as a sustainable solution for both energy crisis and environmental problems in the future. In transition era, hydrogen, alongside ammoniac and synthesis methane derived from hydrogen, can be the primary energy supply in heating and power systems in 4 sectors: industrial, transportation, buildings, and agriculture. To achieve the 2050's target (the net-zero emission of CO_2), 22 million tons of hydrogen will be required [3]. This would be a huge challenge for Japan. This is because, according to EU strategy, a renewable electrolyzers with capacity of 6 GW is needed in order to produce 1 million tons of hydrogen per year [5].

Green hydrogen, which is produced by electrolyzing water with an excess amount of renewable electrical energy input, can be used as an off-grid electrical storage solution and as a direct byproduct of power-to-gas technology [6]. The main challenge in the production of green hydrogen is the production cost. Currently, hydrogen price, which originates mainly from fossil fuels, is approximately 10 $\$kg^{-1}$ depending on the market and is uncompetitive with conventional fuels. With the green hydrogen, the price must be much higher. Hydrogen, for instance, produced from solar PV and wind electrolysis costs from about \$6 to 23 $\$kg^{-1}$ compared with 2 $\$kg^{-1}$ from SMR method without CCS [67]. Production costs primarily constitute capital investment of the electrolyser systems and operating costs. Alkaline water electrolysis (AWE) is a popular and mature technology that uses electricity to split water electrochemically into hydrogen and oxygen. Fig.1.1a shows for the operating principle of AWE. AWE is considered quite reliable, safe, and highly durable (lifetime of 15 years) [8], and has been widely used to produce hydrogen in the large scale. In Japan, the largest alkaline electrolyser of 10 MW has been operating since 2020 in the Fukushima Hydrogen Research Field in Namie, Futaba, Fukushima, using 20 MW of solar power to produce around 900 metric tons of hydrogen per year. However, current capital cost of a large scale AWE remains relatively high, from 1109 – 1330 $\$kW^{-1}$ [9]. Moreover, the electrical energy input for producing 1 kg hydrogen of AWE ranges from 50 to 70 kWh [8]. According to the price of renewable electricity in Europe ranging around 0.083 - 0.2126 $\$kWh^{-1}$ [10], electricity costs around 4.13 –14.9 $\$kg^{-1}$hydrogen. This is really a huge challenge in reducing the green hydrogen price to the 2030's target of 2-3 $\$kg^{-1}$[4]. Besides, AWE has some negative aspects including low operating current density, low pressure, slow response with the variation of solar irradiation and wind speed [11].

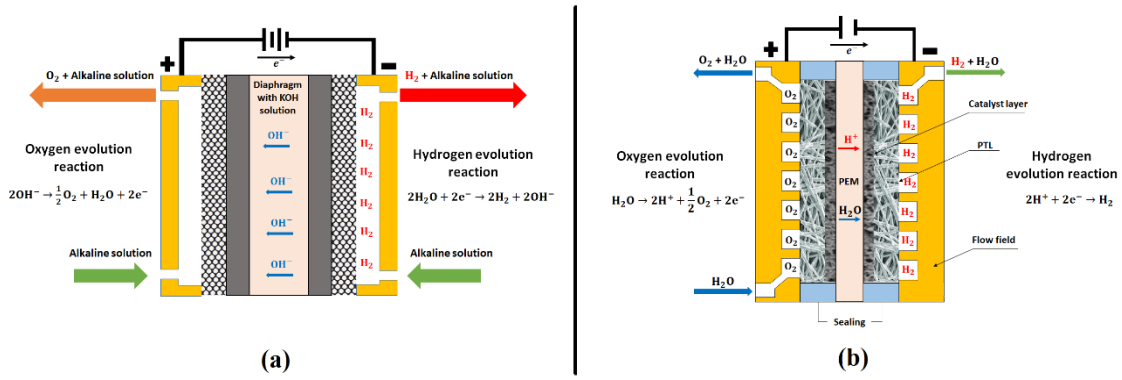

Fig. 1. 1. Schematic images illustrating for (a) AWE cell, and (b) PEMWE cell.

Proton exchange membrane water electrolyzers (PEMWE), as shown in Fig. 1.1b, are being optimized alongside alkaline water electrolyzers to produce green hydrogen. PEMWE uses a thin, solid membrane and can operate with a high current density (1-3 Acm^{-2}), and at high operating pressures. Besides, PEMWE can respond more quickly to the power intermittency of renewable sources than AWE. Hence, PEMWE is a promising method to efficiently harness the excess electrical energy from renewable sources for producing hydrogen. However, PEMWE also has some typical drawbacks. Predominantly, investment costs are higher than AWE, ranging from 2,103 to 2,546 $\$kW^{-1}$ [9] due to the expensive membrane and

noble metals in the catalyst layers. The second is the lifetime of the stack, especially the membrane durability.

In summary, green hydrogen with an acceptable cost is the key to solving two of the most important issues for human beings: fossil fuel exhaustion and the environmental crisis. In the present, hydrogen currently plays the part of balancing the supply and demand of electricity generated from renewable energy sources. With some hydrogen storage and a hydrogen fuel cell (or combustion engines), hydrogen generated from surplus renewable energy can balance out the erratic power generation from renewable sources. However, in order to achieve the acceptable cost of 2 $\$kg^{-1}$ of hydrogen and the net-zero CO_2 emission's target by 2050, some required actions must be taken in the future as follows: increasing efficiency, lowering capital as well as operating costs of the electrolysis systems; and lowering renewable electricity prices. Furthermore, promoting widespread usage of hydrogen in all sectors will increase demand. As a result, large-scale green hydrogen production plants, such as mega or Giga scale renewable hydrogen electrolysis, will have the chance to be deployed.

Direct burning of hydrogen in conventional energy systems will lead to the emission of NOx and a low energy conversion efficiency due to the Carnot cycle limitation. Meanwhile, fuel cell systems are able to convert chemical potential energy from hydrogen and oxygen in air directly into electricity and heat with very high energy conversion efficiency and no emission. The initial experiments about fuel cell were carried out by William Grove since 1839. Based on membrane type, fuel cell is categorized in seven types as follows: Polymer electrolyte membrane fuel cells (PEMFCs), direct methanol fuel cells, alkaline fuel cells, phosphoric acid fuel cells, molten carbonate fuel cells, solid oxide fuel cells, reversible fuel cells.

A PEMFC is a low-temperature fuel cell that uses the polymer electrolyte membrane to conduct protons during operation. It was invented in 1955 by William Grubb, as described in Fig.1.2. The application of PEMFC to the Gemini missions (NASA) in the United States has attracted much attention. At the beginning stage, hydrocarbon-based polymer membranes were used that had poor durability. Afterwards, the invention of the PSFA membrane, in which PTFE plays as the backbone, has shown a brilliant stability. DuPont was a pioneer in producing PFSA membranes, namely Nafion. Today, many other companies also participate in supplying PSFA membranes to the market, including Asahi Glass Company (Flemion® products, Chiyoda, Japan), 3M Company (Saint Paul, MN, USA), W. L Gore (GORE-SELECT® membranes, Newark, DE, USA), and Solvay S.A. (Aquivion® products, Brussels, Belgium). PEMFCs have distinct advantages, such as high power density, quick start-up, and high efficiency. That's why PEMFCs are suitable for transportation applications such as light duty vehicles (cars, motorbikes), heavy duty vehicles (trucks, buses, trains, forklifts, ships), even airplanes. The major automobile companies have focused on the development of fuel cell vehicles (FCVs). In 2014, Toyota was the first company to release a commercial sedan model, the so-called Mirai Besides, PEMFCs are also suitable for household applications that can supply both power and hot water demands (CHP). An Ene-Farm is a typical residential fuel cell system that can use direct city gas or liquefied petroleum gas. These

systems have been commercialized in the Japanese market since 2009. Up to 2021 June, around 402,039 units (including both PEMFC and SOFC types) have been sold throughout Japan [12]. It is targeted to achieve 5,300,000 units by 2030 [13].

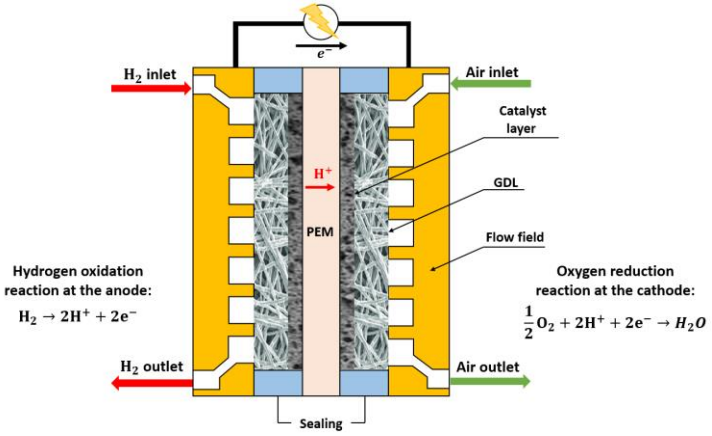

Fig. 1. 2. Schematic illustration of a single PEMFC.

In the automobile applications, BEVs and FCVs are two candidates for substituting internal combustion engine vehicles. However, regarding longer driving distance for one fuel charge, shorter refueling time (3-5 min), higher specific power, FCVs are more promising and viable, especially in medium and heavy duty vehicles [14]. At the end of 2020, more than 34,800 fuel cell vehicles were on the market [15]. The number of fuel cell vehicles distributed mainly in Asian countries including Korea, China and Japan. Among them, South Korea and Japan increased their number of passenger vehicles, while the number of buses and medium-duty trucks represented a large share in China. The number of fuel cell vehicles produced in small quantities, the shortage of hydrogen refueling stations and high hydrogen price are the key causes that constrain the popularity of the FC vehicles on the market.

1.2. Challenges of the fuel cell vehicles (FCVs)

1.2.1 Production cost

In the market, there are only two automobile makers, Toyota and Huyndai, that have commercial products. In 2022, the price of the Toyota Mirai sedan is higher than $50,000 [16] and the Huyndai Nexo is over $60,000 [17]. These prices are much higher than conventional cars. The main cost of FCVs is accounted for by the fuel cell system and hydrogen tanks. The fuel stack in a fuel cell system was projected to account for 66% to 43% of the total price of a fuel cell car, corresponding to 100,000 and 500,000 units produced per year, respectively [18]. There have several hundreds of cells in a stack. And, each cell contains a membrane, catalyst layers, GDLs and bipolar plates. Because PEMFC can operate at low temperature, expensive catalyst must be used like Pt. This is Achilles' heel of the PEM fuel cell. Thank for advance in catalyst material and preparation method, amount of Platinum has been reduced significantly. Toyota has succeeded in reducing the amount of platinum in the catalyst of a passenger car from 100 g to around 30 g

[19]. However, in order to compete with ICEVs, the ultimate reduction of Pt in a fuel cell passenger car must be as low as 8 g [4].

Furthermore, the membrane is a rather expensive component with small volume of fuel cell vehicle produced. Perfluorosulfonic acid (PFSA) membranes are intensively used in fuel cell vehicle. A 25 μm thickness PFSA membrane has price of 250 $\$m^{-2}$, so a 100 kW FC vehicle will use 15 m^2 of membrane, then costing around $3,750 [20]. Membrane price can be reduced significantly to approximate 10 $\$m^{-2}$ by mass-producing fuel cell vehicles. In contrast, even with mass production, the price of bipolar plates tends to rise due to the metal resource limitation. The solution is to find a less expensive and more durable alternative, such as a composite bipolar plate. Ultimate cost target of the fuel cell system has to achieve 30 $\$kW^{-1}$ [18].

1.2.2. Durability

FCVs are divided to three categories: Light-duty- vehicles (passenger cars, light duty goods vehicles, two-wheeled vehicles), medium duty vehicles (buses) and heavy – duty vehicles (trucks, coaches, trains, ships). In order to replace the ICEVs, they must be durable enough to satisfy the life time targets. In particular, the light-duty fuel cell vehicles must achieve the lifetime of 5,000 h (equivalent to 150,000 miles of driving) with less than 10% loss of performance by 2020, and the ultimate target of 8,000 h [21]. However, lifetime of the light-duty fuel cell vehicles was reported at 4,130 h in 2016 [22]), which is just over a half of the above ultimate target.

Heavy-duty vehicles, in particular, must require special attention due to their high fuel consumption and emissions in the transportation sector. The advantages of fuel cell vehicles over BEVs will be accentuated by their long range operation and high cargo capacity. Meanwhile, light-duty fuel cell vehicles (or passenger cars) have been commercialized by some automakers like Toyota and Hyundai. It will be incredibly challenging for the heavy-duty fuel vehicles to meet their lifetime target of 1 million miles of driving range (or 30,000 h) [23] due to the severe operations.

To achieve the durability for the fuel cell vehicles, especially the heavy-duty fuel cell vehicles, a durable membrane is indispensable. The membrane in a PEMFC is a key component that serves three important functions: it conducts protons, separates reactant gases, and insulates electrons. As a result, membrane integrity is a critical factor in determining the overall durability of the stack. The membrane in fuel cell vehicles is extremely thin (less than 25 micrometers) and is subjected to a variety of dynamic impacts during operation, including idling, open-circuit voltage (OCV) holding, dynamic load, startup-shutdown, full-power running, overload, and freezing-thawing. Therefore, improving durability of the membrane is constantly a top priority to achieve the lifetime target of fuel cell vehicles.

1.3. Membrane degradation mechanisms in the PEMFC regarding to automobile application

PFSA membrane failure is mainly caused by chemical and mechanical degradation. Hydroxyl radicals, formed in the presence of H_2O_2 and metallic impurity cations, are responsible for the chemical

decomposition of the membrane structure. The membrane is mechanically deformed as a result of the residual stress caused on by changes in water content and temperature.

1.3.1. Chemical degradation of the PFSA membrane

The PFSA ionomer membranes are modified polymers which are composed of a main chain and a side chain. The main chain is the backbone of the membrane. Meanwhile, the side chain, which terminates in sulfonic acid groups in a cluster region, helps to transport protons [24]. Fig 1.3 is a schematic image of the chemical structure of PFSA ionomer membrane.

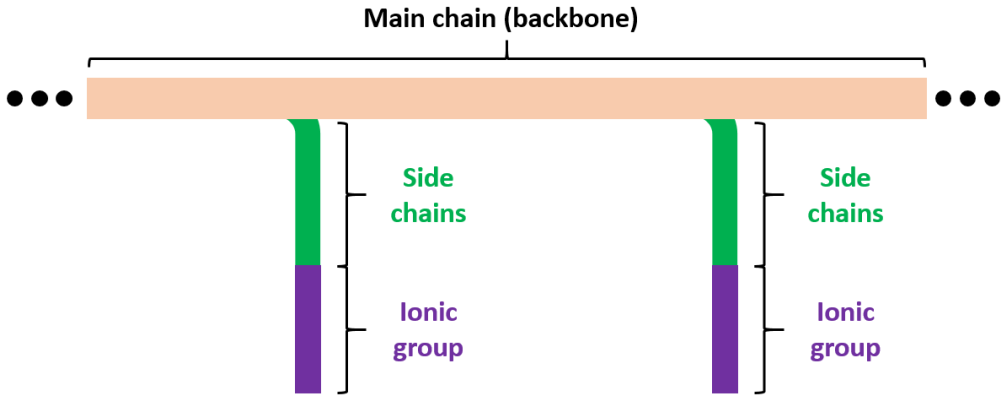

Fig. 1. 3. Schematic image of the chemical structure of a PFSA ionomer membrane.

Chemical stability of PFSA ionomer membrane has been well investigated in the literature in recent decades. The membrane is attacked by hydroperoxyl radicals (•OOH), hydroxyl radicals (•OH), hydrogen radicals (•H), carboxyl radicals (•COOH), leading to the scission of the polymer chains. According to Gubler et al. [25], the oxidative damage potential of radicals is categorized as following order •OH > •H > •OOH. Reactants crossing through the membrane, and then undergo parasitic electrochemical and chemical reactions that entail the formation of hydrogen peroxide and thus free radicals. H_2O_2 can form at both electrodes of the cell and is dependent on the reactant gas crossover rate and potential, as depicted in Fig.1.4. Particularly, H_2O_2 can be formed electrochemically via reduction of O_2 at the cathode electrode at a potential less than 0.695 V [26]). At the anode electrode, Pt-H_{aq} is formed and then reacts with O_2 crossing through the membrane from the cathode side, leading to the formation of H_2O_2. Besides, H_2O_2 can be generated inside the membrane on the surface of nanocrystals of Pt [27]. Under the operation of FCVs, Pt ions are detached from the catalyst layer, then immigrated into the membrane, eventually forming a Pt band. The presence of H_2O_2 and metal ions, such as Fe^{2+}, Cu^{2+}, etc., coming from corrosion of metallic flow fields, supplied gases, MEA preparation etc., causes Fenton's reactions (from Eqs. (1.1) to (1.5)), which result in the formation of free radicals. The operation of a PEMFC under low electrochemical load or OCV conditions [28, 29], high temperature [30], low relative humidity of the gas streams [31], and high reactant

gas pressures [32] can all accelerate chemical membrane degradation. These harsh conditions facilitate the crossover of the reactant gases through the membrane, consequently increasing the formation rate of H_2O_2.

$$M^{2+} + H_2O_2 \rightarrow M^{3+} + \bullet OH + OH^- \quad (1.1)$$

$$M^{3+} + H_2O_2 \rightarrow M^{2+} + \bullet OOH + H^+ \quad (1.2)$$

$$H_2O_2 + \bullet OH \rightarrow \bullet OOH + H_2O \quad (1.3)$$

$$H_2 + \bullet OH \rightarrow \bullet H + H_2O \quad (1.4)$$

$$O_2 + \bullet H \rightarrow \bullet OOH \quad (1.5)$$

Chemical degradation not only reduces the membrane thickness but also weakens the mechanical strength of the membrane. Free radicals decompose both the main and the side chains of the membrane structure. As a result, the membrane loses weight and releases some tracers such as hydrofluoric acid HF, CO_2, and H_2SO_4 in the exhaust streams. The fluorine emission rate (FER) is an important indicator for evaluating chemical degradation. The result of the mass loss is membrane thinning, as indicated by Macauley et al. [33], for instance. The reduction of membrane thickness will increase the crossover rate of the reactant gases, decaying fuel cell performance. The mechanical strength of the membrane depends on its structural integrity, including the main chain, the side chains, and the ionic groups. The free radicals cause the scission of the main chain and unzipping of the end chains (including the side chains and the ionic groups), so that the membrane changes from ductile to brittle, resulting in the reduction of the crack propagation resistance of the membrane [34].

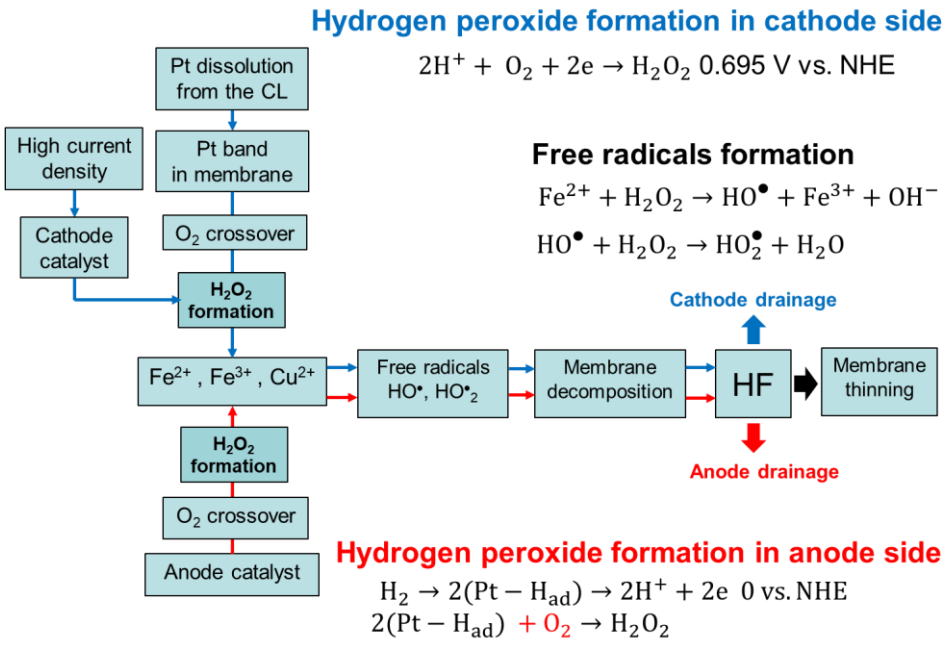

Fig. 1. 4. The illustration for the H_2O_2 formation mechanism at both electrodes of the PEMFCs.

In order to investigate chemical membrane degradation, the accelerated stress test has been proposed and employed. As mentioned above, holding the cell under OCV [28, 29] and near OCV conditions [35], which are conducive to the formation of free radicals, are two popular in situ chemical stress tests. While Fenton's test [36] is an ex-situ chemical durability test. At these tests, free radicals are facilitated to form, and then chemical membrane degradation is surely detected.

There are two strategies mitigating the chemical degradation on the membrane. The first one is decreasing gas leaked rate through membrane by increasing the membrane thickness or membrane type with low permeable coefficient and making less chance to produce H_2O_2. This solution is difficult because thicker membrane will lower power density and cell performance. The second approach is adding chemical degradation stabilizer to the MEA such as doping Ce^{3+} to the PFSA membrane. The scavenge of free radicals is proceeded via reactions from Eqs. (1.6) to (1.10). Apparently, the Ce^{3+} ion scavenges the strongest radical ·OH to H_2O and Ce^{4+} ion, and then Ce^{4+} ion is decomposed by H_2O_2 and regenerated to Ce^{3+}. The final result is the depletion of both free radicals and H_2O_2.

$$\bullet OH + Ce^{3+} + H^+ \rightarrow H_2O + Ce^{4+} \quad \text{(1.6) Un-catalyzed reaction}$$

$$Ce^{4+} + H_2O_2 \leftrightarrow Ce^{3+} + \bullet OOH + H^+ \quad \text{(1.7) Un-catalyzed reaction}$$

$$Ce^{4+} + \bullet OOH \rightarrow Ce^{3+} + O_2 + H^+ \quad \text{(1.8) Un-catalyzed reaction}$$

$$2Ce^{4+} + H_2 \rightarrow 2Ce^{3+} + H^+ \quad \text{(1.9) Catalytic reaction}$$

$$4Ce^{4+} + H_2O \rightarrow 4Ce^{3+} + 4H^+ + O_2 \quad \text{(1.10) Catalytic reaction}$$

1.3.2. Mechanical degradation of the PFSA membrane

The dimensional change of the constrained membrane in the fuel cell is primarily caused by variations in water uptake and temperature [37], which leads to the generation of compressive and tensile stresses in the membrane, as described in Fig.1.5. Membrane shrinkage and swelling due to water content variation is dominant over the temperature dependence because the thermal expansion coefficient of the membrane material is very small. For instance, the Nafion 1100 EW has thermal expansion coefficient of 1.23×10^{-4} K^{-1} [38] which is much smaller in comparison with hygral-swelling coefficient of 90×10^{-4} $(mol_{H_2O}mol_{SO_3H}^{-1})^{-1}$ [39].

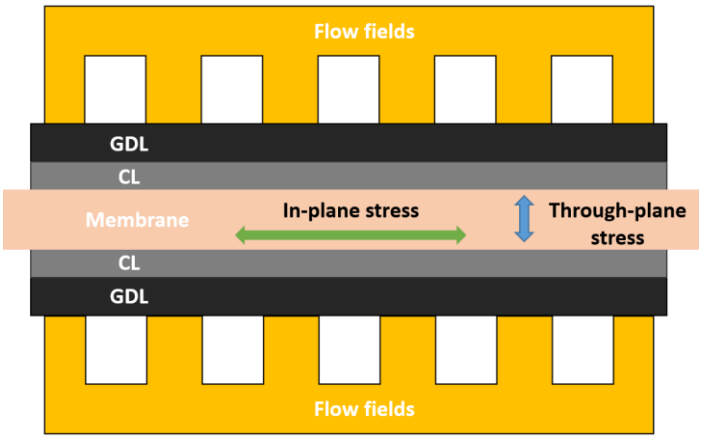

Fig. 1. 5. Stress direction induced by variations of water content and temperature in the membrane. GDL and CL are the gas diffusion layer and the catalyst layer, respectively.

Although these stresses are small compared with the mechanical strength of the membrane, and thus cannot destroy the membrane instantly, they behave like mechanical fatigue loads. The membrane irreversibly deforms under in-plane stresses, mainly [37], resulting in the formation and propagation of physical defects. The mechanical degradation rate is predominantly dependent on the frequency and amplitude of the stresses formed in the membrane. Besides, residual stress can be formed inside the membrane due to false assembly, for example, the uneven compression pressure of the flow field plates on the membrane. Finally, vibration during operation increases the mechanical stress on the membrane.

During operation of a fuel cell vehicle, load variation and start/shutdown cycles are two mechanical stress initiators. These operating conditions cause the water content and temperature variations in the membrane resulting in the formation of some typical defects such as cracks, creeps, and delamination between the membrane and catalyst layers. To investigate membrane mechanical durability, the RH cycling test (or dry/wet cycling test) is used extensively with nitrogen gas or air feeding to the cell. During the dry portion, the membrane shrinks and tensile stress is formed. Whereas, the membrane expands and compressive stress is formed during the wet portion. Based on DOE's protocol, the RH cycling test is carried out with 2 minutes in 0%RH and 2 minutes 150%RH [40] at the cell temperature of 80 °C.

Mechanical membrane lifetime target is 20,000 RH cycles with crossover rate under the threshold of 15 $mAcm^{-2}$ [41]. In the literature, mechanical membrane durability has been well-investigated. Membrane failed after experiencing from hundreds of cycles to 6,000 - 20,000 cycles depending on type of membranes (hydrocarbon, PFSA…), and testing conditions (cell temperatures, RH cycling swings). Typical defects appearing in the membrane under the mechanical degradation are cracks, and delamination between membrane and catalyst interface [42].

In order to mitigate the mechanical stress and increase the membrane durability, using a composite membrane (reinforced membrane) is the most promising solution. A porous PTFE layer is laid in the middle of the reinforced membrane. This type of membrane has been reported almost intact after being subjected to 20,000 RH cycles [20]. However, it appears that the additional PTFE layer with non-proton conductivity may increase ionic resistance, thus decreasing cell performance. Therefore, a balance between the membrane durability and the cell performance needs to be established.

1.3.3. Catalytic combustion and thermal polymer decomposition in the PEMFC

The membrane in the fuel cell stack of a vehicle is super thin (20-30 μm). Leakage through the membrane is inevitable due to the existence of the partial pressure gradient of the reactant gases. When the membrane is free of defects, the leaking rate is low (around 5 $mAcm^{-2}$ with a 25 μm thick membrane at 80 °C [43]). Parasite reactions of the reactant gases at the electrodes cause the drop of actual OCV (0.9-1.0V) from the theoretical value of 1.23 V [44]. Besides, the combustion reaction between hydrogen and oxygen (in the air stream) also occurs in the presence of Pt. Hydrogen combustion releases high thermal energy, approximately -285 $kJmol^{-1}$ at 25 °C [45], which causes the membrane temperature to rise. The heat flux released from combustion depends mainly on the crossover rate and the catalytic activity. Meanwhile, the cell structure can help to deliver heat liberated inside the cell to the coolant medium or heat dissipation capability of the cell. This heat dissipation capability of the cell depends on the arrangement of components and the cell temperature. For instance, GDL oversizing the catalyst is considered a high dissipated heat flux structure [46]. And the maximum dissipated heat flux is defined as the maximum heat flux that the cell can transfer without causing the membrane to burn.

Depending on the correlation between combustion heat flux and the maximum dissipated heat flux of the cell, the temperature rises of the membrane induced by combustion will be at different scale. In the fresh CCM, because the hydrogen crossover rate is small and uniform, combustion is in the moderate scale and the released heat flux must be lower than the dissipated heat flux of the cell. Membrane temperature rise is marginal and does not cause any defects, as described in Fig.1.6a. In a degraded membrane, the hydrogen crossover rate increases appreciably through the serious defects such as through-membrane cracks and membrane thinning (see Fig.1.6b) induced by mechanical and chemical stresses, respectively. As a result, the combustion heat flux could reach close to the maximum dissipated heat flux, the membrane temperature rises locally but still under the auto-ignition temperature of the membrane (approximately

300 °C [47]), then this combustion situation can be categorized in the transient scale. In accidental combustion, the released heat flux is beyond the maximum dissipated heat flux, resulting in the surge of membrane temperature. As membrane temperature exceeds the auto-ignition temperature, the membrane can be ignited and decomposed, leading to the formation of pinholes as described in Fig.1.6c, consequently resulting in fuel shorting and instant failure of the membrane in the PEMFCs [46-48] and PEMWEs [49].

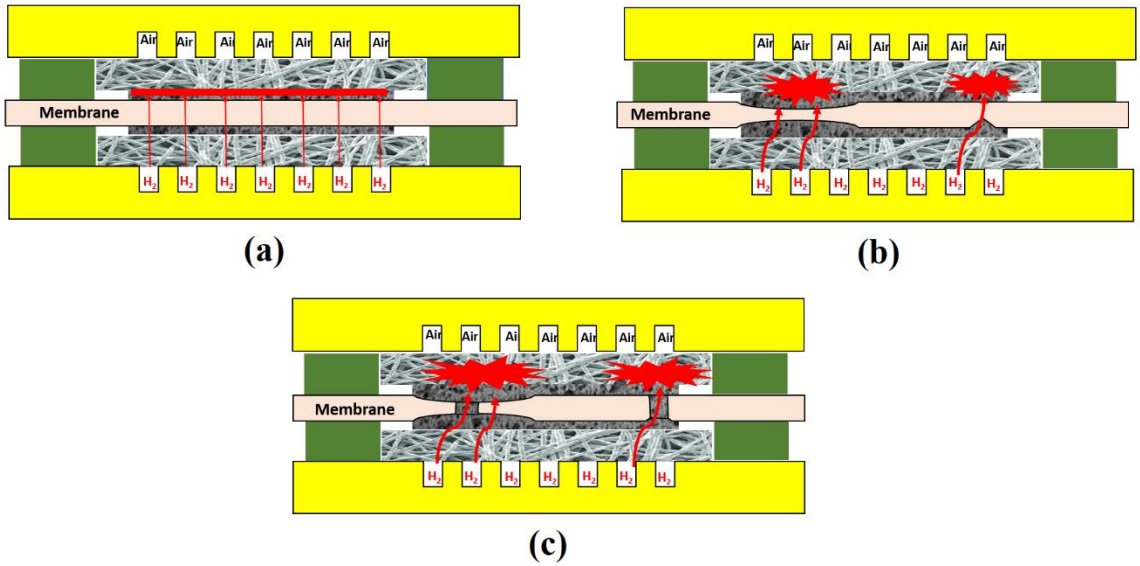

Fig. 1. 6. Schematic illustration for combustion in a PEMFC (a) moderate combustion with the intact membrane, (b) transition of the combustion process from moderate to accidental scale at membrane thinning positions and cracks caused by the mechanical and chemical stresses, and (c) pinhole formation induced by accidental combustion through the degraded membrane.

As mentioned above, accidental combustion is the worst scenario that can lead to the sudden and premature "death" of the PEMFCs, reducing the FCV's lifetime as well as the reliability. In the literature, some authors have reported the catastrophic damage caused by accidental combustion in the PEMFCs [27, 46, 48]. Therefore, the top priority is to prevent the occurrence of accidental combustion in the PEMFCs. In order to do that, it is of paramount importance to develop reliable diagnostic tools for tracking the transition of the combustion process from a moderate to an accidental scale.

1.4. The objectives and methodology of dissertation

1.4.1. Objectives

In automotive applications of the PEMFCs, the membrane is the crucial component and is highly vulnerable when subjected to various degradation mechanisms. For heavy-duty fuel cell vehicles, where the membrane must fulfill an exceptionally high lifespan target of 30,000 h, a more resilient membrane is highly desirable. Therefore, in addition to creating new, more durable membranes, a deeper understanding of membrane degradation mechanisms is essential to advancing mitigation measures, which in turn prolong the lifetime of the membrane. This is one of the objectives of the current study. Furthermore, as combustion

shifts to the accidental scale, the membrane may suffer catastrophic destruction, as depicted in Fig. 1.6c. Based on this background, the author dedicates effort to clarifying the transition of combustion from the moderate to accidental scale in order to identify transient combustion signals and provide reliable diagnostic methods. More details of the objectives and method of this study are listed as follows.

(1) Proposing a mathematical model to diagnose membrane integrity based on the correlation between OCV and hydrogen crossover rate

The hydrogen crossover rate is recognized as a reliable indication of membrane integrity. However, measuring the hydrogen crossover rate demands the employment of additional equipment and inert gases supplied from the cathode compartment. Furthermore, there are several hundred cells in the fuel stack of a FCV, so measuring the hydrogen crossover rate in every single cell could be costly and time-consuming. Meanwhile, OCV is a useful and crucial parameter in the PEMFCs and can be scanned quickly across the whole fuel stack of a FCV. In the RH cycling test using nitrogen gas, the membrane is subject to purely mechanical degradation, thus the decrease in OCV from the theoretical value is dominantly due to hydrogen crossover. The current study aims to develop a reliable mathematical model that translates the OCV data into the hydrogen crossover rate. This model can be a diagnostic tool to evaluate membrane integrity based on the practical parameter, OCV.

(2) Investigating the catalytic combustion by using thermal imaging method

The formation of pinhole induced by accidental combustion has been confirmed as being responsible for the early and sudden failure of the cell. Once we succeed to track the transition of the combustion process in the PEMFCs, we can recognize to some physical signs of the transition, and can design a reasonable diagnose method, which lead to a more safety operation and enhancing the durability and the reliability of the fuel cell vehicles. In the current study, the catalytic combustion of the crossing reactant gases through the membrane is investigated in situ manner with the visualization cell. Thermal imaging method is employed with the support of an IR camera and a high transmittance glass window (ZnS) at the cathode compartment. Temperature distribution on the GDL's surface is proportional to hydrogen crossover rate. When and where the combustion transition from moderate to accidental scale corresponding to hot-spot appearance. Correlation between temperature increase due to combustion and hydrogen crossover rate is clarified.

(3) Investigating the effect of current density on the membrane durability under the combined chemical and mechanical stress test

This study aims to investigate the effects of current density on membrane durability and elucidate the catalytic combustion phenomenon in PEMFCs under combined mechanical and chemical stress tests. RH cycling durability tests using hydrogen gas and air were carried out under the open circuit voltage (OCV) condition and at current densities of 0.05 and 0.3 Acm^{-2}. The effects of mechanical and chemical stress on the membrane during the durability tests are represented, respectively, by residual stress and the

rate of H_2O_2 formation. While comparing the results under the three testing conditions, the effect of different current densities on the degree of mechanical and chemical degradation was examined through the following questions:

(i) Does the large amount of water produced at higher current density operation moderate the water content variation in the membrane, resulting in the suppression of mechanical degradation?

(ii) Does lowering the cell voltage by higher current density operation moderate the formation rate of hydrogen peroxide (H_2O_2) at the anode side, resulting in the suppression of chemical degradation?

1.4.2. Methodology

In order to achieve the above objectives, membrane durability tests will be proposed and employed in a single PEM fuel cell that embeds the CCM using Nafion membrane NRE211 (Normal thickness of 25 μm). The mechanical stress test will be conducted on the normal cell. In particular, RH cycling test using nitrogen gas is implemented. Meanwhile, the RH cycling test using hydrogen and air is employed to the visualization cell, in which a high infrared transmitting glass window-ZnS glass is installed at the cathode compartment, to investigate membrane durability as well as the catalytic combustion phenomenon in-situ manner at different current density conditions e.g., 0, 0.05 and 0.3 Acm^{-2}.

During these tests, electrochemical methods like linear sweep voltammetry (LSV), Cyclic voltammetry (CV) will be employed. Based on these methods, some important indicators, including the hydrogen crossover rate, electrochemical surface area (ECSA) of the catalyst, and OCV, will help to elucidate the membrane degradation mechanism.

In the visualization cell, an IR camera will be used to take images of the cathode's GDL during the OCV measurements through a high transmittance glass window (ZnS glass). The thermal imaging method will aid in identifying hot spots that appear as a result of the catalytic combustion transitioning from moderate to accidental scale.

Finally, focused ion beam scanning electron microscope (FIB-SEM) will be used in the postmortem analysis to investigate directly the changes in the membrane's morphology under the durability tests. The SEM images contribute to revealing the location where cracks and pinholes tend to appear under different testing conditions. Furthermore, the cross-sectional images created by the FIB can give information about the size of pinholes, membrane thickness, and the width and depth of cracks.

1.5. Structure of dissertation

This dissertation is structured as follows:

- Chapter 1 is the introduction section where the chemical and mechanical membrane degradation mechanisms are reviewed. Furthermore, catalytic combustion and its transition to accidental scale in the PEMFCs is introduced. The final contents are the study objectives and methodology.

- The purpose of Chapter 2 is to investigate the durability of the membrane under mechanical stress in a normal cell. An RH cycling test using nitrogen gas will be conducted. Additionally, a model based on the relationship between the hydrogen crossing rate and OCV will be proposed to evaluate the membrane health.
- The goals of Chapter 3 are to investigate in situ catalytic combustion in the PEMFC during a combined chemical and mechanical stress test in the visualization cell. The cell is kept at OCV condition at 80°C during the RH cycling test in which hydrogen and air are fed to the cell. The IR images are taken through a high transmittance glass by using an IR camera, so that the temperature increase of cathode's GDL caused by combustion can be identified.
- In Chapter 4, effects of the current density on membrane durability under the under the combined mechanical and chemical accelerated stress test will be elucidated. The RH cycling tests will be conducted at the OCV condition, at 0.05 and 0.3 Acm^{-2} in a visualization PEMFC. Furthermore, catalytic combustion will be investigated in-situ manner in these three testing conditions.
- The content of Chapter 5 is the overall conclusions of the study and membrane degradation mitigation strategy promotion.
- The appendix includes two parts. The appendix A is the iteration calculation procedure which is proposed to predict the cathode's GDL temperature rise induced by combustion. The appendix B is to investigate the chemical stress on the membrane's durability. An OCV hold test is conducted to intensify the formation of free radicals that can decompose membrane structure chemically. During the OCV hold test, the IR imaging method is also employed to track the transition of catalytic combustion in the OCV measurements.

1.6. References

1. BP Statistical Review of World Energy June 2016. bp.com/statisticalreview. http://oilproduction.net/files/especial-BP/bp-statistical-review-of-world-energy-2016-full-report.pdf. Accessed on 17 February 2022.
2. Understanding the current energy situation in Japan (Part 1), August 2019. https://www.enecho.meti.go.jp/en/category/special/article/energyissue2019_01.html#topic01. Accessed on 17 February 2022.
3. Tasuku Kuwabara, Detlev Mohr, Benjamin Sauer, and Yuito Yamada, "How Japan Could Reach Carbon Neutrality by 2050 | McKinsey." Www.mckinsey.com, 4 Aug. 2021, www.mckinsey.com/business-functions/sustainability/our-insights/how-japan-could-reach-carbon-neutrality-by-2050. Accessed on 17 February 2022.

4. Ohira, Eiji. “Japan Policy and Activity on Hydrogen Energy”. 4 Mar. 2019. https://www.nedo.go.jp/content/100890039.pdf. Accessed on 17 February 2022.
5. “A hydrogen strategy for a climate - neutral Europe”, Brussels, 8.7.2020 COM (2020) 301 final. http://extwprlegs1.fao.org/docs/pdf/eur208381.pdf. Accessed on 17 February 2022.
6. 6 Borm, Oliver, and Stephen B Harrison. “Reliable Off-Grid Power Supply Utilizing Green Hydrogen.” Clean Energy, vol. 5, no. 3, 1 Aug. 2021, pp. 441–446, 10.1093/ce/zkab025.
7. Muhammet Kayfeci, Ali Keçebaş, Mutlucan Bayat, Chapter 3 - Hydrogen production, Editor(s): Francesco Calise, Massimo Dentice D’Accadia, Massimo Santarelli, Andrea Lanzini, Domenico Ferrero, Solar Hydrogen Production, Academic Press, 2019, Pages 45-83, ISBN 9780128148532, https://doi.org/10.1016/B978-0-12-814853-2.00003-5
8. J. Ivy, “Summery of electrolytic hydrogen production: Milestone completion report,” NREL Tech. Rep. MP-560-36734, Sep. 2004. https://www.nrel.gov/docs/fy04osti/36734.pdf
9. L. Bertuccioli, A. Chan, D. Hart, F. Lehner, B. Madden, and E. Standen, Study on Development of Water Electrolysis in the EU by E4tech S`arl with Element Energy Ltd for the Fuel Cells and Hydrogen Joint Undertaking (2014). https://www.fch.europa.eu/sites/default/files/FCHJUElectrolysisStudy_FullReport%20(ID%2019 9214).pdf
10. “Electricity Price Statistics - Statistics Explained.” Ec.europa.eu, 2022, ec.europa.eu/eurostat/statistics-explained/index.php?title=Electricity_price_statistics. Accessed 17 Feb. 2022. Accessed on 17 February 2022.
11. Shiva Kumar, S., and V. Himabindu. “Hydrogen Production by PEM Water Electrolysis – a Review.” Materials Science for Energy Technologies, vol. 2, no. 3, Mar. 2019, www.sciencedirect.com/science/article/pii/S2589299119300035, 10.1016/j.mset.2019.03.002.
12. Ene-farm partners, 2022. https://www.gas.or.jp/user/comfortable-life/enefarm-partners/. Accessed on 17 February 2022.
13. Residential Fuel Cell ENE-FARM: Challenge Zero. チャレンジ・ゼロ - イノベーションを通じた脱炭素社会へのチャレンジ -. https://www.challenge-zero.jp/en/casestudy/469. Accessed on 17 February 2022.
14. Fuel Cell and Battery Electric Vehicles Compared, By C. E. (Sandy) Thomas, Ph.D., President
15. Remzi Can Samsun, Laurent Antoni, Michael Rex, Detlef Stolten, Deployment Status of Fuel Cells in Road Transport: 2021 Update, Energie & Umwelt / Energy & Environment, Band / Volume 542, ISBN 978-3-95806-556-7

16. Dorian, Drew. "2020 Toyota Mirai." Car and Driver, Car and Driver, 14 May 2019, www.caranddriver.com/toyota/mirai. Accessed on 17 February 2022.
17. "2022 Hyundai Nexo Review, Pricing, and Specs." Car and Driver, 2 Nov. 2021, www.caranddriver.com/hyundai/nexo. Accessed on 17 February 2022.
18. Adria Wilson, Gregory Kleen, and Dimitrios Papageorgopoulos, 2017, Fuel Cell System Cost-2017, DOE Hydrogen and Fuel Cells Record Program. U.S. Department of Energy <https://www.hydrogen.energy.gov/pdfs/17007_fuel_cell_system_cost_2017.pdf>
19. "Insight: In Green Car Race, Toyota Adds Muscle with Fuel-Cell Launch." Reuters, 17 Apr. 2014, www.reuters.com/article/us-autos-hydrogen-toyota-motor-insight/insight-in-green-car-race-toyota-adds-muscle-with-fuel-cell-launch-idUSBREA3F1UN20140417.
20. M.F. Mathias, et al. "Two Fuel Cell Cars In Every Garage?" Interface 14 (2005) 24.
21. Department of Energy of the United States. Fuel Cell Technologies Office Multi-Year Research, Development, and Demonstration Plan. https://www.energy.gov/sites/prod/files/2017/05/f34/fcto _ myrdd _ fuel _ cells.pdf
22. Fuel Cell Technical Team Roadmap I Hydrogen Storage Technologies Roadmap Fuel Cell Technical Team Roadmap. 2017. https://www.energy.gov/sites/prod/files/2017/11/f46/FCTT_Roadmap_Nov_2017_FINAL.pdf. Accessed 12 July 2022.
23. Cullen, David A., et al. "New Roads and Challenges for Fuel Cells in Heavy-Duty Transportation." Nature Energy, vol. 6, no. 5, 25 Mar. 2021, pp. 462–474, 10.1038/s41560-021-00775-z
24. Shin, Sung-Hee, et al. "Improving the Mechanical Durability of Short-Side-Chain Perfluorinated Polymer Electrolyte Membranes by Annealing and Physical Reinforcement." ACS Omega, vol. 4, no. 21, 5 Nov. 2019, pp. 19153–19163, 10.1021/acsomega.9b02436.
25. 25Gubler, Lorenz, et al. "Radical (HO•, H• and HOO•) Formation and Ionomer Degradation in Polymer Electrolyte Fuel Cells." Journal of the Electrochemical Society, vol. 158, no. 7, 27 Apr. 2011, pp. B755–B769, 10.1149/1.3581040.
26. 26Liu, Wen, and David Zuckerbrod. "In Situ Detection of Hydrogen Peroxide in PEM Fuel Cells." Journal of the Electrochemical Society, vol. 152, no. 6, 2005, p. A1165, 10.1149/1.1904988.
27. 27T. Madden, D. Weiss, N. Cipollini, D. Condit, M. Gummalla, S. Burlatsky and V. Atrazhev, J. Electrochem.Soc.156 (2009) B657.

28. Zhang, Shengsheng, et al. “Effects of Open-Circuit Operation on Membrane and Catalyst Layer Degradation in Proton Exchange Membrane Fuel Cells.” Journal of Power Sources, vol. 195, no. 4, 15 Feb. 2010, pp. 1142–1148. https://doi.org/10.1016/j.jpowsour.2009.08.070.

29. Ohma, Atsushi, et al. “Phenomenon Analysis of PEMFC for Automotive Use (1) Membrane Degradation Behavior during OCV Hold Test.” ECS Transactions, vol. 3, no. 1, 21 Dec. 2019, pp. 519–529, 10.1149/1.2356173.

30. Endoh, Eiji. “Development of Highly Durable PFSA Membrane and MEA for PEMFC under High Temperature and Low Humidity Conditions.” ECS Transactions, vol. 16, no. 2, 3 Oct. 2008, pp. 1229–1240, 10.1149/1.2981964.

31. Inaba, Minoru, et al. “Gas Crossover and Membrane Degradation in Polymer Electrolyte Fuel Cells.” Electrochimica Acta, vol. 51, no. 26, Aug. 2006, pp. 5746–5753, 10.1016/j.electacta.2006.03.008.

32. Liu, Han, et al. “Impact of Gas Partial Pressure on PEFC Chemical Degradation.” ECS Transactions, vol. 3, no. 1, 20 Oct. 2006, pp. 493–505, 10.1149/1.2356171.

33. Macauley, N., et al. “Pt Band Formation Enhances the Stability of Fuel Cell Membranes.” ECS Electrochemistry Letters, vol. 2, no. 4, 5 Feb. 2013, pp. F33–F35, 10.1149/2.007304eel.

34. Sadeghi Alavijeh, A., et al. “Decay in Mechanical Properties of Catalyst Coated Membranes Subjected to Combined Chemical and Mechanical Membrane Degradation.” Fuel Cells, vol. 15, no. 1, 28 Nov. 2014, pp. 204–213, 10.1002/fuce.201400040

35. Wu, Jinfeng, et al. “Proton Exchange Membrane Fuel Cell Degradation under close to Open-Circuit Conditions.” Journal of Power Sources, vol. 195, no. 4, Feb. 2010, pp. 1171–1176, 10.1016/j.jpowsour.2009.08.095.

36. Mittal, Vishal O., et al. “Is H_2O_2 Involved in the Membrane Degradation Mechanism in PEMFC?” Electrochemical and Solid-State Letters, vol. 9, no. 6, 2006, p. A299, 10.1149/1.2192696.

37. Lai, Yeh-Hung, et al. “Viscoelastic Stress Analysis of Constrained Proton Exchange Membranes under Humidity Cycling.” Journal of Fuel Cell Science and Technology, vol. 6, no. 2, 20 Feb. 2009, 10.1115/1.2971045.

38. Kusoglu, Ahmet, et al. “Mechanical Response of Fuel Cell Membranes Subjected to a Hygro-Thermal Cycle.” Journal of Power Sources, vol. 161, no. 2, Oct. 2006, pp. 987–996, 10.1016/j.jpowsour.2006.05.020.

39. Adam Z. Weber. “New Insights into Perfluorinated Sulfonic-Acid Ionomers.” Chemical Reviews, vol. 117, no. 3, 23 Jan. 2017, pp. 987–1104, 10.1021/acs.chemrev.6b00159.]

40. US Department of Energy, DOE cell component accelerated stress test protocols for PEM fuel cells, March 2007. https://www1.eere.energy.gov/hydrogenandfuelcells/fuelcells/pdfs/component_durability_profile.pdf. Accessed on 17 February 2022.

41. A.B. LaConti, M. Hamdan, and R.C. McDonald, Handbook of Fuel Cells: Fundamentals, Technology, and Applications, Vol. 3, W. Vielstich, A. Lamm, and H. A. Gasteiger, Editors, Wiley, New York (2003)

42. Alavijeh, Alireza Sadeghi, et al. "Microstructural and Mechanical Characterization of Catalyst Coated Membranes Subjected to in Situ Hygrothermal Fatigue." Journal of the Electrochemical Society, vol. 162, no. 14, 2015, pp. F1461–F1469, 10.1149/2.0471514jes.

43. Ngo, Phi Manh, et al. "Investigation of In-Situ Catalytic Combustion in Polymer-Electrolyte-Membrane Fuel Cell during Combined Chemical and Mechanical Stress Test." Journal of Power Sources, vol. 542, Sept. 2022, p. 231803, 10.1016/j.jpowsour.2022.23180.

44. Francia, Carlotta, et al. "Estimation of Hydrogen Crossover through Nafion® Membranes in PEMFCs." Journal of Power Sources, vol. 196, no. 4, Feb. 2011, pp. 1833–1839, 10.1016/j.jpowsour.2010.09.058.

45. M.R. Tarasevich, A. Sadkowski, E. Yeager, B.E. Conway, J. O'M. Bockris, in: E. Yeager, S.U.M. Khan, R.E. White (Eds.), Comprehensive Treatise of Electrochemistry, vol. 7, Plenum Press, New York, 1983, p.301.

46. Lakshmanan, Balasubramanian, et al. "Polyetheretherketone Membranes for Elevated Temperature PEMFCs." Electrochemical and Solid-State Letters, vol. 6, no. 12, 2003, p. A282, 10.1149/1.1619647.

47. Stanic, Vesna. "Mechanism of Pinhole Formation in Membrane Electrode Assemblies for PEM Fuel Cells." ECS Proceedings Volumes, vol. 2004-21, no. 1, Jan. 2004, pp. 391–401, 10.1149/200421.0391pv.

48. Gunji, Hiroyuki, et al. "Gas-Leak-Induced Pinhole Formation at Polymer Electrolyte Membrane Fuel Cell Electrode Edges." International Journal of Hydrogen Energy, vol. 42, no. 1, Jan. 2017, pp. 562–574, 10.1016/j.ijhydene.2016.11.038.

49. Millet, P., et al. "Cell Failure Mechanisms in PEM Water Electrolyzers." International Journal of Hydrogen Energy, vol. 37, no. 22, Nov. 2012, pp. 17478–17487, 10.1016/j.ijhydene.2012.06.017.

Chapter 2

Investigation of membrane mechanical durability in the polymer electrolyte membrane fuel cells

Abstract

Membrane durability is the main hurdle preventing the widespread commercialization of fuel cell vehicles. Thus, understanding degradation mechanisms and developing diagnostic methods for checking the integrity of the membrane in polymer electrolyte membrane fuel cells are apparently vital. In this chapter, the mechanical stability of the membrane will be investigated, and the correlation between two indicators, the hydrogen crossover rate, and open-circuit voltage will also be established with the aim of finding a reliable and practical membrane health diagnostic tool. A single membrane fuel cell, which embeds a catalyst-coated membrane (CCM) using Nafion NRE211 membrane, is subjected to the relative humidity (RH) cycling test, an accelerated stress test, at the cell temperature of 80 °C, feeding N_2 to both the cathode and anode at atmospheric pressure. After every 500 RH cycles, the hydrogen crossover rate and open-circuit voltage (OCV) were checked, so that any sudden change of these two indicators could be a signal for fatal damage to the membrane. An empirical model was used to predict membrane integrity based on the correlation between OCV and the hydrogen crossover rate. As a result, the hydrogen crossover was more sensitive and able to detect the formation of small pinholes in the membrane after 10,500 RH cycles. After 12,500 RH cycles, both the hydrogen crossover rate and OCV showed an appreciable change, which reveals the impact of catastrophic defects in the membrane. The model can predict quantitatively membrane degradation. Finally, the scanning electron microscope images, which indicate the cross-section of the CCM after the durability test, clearly showed the presence of the through-membrane cracks.

2.1. Introduction

The durability of the fuel cell stack will predominantly determine the lifetime, stability, and safety of the fuel cell vehicles (FCVs). Among the components of the fuel cell stack, the polymer electrolyte membrane (or membrane for short) plays three main crucial roles, including proton conduction, electron insulation, and reactant gas separation [1]. However, the thickness of the membrane in applications for mobile applications in general and vehicles, in particular, is really thin, typically 20–25 μm [2]. The thinner the membrane, the higher the specific power density, and thus the smaller the system and the lower the cost.

During the operation of the FCVs, the membrane must experience several dynamic changes, such as cyclic changes in humidity and temperature of the reactant gases induced by load demand variation. The variation of the membrane dimension due to water content and temperature changes leads to the formation of compressive and tensile stresses in the membrane, consequently deteriorating the membrane. As

mentioned in Chapter 1, the shrinkage and expansion of the membrane induced by the oscillation of water content is the primary cause of mechanical membrane failure. The membrane is under the impact of the mechanical degradation process, which will lead to the formation of typical defects, e.g., cracks and delamination between the membrane and catalyst layers. The presence of these defects, respectively, increases the fuel crossover rate and the ohmic resistance, resulting in fuel cell performance decay. In addition, mechanical degradation can also enhance chemical degradation when it leads to an increase in reactant gases crossing through the membrane, resulting in the formation of hydrogen peroxide at the electrodes and inside the membrane, as mentioned in detail in Chapter 1. Then, free radicals such as •OOH and •OH are formed with the appearance of hydrogen peroxide and metal cations (Fe^{2+}, Fe^{3+}, Cu^{2+}...). As a result, the membrane is chemically decomposed by these radicals and becomes thinner. Furthermore, the appearance of cracks in the mechanically-degraded membrane might be largely responsible for the sudden, unpredictable death of the fuel cell stack due to an accidental catalytic combustion between hydrogen and oxygen in the air, thus seriously affecting the safety of the fuel cell stack [3, 4]. According to the aforementioned viewpoints, membrane mechanical degradation should be continuously and in-depth explored. The effort concentrates to clarify the transient process of catalytic combustion from moderate to accidental scale in quantitative manner. This effort contributes to develop suitable mitigating tactics, and diagnostic techniques, in addition to producing new durable membranes.

In the PEMFC, the hydrogen crossover rate is a popular and reliable indicator for diagnosing membrane health because it is certainly proportional to the degree of membrane damage (pinholes and cracks). Thus, the membrane failure criterion is usually set by the rate of hydrogen gas passing through the membrane. In particular, when the hydrogen crossover rate exceeds a predetermined threshold of 15 $mAcm^{-2}$, a membrane is deemed to be entirely failed [5]. Currently, there are a number of methods being used to measure the hydrogen crossover rate for diagnosing the presence of cracks, or pinholes in the membrane. The first method is the mechanical gas leakage test. Specifically, a pressure difference of some selected gases (e.g., N_2 or air or He...) between the anode and the cathode is intentionally imposed. Then, the flow rate of the gases through the membrane is measured using mass spectrometry, which is installed at the outlet of the cell. If the membrane is intact, the flow rate through the membrane will be a small and stable value, which can be estimated by the gas permeability of the membrane. In the deteriorated membranes, the mechanism of gas leakage between the anode and the cathode of the fuel cell will be governed by convection and increase dramatically with the appearance of cracks or pinholes. This is an ex-situ method and quite accurate, but cannot be performed while the fuel cell is in operation. Moreover, it requires a complex design for the testing systems [3]. In addition to the ex-situ method, hydrogen crossing through the membrane can be measured electrochemically by using, e.g., the linear sweep voltammetry (LSV) method. The molecular hydrogen passing through the membrane from the anode to the cathode is oxidized and represented in units of current and then can be translated easily to traditional flow rate units e.g. cm^3/min, ml/min… by using Faraday's equation. The advantages of this method are that it is simple, non-

destructive, quick, and can be done in-situ. However, during measurement, inert gases like argon or nitrogen must be supplied into the cathode compartment.

It has been well-known that there is a correlation between the reactant gas crossover rate and the open-circuit voltage (OCV) [6,7]. Hence, OCV can also be an indicator for checking the membrane integrity. Hydrogen gas crossing through the membrane is oxidized at the cathode (at the potential of 0 V vs. NHE (Normal Hydrogen Electrode)), resulting in the reduction of the cathode potential. At the same time, oxygen gas permeates through the membrane to the anode side and is reduced, leading to the rise in anode potential. Mixed potentials caused by the oxygen reduction reaction at the anode and the hydrogen oxidization reaction at the cathode lead to the decrease of OCV. Based on this relation, it is possible to predict indirectly the occurrence of serious damage on the membrane. Specifically, when cracks or pinholes appear in the deteriorated membrane, the OCV will decrease significantly due to hydrogen crossover increase [8]. OCV is therefore regarded as an important and practical measure for evaluating the integrity of the membrane. Furthermore, checking OCV is quick, and easy and can be carried out while the fuel cell is running. The OCV decay rate can be converted to the rate of hydrogen passing through the deteriorated membrane, although there is no accurate quantitative formula for doing so.

The objectives of this chapter are to investigate membrane mechanical durability and develop a membrane health diagnostic method based on the correlation between OCV and hydrogen crossing rate through the degraded membrane. In order to achieve these objectives, a Nafion membrane NRE211 (25 μm thickness) in the catalyst-coated membrane (CCM) is first subjected to an RH cycling test using nitrogen for both sides of the cell. Without flowing H_2 and air to the cell during the RH cycling test, the formation of H_2O_2, which is a precursor of free radicals, will be excluded. Hence, the membrane will only experience the mechanical degradation mechanism in the RH cycling test using nitrogen gas. Secondly, membrane integrity is evaluated through two indicators after every 500 RH cycles, including the hydrogen crossover rate and OCV. Thirdly, a mathematical model is applied to translate the OCV drop rate into the hydrogen crossover rate through the degraded membrane induced by the RH cycling test. And finally, FIB-SEM is employed to investigate the morphology change from the degraded CCM induced by the mechanical durability test.

2.2. Experimental

2.2.1. Experimental apparatus

Fig. 2.1 presents the flow diagram of the experimental system, which is designed to conduct both accelerated stress tests and periodic electrochemical evaluations for the visualization cell. A catalyst ink is spray-printed on an NRE211 (DuPont) membrane with a normal thickness of 25 μm and an overall area of 80 × 80 mm with a spray-printing system (Nordson). The ink is composed of Pt/C powder (46.6%wt Pt in Pt/C, TEC10E50E, Tanaka), Nafion perfluorinated resin solution (1100 EW, 5%wt, Aldrich), ethanol (99.5%vol), and deionized water. As the result, a rectangular CCM with a 10-mm width and a 34-mm

length was formed in the center of the membrane with a platinum loading of 0.5 mg cm^{-2} at both electrodes. Subsequently, the CCM was hot-compressed at 130 °C for 180 s at a pressure of 7.5 kN m^{-2}. The CCM was then sandwiched between two carbon paper GDLs (Sigracet 34BC, thickness of 315 mm), two co-current serpentine flow fields with 2-mm-wide channels and 3-mm lands, and two SS316 clamp plates. The preparation of the testing cell is shown in Fig.2.2.

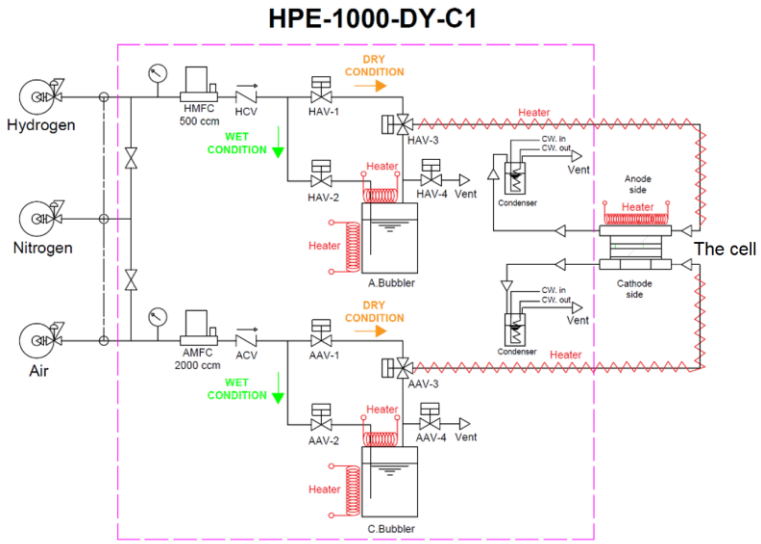

Fig. 2. 1. Flow diagram of the experimental device.

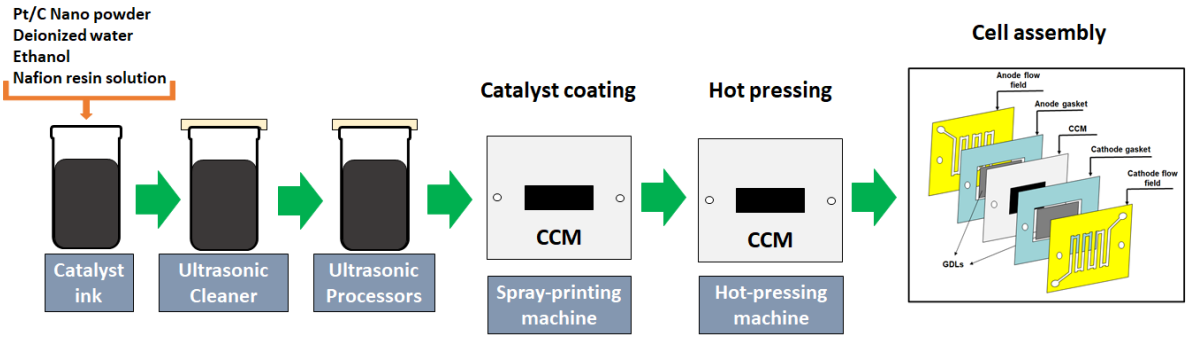

Fig. 2. 2. An illustration for the testing cell preparation.

2.2.2. The RH cycling protocol and experimental procedure

The membrane in a PEFC is partially constrained by the electrodes, gas diffusion layers, and flow fields. Meanwhile, the dimension of the membrane reacts sensitively to the variation of temperature and humidity of the reactant gases [9]. Thus, the cyclic change of temperature and water content of the membrane during the operation of the FCVs can cause contraction and expansion, consequently forming residual stresses in the membrane. The influences of temperature and the water content on the membrane's dimensional change are based on the thermal expansion coefficient and the hygral expansion coefficient, respectively. In the operation of the FCVs, the dimensional change of the membrane caused by the water content fluctuation is dominant due to the high hygral expansion coefficient. In engineering materials,

residual stresses induced by the repeated dimensional change behave like the fatigue load which is largely responsible for the mechanical damages. Therefore, the membrane becomes deteriorated gradually with the appearance of dangerous damages like micro-cracks and pinholes, ultimately the membrane failure [10].

The purpose of the RH cycling durability test is to accelerate the mechanical degradation of the membrane by applying a cyclic variation of the relative humidity of the gas streams. In the present chapter, a testing protocol has been built, which is partially based on the mechanical membrane stress test protocol of DOE [11]. Particularly, nitrogen gas at atmospheric pressure is supplied into the anode and cathode at a constant flow rate of 500 Nccm (Normal cm^3min^{-1}), at the cell temperature of 80 °C. The durations for keeping the cell in the dry portion (dry gas) and wet portion (100%RH) are 3 min and 2 min, respectively. The wet and dry transition of the nitrogen gas streams at both compartments of the cell was achieved by controlling the series of air-compressed valves (HAV-1, HAV-2, HAV-3, AAV-1, AAV-2, and AAV-3) in Fig. 2.1.

The experimental procedure is shown in Fig. 2.3. First of all, the Beginning-of-Life (BOL) check will be proceeded after incubating the cell at the fully hydrated condition in a day. In this stage, some important parameters e.g. the electrochemical active surface (ECSA), crossover rate, and OCV will be evaluated. Next, after every 500 RH cycles, there will be a periodic evaluation. Once again, the above indicators will be checked and compared with the result from the BOL. In order to eliminate the influence of the hydration level of the membrane on the electrochemical measurements, e.g., the hydrogen crossover rate, cyclic voltammetry, and OCV, and to secure the consistency with the measurements carried out at BOL, the membrane was fully hydrated before all periodic checks. Finally, there will be the End of Life (EOL) evaluation after finishing 20,000 cycles.

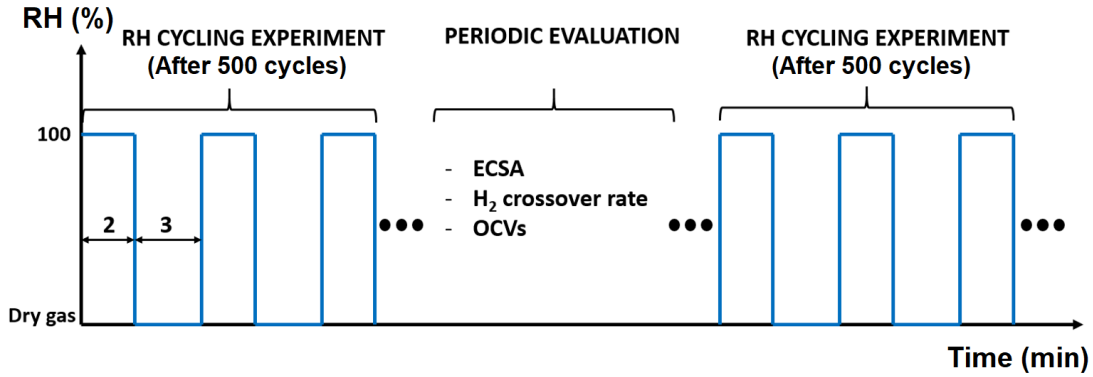

Fig. 2. 3. Experimental procedure.

2.2.3. Electrochemical testing and the OCV checking condition

2.2.3.1. Electrochemical surface area (ECSA) and hydrogen crossover rate measurements

Cyclic voltammetry (CV) and linear sweep voltammetry (LSV) are widely used to measure the ECSA and hydrogen crossing the membrane, correspondingly. Herein, a voltammetry system which is the so-called BioLogic Science Instruments - SP300, was utilized to conduct these techniques. Fully-hydrated

hydrogen and nitrogen at atmospheric pressure were fed into the anode and cathode at the flow rates of 150 Nccm and 200 Nccm, respectively. In order to achieve a 50-kPa anode backpressure, the hydrogen flow rate was chosen at least over 150 Nccm to overcome the pressure losses in the cell and the exhausted pipe. The cell temperature was kept at T_{cell} = 80 °C and nitrogen gas was stopped right before starting CV measurement. The hydrogen desorption area at the cathode electrode is so called as ECSA. The voltage applied to the cathode ranges from 0.05 V to 0.9 V vs. NHE (Normal Hydrogen Electrode (H_2/H^+)) with a scan rate of 50 mVs^{-1}. In general, in the RH cycling test using N_2, catalyst degradation is not a concern. However, during measuring OCV, hydrogen gas and air were used, and carbon oxidation can occur at the cathode, leading to the reduction of ECSA. Besides checking the catalyst degradation based on ECSA, the CV technique can also indicate when the fatal defects appear in the membrane. In particular, the CV curves tend to shift upward when the hydrogen crossover rate increases appreciably through the deteriorated membrane.

Meanwhile, the LSV technique can reveal the hydrogen crossover rate, expressed in units of the current density. The applied potential is swept from 0.05 to 0.5 V versus NHE, with a scan rate of 0.5 mV s^{-1}. The crossover current density is then calculated at an applied potential of 0.4 V versus NHE, at which the leaked hydrogen gas from the anode gets completely oxidized on the cathode catalyst [8]. When fatal defects appear in the membrane, the hydrogen crossover rate increases, and the voltammetry curves fluctuate vigorously. It is difficult to obtain correctly the hydrogen crossover current. The author recommended obtaining the maximum current density in the potential range of 0.4 to 0.5 V as the hydrogen crossover rate. This recommendation might not be perfect, but at least the obtained values can indicate the maximum hydrogen crossover rates through the degraded membrane. Two different pressure cases were used to measure the hydrogen crossover rate: (a) atmospheric pressure in the anode and cathode compartments and (b) the introduction of 50-kPa backpressure alone in the anode compartment. The "50-kPa anode backpressure," despite having a differential pressure of only 50-kPa, facilitates the early detection of serious membrane defects, such as pinholes and through-thickness cracks.

2.2.3.2. OCV checking condition

In order to measure the OCV, atmospheric, humidified hydrogen and air flowed into the anode and cathode at flow rates of 90 Nccm and 200 Nccm, respectively. These flow rates correspond to the anode stoichiometry of 2.92 and the cathode stoichiometry of 3.24 at the current density of 1 Acm^{-2}. This condition was maintained at the cell temperature of 80°C within 10 min during the OCV measurement to obtain the data.

2.2.3.3. FIB-SEM

The Focused Ion Beam Scanning Electron Microscope (FIB-SEM, Helios Nanolab 600i) is employed to confirm the appearance of mechanical defects on the degraded CCM after finishing the durability test. Three samples from the deteriorated CCM will be cut and observed.

2.3. Results and discussion

2.3.1. Mechanical degradation on the membrane

In Fig. 2.4a, b, and c are the snapshots of 10 RH cycles (50 min) which depict the cyclic change of the membrane resistance (highlighted by the green lines), which is induced by the RH cycling test, from 3 testing periods: (i) at the beginning of the test (500–1,000), (ii) at the middle (10,000–10,500), and (iii) at the end (19,500–20,000). These diagrams indicate that the water content of the membrane synchronizes with the repeated variation of the RH of the nitrogen streams. Thus, the constrained membrane in the cell must expand and shrink repeatedly during the durability test. As a result, the stress, which is dominated by the in-plane stress, is formed and accumulated in the membrane, leading to the formation of mechanical defects like cracks and tears in the membrane. It's well-known that the amplitude and frequency of the stress induced by the RH cycling test are the key factors in the formation speed and degree of damage of the defects in the membrane. However, it is quite difficult to directly measure the amplitude and frequency of the stress. Therefore, in the literature, many authors have tried to simulate and extract the stress fatigue as well as the frequency during the RH cycling test [12,13].

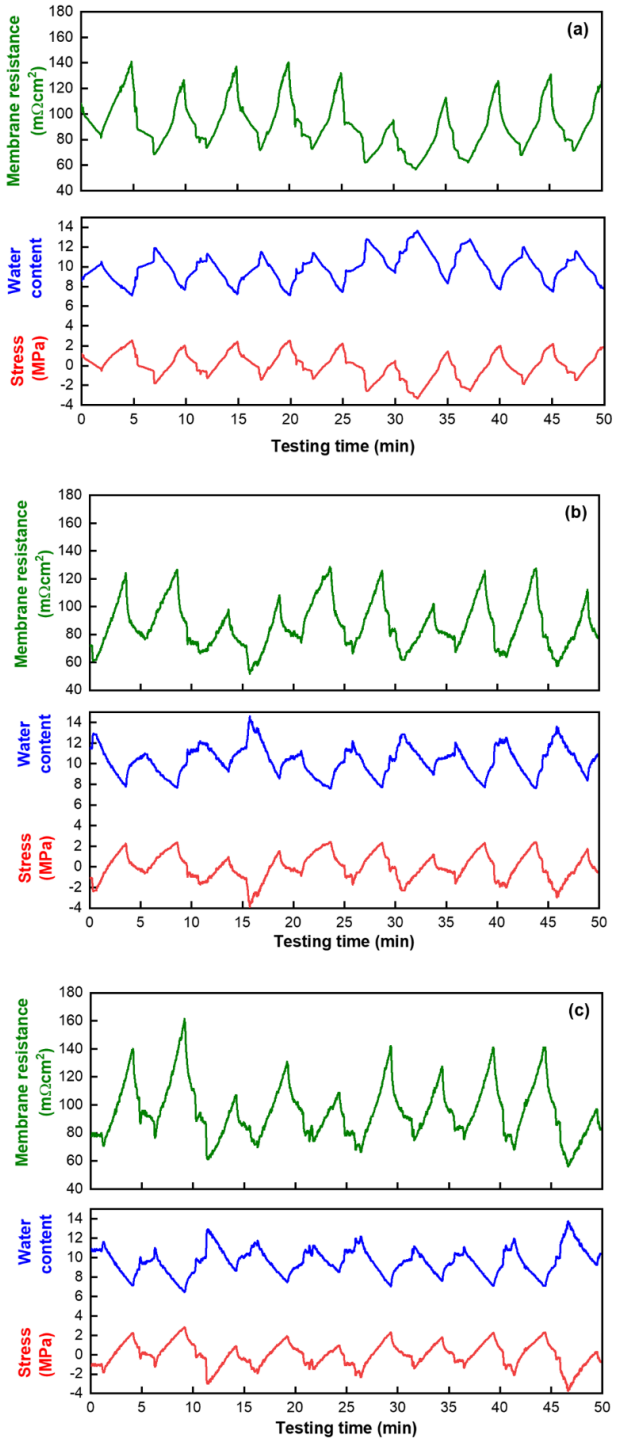

Fig. 2. 4. Snapshots of 10 RH cycles (a) in the testing period from 500 to1000 cycles, (b) in the testing period from 10,000 to 10,500 cycles, and (c) in the testing period from 19,500 to 20,000 cycles. Cyclic changes in membrane resistance (highlighted by the green lines) lead to the repeated change of water content (highlighted by the blue lines) and in-plane stress (highlighted by the red lines) formation during the RH cycling test.

In this chapter, the in-plane stresses (tensile and compressive stresses), which are induced by the repeated dimensional change in the constrained membrane as the water content changes during the

durability test, are quantified based on the membrane resistance data. The alternation of the tensile and compressive stresses acts as a fatigue load, causing the membrane to mechanically degrade over time. It is noticed that the water absorption and water desorption processes of the membrane are different. In particular, the Nafion membranes require less time to be fully humidified than they do to be fully dehumidified. Thus, the membrane can be fully hydrated in the wet portion in 2 min. Conversely, the membrane may not be dried fully in the dry portion (in 3 min) of the RH cycling test. Therefore, if equation (2.1) [12] is used to calculate the water content in the dry state (0% RH), the results will definitely be overestimated, especially given that the dry phase only lasts for 3 min. In light of the above considerations, an additional experiment was conducted to establish the correlation between membrane resistance and the relative humidity. In this experiment, the membrane resistance was measured at different relative humidity levels at the constant cell temperature of 80 °C by feeding 450 Nccm of nitrogen gas to the cell. As a result, the actual correlation between membrane resistance and the RH was established and shown in Fig. 2.5. Then, the actual relative humidity of the nitrogen gas stream can be determined at any resistance during the RH cycling test by interpolating the experimental data shown in Fig. 2.4. Next, the water content of the membrane (λ ($mol_{H_2O}mol^{-1}_{SO_3H}$)) as a function of gas stream relative humidity at 80°C was derived by applying an empirical equation (Eq. (2.1)) [12].

$$\lambda=\left[1+0.1913\times\left(\frac{RH}{100}\right)^2\left(\frac{T-30}{30}\right)\right]\left[14.15\times\left(\frac{RH}{100}\right)^3-18.97\times\left(\frac{RH}{100}\right)^2+13.41\times\left(\frac{RH}{100}\right)\right] \quad (2.1)$$

where RH (%) is relative humidity, and T (°C) is gas stream temperature.

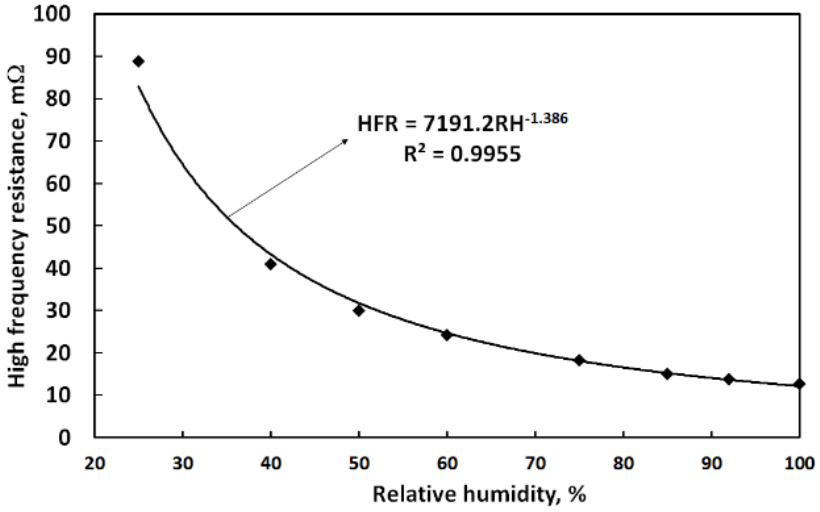

Fig. 2. 5. The correlation between membrane resistance and RH. The cell temperature is 80 °C. 450 Nccm of nitrogen gas at atmospheric pressure is fed into the cathode and anode compartments.

During the RH cycling test, the water content of the membrane changes repeatedly around an average value ($\lambda_{average}$), as illustrated in Fig. 2.6. The membrane contracts, and tensile stress ($\sigma > 0$) is created when the water content of the membrane is lower than the average. In contrast, when the membrane's water

content is higher than average, compressive stress ($\sigma < 0$) is formed as a result of membrane expansion. There is an approximate equation that represents the correlation between the hygral strain and water content of the membrane (Eq. (2.2) [14]).

$$\varepsilon = \frac{\Delta L}{L_o} = \beta_{swe}(\lambda_i - \lambda_{average}) \quad (2.2)$$

where $\beta_{swe} = 0.009$ is an experimental hygral expansion coefficient. λ_i is the water content of the membrane at time *t*. Because the cell temperature was maintained at 80 °C and no load was applied to the cell during the RH cycling test and the thermal expansion coefficient of the PFSA membrane is much smaller than the hygral expansion coefficient, thermal strain can be negligible in the current calculation.

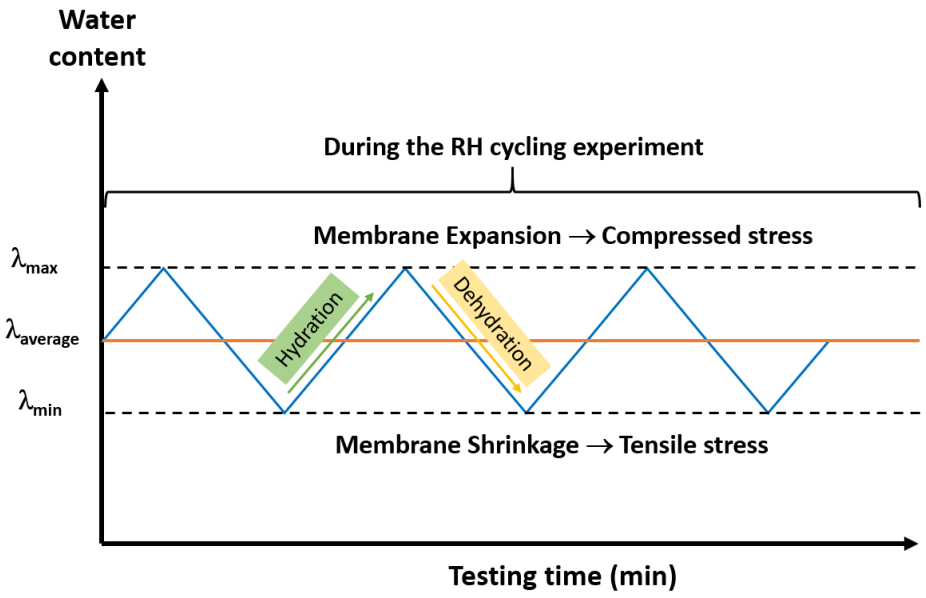

Fig. 2. 6. Schematic illustration of the water content variation during the RH cycling test.

Therefore, the in-plane stresses on the membrane can be estimated by Eq. (2.3) as follows

$$\sigma = \varepsilon \bar{E} \quad (2.3)$$

where $\bar{E}$ is the average Young's modulus of the membrane. At 25 °C, and 50%RH the Young's modulus of the NRE211 membrane is 233.5 MPa (244 MPa in the transverse direction, 223 MPa in the machine direction) [15]. Because Young's modulus decreases with temperature, it was obtained by interpolating at 80 °C from the experimental data in reference 15, approximately 100 MPa.

The results of water content change (highlighted by the blue lines) of the membrane and the corresponding in-plane stress (highlighted by the red lines), which is based on the resistance data, is shown in Fig. 2.4. And, Table 2.1 summarizes the average of water content changes and the corresponding stresses in the three testing periods. It is clear that the cyclic change of the RH of gas stream induces the water content of the membrane, eventually causing the repeated variation of the stress. The stress amplitude

($\Delta\sigma/2$), which influences predominantly the mechanical degradation, is approximately 2 MPa in all three periods. The results indicate that the current RH cycling test only targets membrane mechanical degradation. Hence, the side chain of the membrane, which determines its water absorption and desorption capability, was not decomposed by the free radicals. Therefore, the water content changes are almost the same, leading to the marginal difference in the stress amplitude in three periods, as shown in Table 2.1.

Table 2. 1. The summary from the in-plane stress calculation based on the membrane resistance data of 10 RH cycles at three testing periods

Testing periods	Membrane resistance change ΔR ($m\Omega cm^2$)	Average membrane water content $\lambda_{average}$ (-)	Water content change $\Delta\lambda$ (-)	Stress amplitude $\Delta\sigma/2$ (MPa)
500-1,000	57.7	9.90	4.20	1.90
10,000-10,500	53.2	10.3	4.39	1.98
19,500-20,000	60.4	9.60	4.23	1.87

2.3.2. The appearance of cracks/pinholes in the membrane

As shown in Figs. 2.7b and 2.8b, the hydrogen crossover rates, which were measured at atmospheric pressure and 50-kPa anode backpressure, respectively, vary slightly around 4.4 and 5.7 $mAcm^{-2}$ from the BOL until after 10,000 cycles. These crossover rates correspond to the rate estimated by H_2 permeability through the intact membrane. After the membrane experienced 10,500 RH cycles (875 h of testing), there was a sudden increase and a cyclic change in the detected current density in the voltammograms, as shown in Figs. 2.7a and 2.8a. But, apparently, the hydrogen crossover rate increased faster and at a higher magnitude at 50-kPa anode backpressure. The phenomenon implies serious damage to the membrane microstructure. When the membrane is subjected to the RH cycling test, cracks initiate on its surface and gradually propagate in depth. Thus, the cracks might have been fully developed through the membrane after 10,500 cycles, resulting in the formation of the micro-leaked paths in the membrane. As shown in Fig. 2.8b, the membrane completely failed after experiencing 12,500 RH cycles when the crossover rate reached 27.4 Acm^{-2}, and exceeded the membrane failure threshold of 15 $mAcm^{-2}$ [5]. This crossover rate is about 4.4 times higher than the crossover rate measured at atmospheric pressure (approximately 6.23 $mAcm^{-2}$ in Fig. 2.7b). Gas convection is clearly dominant over molecular diffusion when fatal cracks appear in the membrane. Thereafter, due to the enlargement of the cracks and the increased number of cracks, hydrogen crossover rates continuously increased and reached 256.2 $mAcm^{-2}$ after 19,000 RH cycles, which are far beyond the membrane failure threshold of 15 $mAcm^{-2}$. After 19,500 RH cycles, the author was unable to

measure the crossover rate using the LSV technique because the responded current was too high and exceeded the measured limitation of the BioLogic Science Instruments SP300.

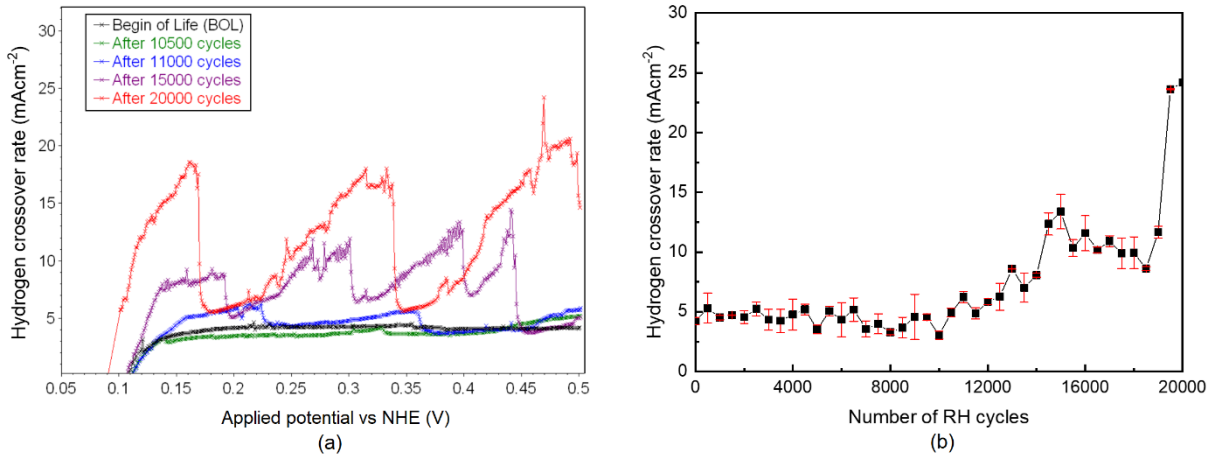

Fig. 2. 7. The (a) LSV and (b) variation of hydrogen crossover rate after the different numbers of RH cycles at atmospheric pressure.

Noticeably, the cyclic change of CVs in the LSV in Figs. 2.7a and 2.8a occurred after 10,500 RH cycles to the end of the durability test. This is an important signal indicating the formation of the fatal cracks in the membrane. However, it is more challenging to accurately obtain the hydrogen crossover rate due to the CVs' strong fluctuations.

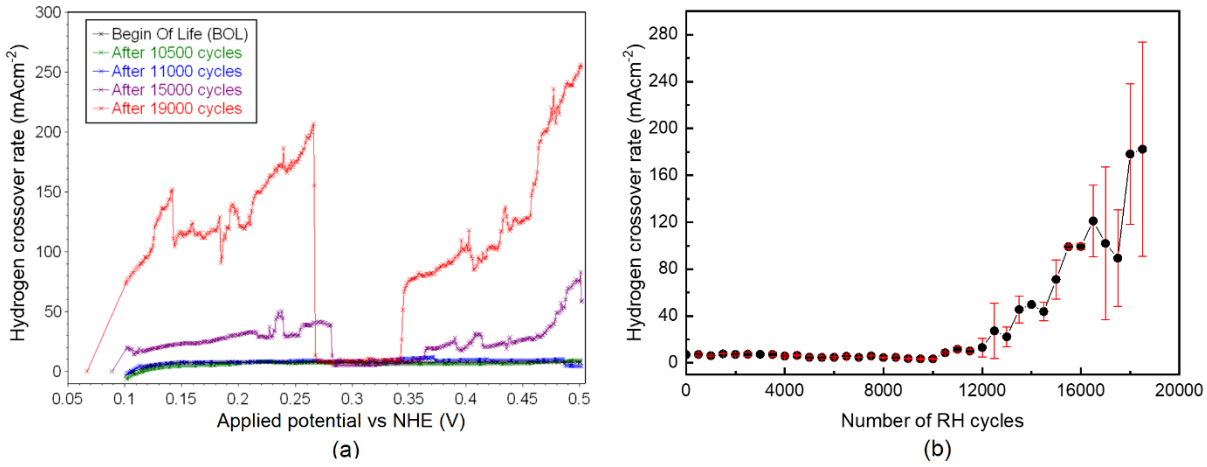

Fig.2. 8. The (a) LSV and (b) variation of hydrogen crossover rate after different number of RH cycles at 50-kPa anode backpressure.

The water blockage in the flow channel and its drainage can explain the significant increase and large fluctuation of crossover current shown in the LSV curves (Figs. 2.7a and 2.8a). During measuring hydrogen crossover, the water vapor in the hydrogen and nitrogen streams condenses and gradually blocks the channels of the flow fields and the drainage. As a result, the temporary pressure gradient formed at both the cathode and anode, as described in Fig. 2.9. The short-lived pressure rise disappears when water droplets

in the channel of flow fields and in the drainage are rejected to the condensers (Fig.2.1). When the pressure is increased only at the anode side (see Fig. 2.9a, c), there will be a pressure difference between the anode and the cathode, causing an increase in hydrogen mole fraction at the anode, thus increasing the crossover rate according to Fick's law of diffusion. Prior to 10,500 cycles, the membrane may be crack/pinhole free. Thus, the crossover rate depends mainly on the gas diffusion mechanism, with the diffusion coefficient through the Nafion membrane in the order of 10^{-6} cm^2s^{-1} [1]. Meanwhile, the convective gas diffusion had a marginal effect, even though there was a pressure gradient between the anode and cathode. Conversely, the effect of temporary pressure build-up is much more tremendous, because the hydrogen crossover is dominated by the convective mechanism with the appearance of pinholes or cracks on the membrane after 10,500 cycles (875 h of testing). According to Vengatesan et.al [16], they also observed an abrupt increase in crossover rate after the membrane subjecting to 350 h of the RH cycling test due to the formation of fatal defects in the membrane [17]. This explains the gradual increase of the hydrogen oxidized current in the voltammogram (see Fig. 2.8b). Right after pressure rise is released at the anode and alternatively, the pressure built up at the cathode (see Figs. 2.9b, d), the oxidized current drops. The gradual pressure increase caused by water blockage in the channels of the anode flow field and its drainage created a resonant effect with the anode backpressure that led to the magnificent variation of hydrogen oxidized current, as shown in Fig.2.8a.

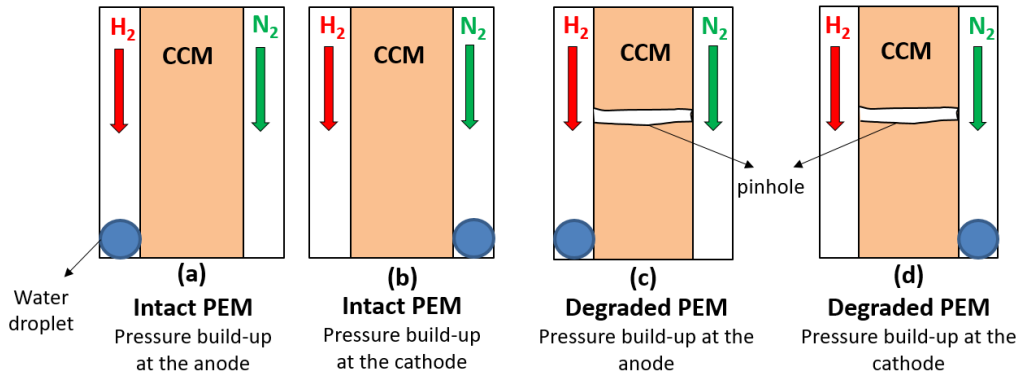

Fig. 2. 9. The schematic illustration for the pressure build-up due to water condensation. PEM is the NRE211 membrane.

2.3.3. The evolution of ECSA

Fig.2.10a displays the cyclic voltammograms (CVs) of the CCM during the durability test. Coincidently, the detected current curve starts shifting in the CVs after 10,500 cycles due to an appreciable increase of hydrogen through the membrane. This indicates that the membrane has deteriorated, and the appearance of cracks or pinholes [16]. The shift of the CVs consolidates the above-aforementioned explanation about the cyclic, sudden increase of hydrogen crossing through the deteriorated membrane. In particular, the hydrogen crossover rate through the membrane follows its permeability when the membrane is intact (or at the BOL). In the CV measurement in this situation, a small amount of hydrogen gas crossing

through the membrane to the cathode is absorbed on the platinum particles in the cathode catalyst layer, and the hydrogen is oxidized and reduced repeatedly during the CV measurements. However, the hydrogen crossover rate increases when the membrane is degraded by catastrophic defects such as cracks or pinholes. In the CV measurement with a large hydrogen crossover rate, the electrochemical hydrogen pumping current increased when the potential at the cathode was swept to a high value. The electrochemical hydrogen-pumping current corresponds to the upper shift of the CV curve. It is obvious that the current curves continue to move upward to the end of the durability test after 11,000 cycles, suggesting a more serious deterioration of the membrane. Conventionally, CV technique is used to evaluate the catalytic activity of the catalyst layer, in the study, the morphological change of the CVs (the shift of CVs) also contributes to the diagnosis of the membrane integrity during the durability test.

Figure 2.10b depicts the evolution of the cathode's ECSA, which is derived from the CVs, after a variety of RH cycles. The ECSA decreases and fluctuates marginally from the BOL up to 14,000 cycles. The slight reduction of the ECSA is caused by Pt particle agglomeration and Ostwald ripening induced, respectively, by carbon oxidation (during OCV measurements) and the variation of the cathode's potential (during electromechanical measurements). However, Ostwald ripening appears to be dominant because the electrochemical (LSV and CV) measurements' duration is much longer than the OCV measurements. After 15,000 RH cycles to the end of the durability test, the ECSA dropped sharply due to the delamination between the electrodes and the membrane induced by the RH cycling condition. The same findings have also been reported by Vengatesan et al. [16] and Uribe [18]. In particular, the hygral coefficient of the membrane is much higher than that of the catalyst layers. Therefore, after a specific number of RH cycles, delamination of the membrane/catalyst interfaces occurs. The separation between the membrane and the catalyst layers increases the ohmic resistance, resulting in the reduction of the ECSA [19]. On the other hand, the significant reduction in ECSA does not relate to the catalyst degradation but the mechanical degradation of the CCM induced by the RH cycling test.

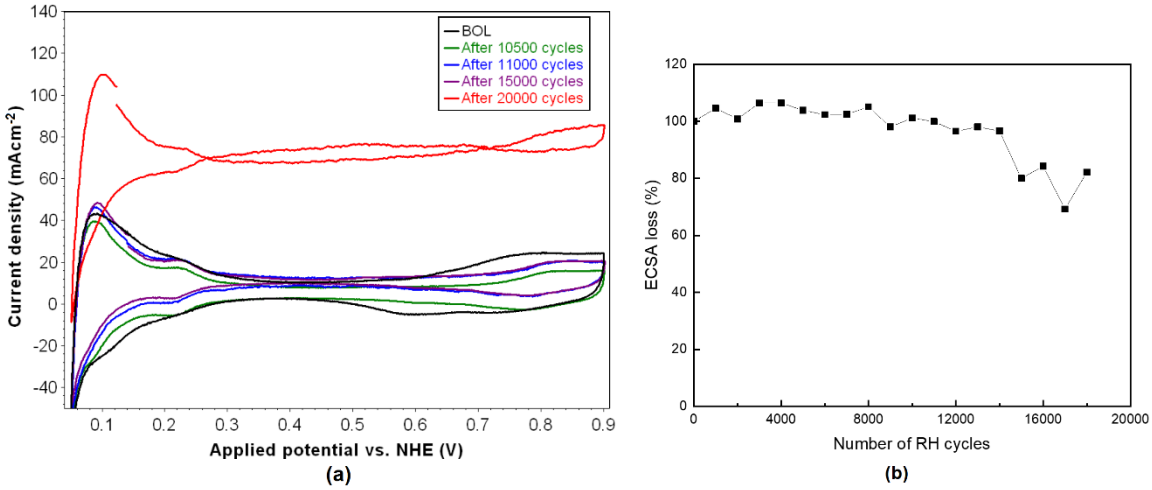

Fig. 2. 10. (a) Cyclic voltammograms of the CCM, and (b) ECSA loss after the different numbers of RH cycles.

2.3.4. The correlation between OCV decay rate and the hydrogen crossover rate

As shown in Fig. 2.11, the measured OCV at the BOL is 0.948 V, which deviates approximately 18.3% from the theoretical value of 1.16 V (computed via Nernst equation (2.4) [20] at 80 °C and atmospheric pressure). This deviation is mainly due to the crossover of hydrogen from the anode to the cathode.

$$V_0 = 1.229 - 8.46\times10^{-4}(T-298) + \frac{RT}{4F}\ln p_{H_2}^2 p_{O_2} \qquad (2.4)$$

where the temperature T =353 K (80 °C); p_{H_2} and p_{O_2} are the partial pressure of hydrogen gas and oxygen gas at the anode and cathode, respectively; R is the universal gas constant; F is Faraday's constant. Furthermore, it can be seen that the OCV decreased with increasing RH cycles which is reversed with the increase of hydrogen crossover rate. That is why OCV also has been widely considered as an important indicator for checking membrane health [21-23]. More specifically, OCV dropped slightly from 0.94 V at the BOL to 0.92 V until 12,500 cycles. Afterward, the OCV dropped significantly from 0.92 V to the minimum value of 0.87 V after 16,000 cycles. Therefore, once again after 12,500 cycles is a milestone indicating the failure of the membrane. Furthermore, after membrane failure, the OCV has a strong fluctuation, which is possibly due to the variation of the hydrogen crossover rate as indicated in Section 2.3.2 and the cathode degradation as shown in Fig. 2.10.

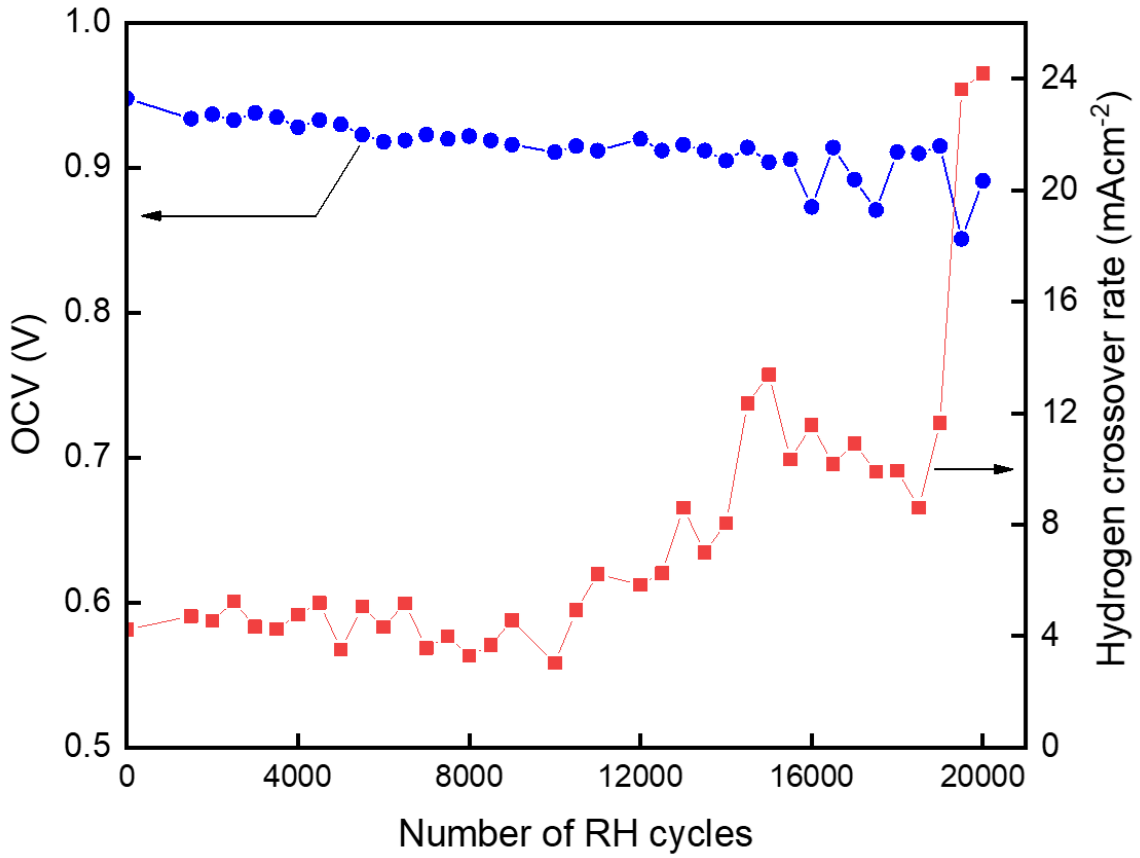

Fig. 2. 11. The correlation between OCV decay and the hydrogen crossover rate during the durability test at atmospheric pressure and the cell temperature of 80 °C.

Despite the fact that the hydrogen crossing rate, which is determined using the LSV method, is a powerful and reliable indicator of the health of the membrane, using nitrogen gas at the cathode for electrochemical measurement appears to be challenging to carry out in actual vehicle operation. Checking OCV is more practical in the interim. As a result, a lot of effort has been devoted to establishing a link between OCV and the hydrogen crossover rate in PEMFCs. From this point of view, the author made an effort to convert the OCV decay to the hydrogen crossover rate through a degraded membrane in this study. The measured OCV departs from the theoretical value (V_0) due to the anode ($\eta_{A,X}$) and cathode ($\eta_{C,X}$) activation overpotentials, as well as the other potentials (η_{others}) by the Pt/PtO anode reaction, carbon-support corrosion, and fuel impurities. Hence, the measured OCV can be predicted using Eq. (2.5).

$$OCV_{measured} = V_0 - \eta_{C,X} - \eta_{A,X} - \eta_{others} \quad (2.5)$$

S.A. Vilekar et al. [7] have proposed a model presented by Eq. (2.6) based on the Butler-Volmer equation that indicates the cathode overpotential caused by hydrogen crossover ($i_{H_2,Ca}$) and electrical short-circuit (i_{SM}) currents.

$$\eta_{C,X} = \left(\frac{RT}{\dot{\alpha}_{ORR}\dot{v}_{ORR}F}\right)\sinh^{-1}\left\{\frac{i_{H_2,Ca} + i_{SM}}{2i_{ORR,0}}\right\} \quad (2.6)$$

where $i_{ORR,0}$ is the oxygen reduction reaction (ORR) exchange current density, which is calculated as below

$$i_{ORR,0} = \gamma_{M,C}\left(\frac{p_{O_2}}{p_{O_2,ref}}\right)\exp\left\{-\frac{E_{\Phi_0}}{R}\left(\frac{1}{T} - \frac{1}{T_{ref}}\right)\right\} i^*_{0,ref} \quad (2.7)$$

where $\gamma_{M,C}$ is the roughness factor of the cathode's catalyst which is extracted from the ECSA data in section 2.3.3; $i^*_{0,ref}$ is the exchange current density at reference condition; $E_{\Phi_{0,ORR}}$ is the activation energy for Pt/C at the cathode (Oxygen reduction reaction); R is the universal gas constant. p_{O_2} and $p_{O_2,ref}$ are the partial pressure of oxygen at 80 °C and at the reference temperature, respectively. In the RH cycling test using N_2, because catalyst degradation can be negligible, $i_{ORR,0}$ is assumed to be constant. This assumption was confirmed to be reasonable because the catalyst thickness in the SEM images of the degraded CCM in Section 2.3.5 did not change. Furthermore, as stated in Section 2.3.3, the mechanical degradation of the CCM caused by the RH cycling test caused only a 30% drop in ECSA compared to the BOL value in Fig. 2.10b after 15,000 RH cycles. The electrical short-circuit (i_{SM}) current at OCV condition is calculated using Eq. (2.8)

$$i_{SM} \approx V_0 \frac{\sigma_{M,e^-}}{L_M} \quad (2.8)$$

At the BOL, the membrane is still intact, the hydrogen crossover current corresponding to the flux of hydrogen crossing through the membrane can be calculated using Fick's law as follow:

$$i_{H_2,BOL} = \frac{(Fv_{HOR,e^-})k_{H_2}}{L_M}\left(p_{H_2,0} - p_{H_2,Ca}\right) \approx \frac{(Fv_{HOR,e^-})k_{H_2}p_{H_2,0}}{L_M} \quad (2.9)$$

where v_{HOR,e^-} is the electron transfer number in the rate-determining-step for anodic hydrogen oxidation reaction; F is Faraday's constant; $k_{H_2}$is hydrogen permeability; $p_{H_2,0}$ and $p_{H_2,Ca}$ are the hydrogen partial

pressure at the anode and cathode compartments, respectively. With the assumption that hydrogen crossing through the membrane is completely oxidized at the cathode's electrode, or $p_{H_2,Ca} \approx 0$.

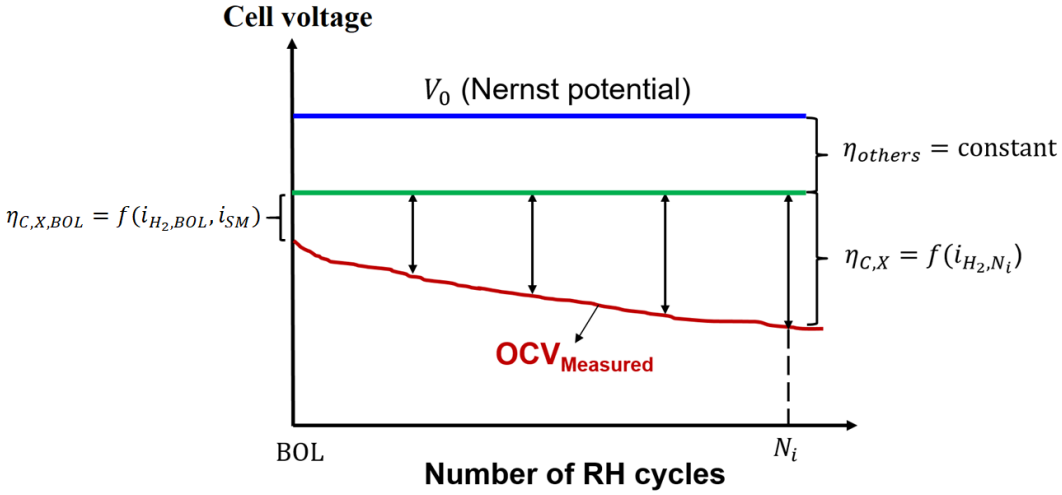

Fig. 2. 12. A proposed approach for predicting the hydrogen crossover rate based on OCV data.

As shown in Fig. 2.12, an approach was proposed to convert the OCV decay to the hydrogen crossover rate during the durability test. The η_{others} in this figure only has an impact on fresh cells and can be supposed to remain constant during the RH cycling test; that can be extracted by using Eq. (2.10) at the BOL. The η_{others} can be estimated by combining Eqs. (2.4–2.9).

$$\eta_{others} = \eta_{others,\,BOL} = V_0 - OCV_{measured,BOL} - \eta_{A,X,\,BOL} = V_0 - OCV_{measured,BOL} - \frac{RT}{\dot{\alpha}_{ORR}\dot{v}_{ORR}F}\sinh^{-1}\left\{\frac{(Fv_{HOR,e^-})k_{H_2}p_{H_2,0} + V_0\sigma_{M,e^-}}{2L_M i_{ORR,0}}\right\} \quad (2.10)$$

In addition, the anode activation overpotential was also confirmed to have a minor contribution to the reduction of OCV [7]. Thus, in the durability test, the overpotential caused by H_2 crossover is primarily responsible for the drop of OCV from the theoretical value in Eq. (2.4). In particular, the hydrogen crossover rate (i_{H_2,N_i}) after any number of RH cycles (N_i) can be predicted based on the measured OCV ($OCV_{measured,\,N_i}$) and $\eta_{others,\,BOL}$ using Eq. (2.11) as follows:

$$V_0 - \eta_{others,\,BOL} - OCV_{measured,\,N_i} = \left(\frac{RT}{\dot{\alpha}_{ORR}\dot{v}_{ORR}F}\right)\sinh^{-1}\left\{\frac{i_{H_2,N_i}}{2i_{ORR,0}}\right\} \quad (2.11)$$

A specific form for estimating the hydrogen crossover current density during the durability was devised by rearranging Eq. (2.11) as follows:

$$\sinh^{-1}\left\{\frac{i_{H_2,N_i}}{2i_{ORR,0}}\right\} = \frac{\dot{\alpha}_{ORR}\dot{v}_{ORR}F}{RT}\left(V_0 - \eta_{others,\,BOL} - OCV_{measured,\,N_i}\right)$$

And, all of the parameters used for calculation are shown in Table 2.2.

Table 2. 2. Calculated parameters

Parameter	Symbol	Value	Unit
Activation energy for Pt/C at the cathode (Oxygen reduction reaction) [24]	$E_{\Phi_{0,}\mathrm{ORR}}$	67	$kJmol^{-1}$
Exchange current density at reference condition [25]	$i^{*}_{0,\mathrm{ref}}$	1×10^{-10}	Acm^{-2}
Roughness factor (Measured at the BOL in the current study)	$\gamma_{\mathrm{M,C}}$	183	$cm^{2}_{Pt}cm^{-2}_{Geo}$
Partial pressure of oxygen at the cathode side (Dry air)	$p_{\mathrm{O_2},0}$	21	kPa
Partial pressure of oxygen at the cathode side at reference condition	$p_{\mathrm{O_2,ref}}$	21	kPa
Partial pressure of hydrogen at the anode side at 80 °C and 100%RH	$p_{\mathrm{H_2},0}$	53.6	kPa
Cell temperature	T_{cell}	353	K
Reference temperature	T_{ref}	293	K
Hydrogen permeability [26]	$k_{\mathrm{H_2}}$	5.1×10^{-13}	$molkPa^{-1}cm^{-1}s^{-1}$
Charge transfer coefficient [27]	$\dot{\alpha}_{\mathrm{ORR}}$	0.593	-
The electron transfer number in the rate-determining-step for the cathodic O_2 reduction reaction [28]	$\dot{\nu}_{\mathrm{ORR}}$	2	-
Faraday's constant	F	96485	$Cmol^{-1}$
The electron transfer number in the rate-determining-step for anodic H_2 oxidation reaction [28]	$\nu_{\mathrm{HOR,e-}}$	2	-

The electronic conductivity of the membrane [1]	σ_{M,e^-}	10^{-6}	Scm^{-1}
Membrane thickness	L_M	0.0025	cm

It can be seen in Fig. 2.13 that the hydrogen crossover rate from the model proposed above shows a quantitative agreement with experimental results. This indicates that the hydrogen crossover is mostly responsible for the OCV drop in the degraded membrane. In addition, the model can predict membrane failure after 12,500 RH cycles in the same way that the LSV technique can. Therefore, the existing model proposed by S.A. Vilekar et al. [7] combined with the author's approach can be a reliable tool to diagnose membrane integrity based on the practical parameter, the OCV. However, there is a slight overestimation of the current model with experimental results in the range of 5,500 to 11,000 RH cycles in the durability test. Noticeably, the model overestimated the hydrogen crossover rate corresponding to the drastic drop of OCV after 16000, 17000, 17500 and 19500 RH cycles. The author doesn't have a clear answer for the deviations because the decrease in OCV can derive from other reasons, like an ECSA drop, for instance. Therefore, further study is necessary to confirm the validity of the current model in predicting the hydrogen crossover rate based on the OCV data. Finally, the current model is applicable when the catalyst degradation is minor. If the cell experiences a durability test that can lead to serious catalyst degradation (the voltage cycle test, for instance), the oxygen reduction reaction (ORR) exchange current density $i_{ORR,0}$ in Eq. (2.7) must be modified.

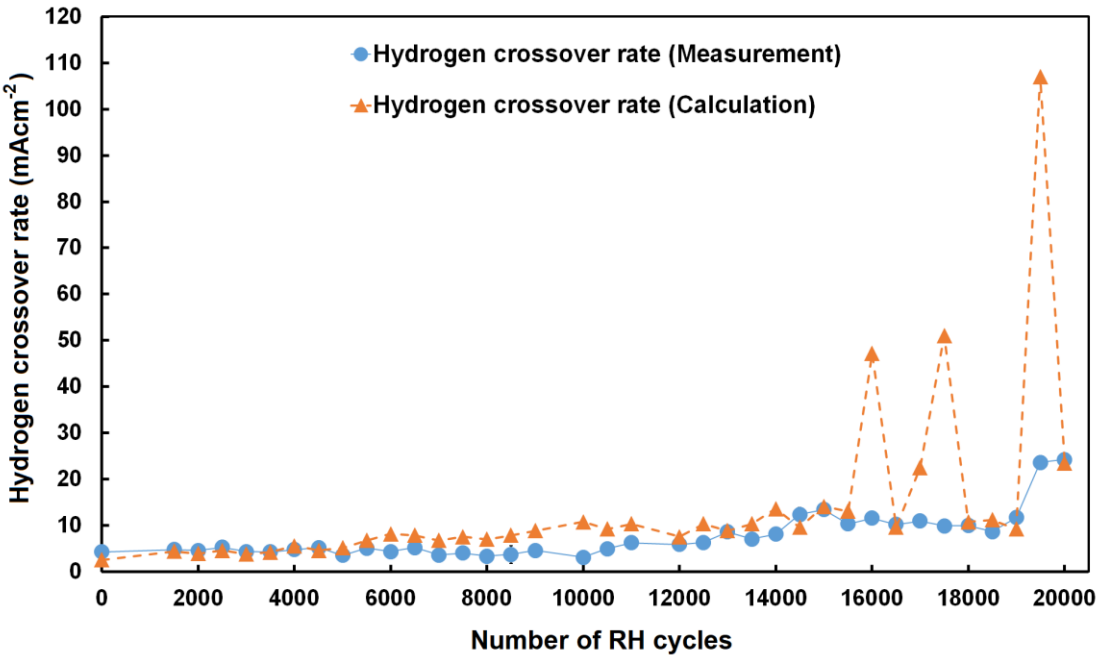

Fig. 2. 13. The hydrogen crossover rate comparison between calculation and measurement.

2.3.5. Postmortem morphological analysis

The changes in the degraded CCM's morphology have been investigated using FIB-SEM after finishing 20,000 RH cycles. In order to identify the occurrence of the cracks and their distribution in the degraded CCM, the author cut three samples located at the inlet regions (anode and cathode) and in the middle of the degraded CCM. Each sample has dimensions of 10 mm in length and 3 mm in width. Fig. 2.14 illustrates the positions of samples which are cut from the degraded CCM. Degraded SEM images from the degraded samples compared with the CCM morphology at the BOL as shown in Fig. 2.15. During the observation, firstly, the SEM will be employed to scan the overall surface of the sample. Then, after addressing the location of cracks, the focused ion beam was applied to obtain the cross-sectional images of the selected positions.

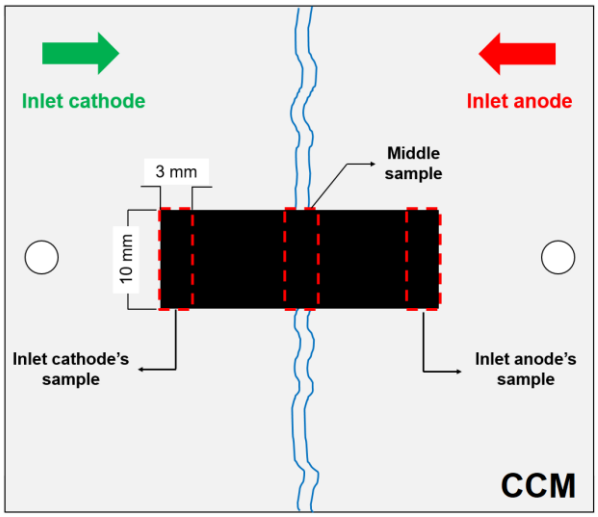

Fig. 2. 14. Three samples from the degraded CCM were cut and investigated with FIB-SEM.

The SEM images displayed in Figs. 2.16a, 2.17a, and 2.18 show that cracks formed in the three examined positions of the CCM as a result of the mechanical stress induced by the current RH cycling test. In more detail, cracks have a variety of sizes, grow perpendicularly to the applied in-plane stress direction, and distribute mainly at the inlets of the cell and on the edges of the channels and the land, as displayed in Figs. 2.16 and 2.17. According to the stress calculation in Section 2.3.1, mechanical stress depends predominantly on the magnitude of the membrane water content oscillation. Owing to the co-current serpentine pattern of the flow fields, the membrane experiences a significant change in water content at the inlets of the CCM compared to the middle part during the RH cycling test. Thus, the membrane endures a higher stress range at these locations, enabling the formation and propagation of cracks throughout the membrane.

Moreover, the edges in the channels and the land (or ribs) tend to have cracks. Because the water content variation of the membrane under land is much narrower than that under the channel regions during the RH cycling test due to the limitation of water transportation, the in-plane tensile stress in the channel regions is expected to have a higher amplitude. The in-plane stress formed in the channel regions is interrupted near the land edge. As a result, the stress concentration in the membrane under the edge between the channel and land is particularly high in comparison to that under the channel and land [29], facilitating the formation and development of cracks.

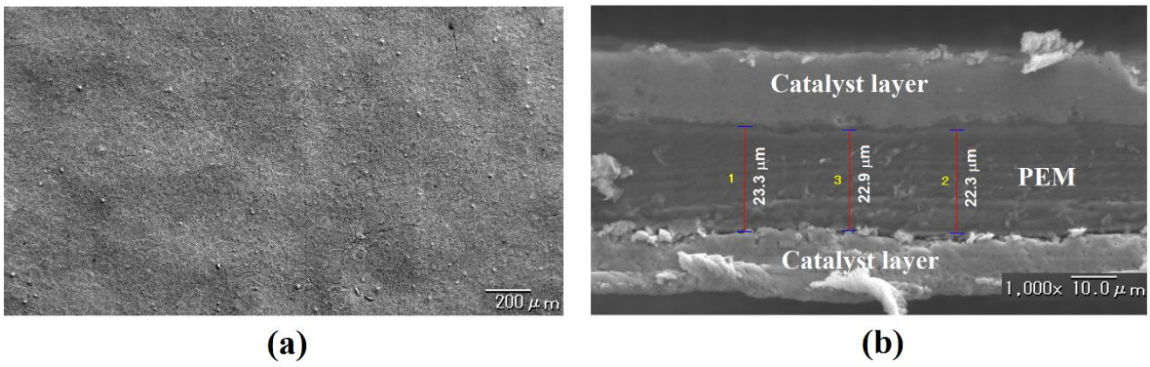

Fig. 2. 15. (a) surface and (b) a cross-section of the fresh CCM. PEM is the Nafion NRE211 membrane.

Based on the cross-sectional images in Fig. 2.16b and Fig. 2.18b, the cracks that have been found in the inlet cathode's sample and in the middle sample, respectively, have propagated through the membrane, thus creating a micro gas leak in the CCM. Therefore, the hydrogen crossover rate increased dramatically. The appearance of these cracks validated the hypothesis of the sudden and cyclic change of the oxidized current during measuring the hydrogen crossover rate that was aforementioned in section 2.3.2. In contrast, no membrane-through crack has been found among these cracks in the inlet anode's sample, as shown in Fig. 2.17. That means the cracks have just initiated on the surface of the anode catalyst, yet have might not propagated deep through enough of the membrane to form the micro-gas leaked paths. Because the stress amplitude at the inlet anode's sample could be smaller than that at the inlet cathode's sample, cracks take a longer time to propagate through the membrane thickness.

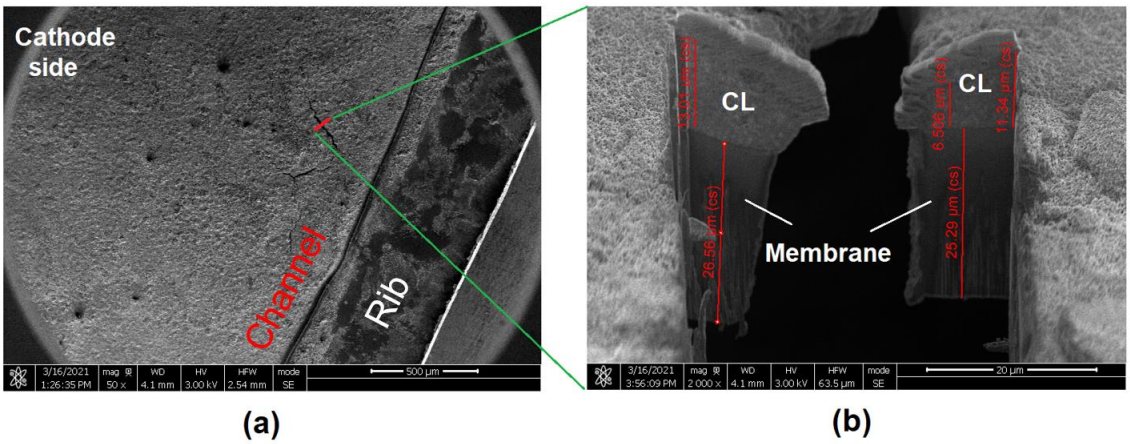

Fig. 2. 16. SEM images of the surface (a) and cross-section of a crack (b) in the inlet cathode sample which were observed from the cathode side. CL is the catalyst layer.

In addition, according to the cross-sectional SEM images in Figs. 2.16b and 2.18b, the membrane thickness does not change in comparison with the fresh membrane in Fig. 2.15b, indicating the absence of chemical stress on the membrane in the current durability test. Moreover, the catalyst thickness remained unchanged, revealing that catalyst degradation is negligible and that the model's assumption regarding the constant value of ECSA is reasonable.

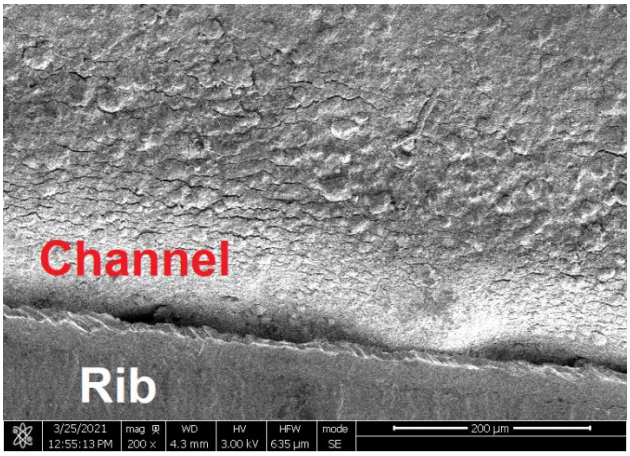

Fig. 2. 17. Cracks distribute in the boundary between the rib and channel of the inlet anode sample which were observed from the anode side.

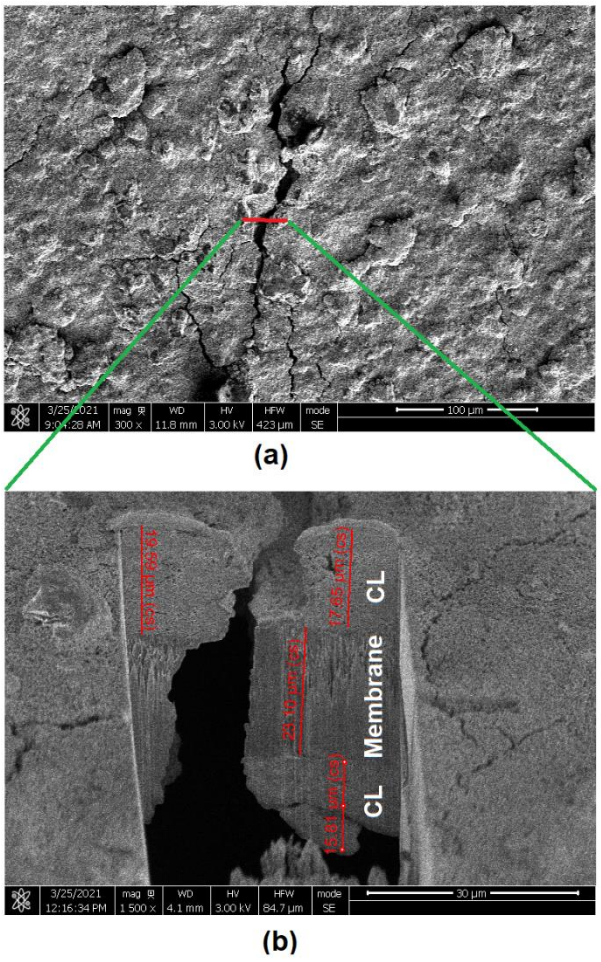

Fig. 2. 18. SEM images of (a) a crack, and (b)a corresponding cross-section from the middle sample which were observed from the cathode side. CL denotes the catalyst layer.

2.4. Conclusions

In this chapter, with an aim to investigate the mechanical durability of the membrane, the author applied the RH cycling test using nitrogen gas to a cell that embedded membrane NRE211. Two indicators including the hydrogen crossover rate and OCV have been used to diagnose the integrity of the membrane subjected to the relative humidity cycling test. These electrochemical measurements at every 500 RH cycles and the postmortem analysis with SEM-FIB suggest followings:

(1) Both the hydrogen crossover rate and OCV have shown the ability to predict the existence of serious damages e.g., cracks, and tears in the membrane.

(2) Comparing with OCV, the hydrogen crossover is more sensitive and possible to indicate the early occurrence of through-membrane cracks after 10,500 cycles via the sudden and cyclical change of the hydrogen oxidized current on the LSV curves. After 12,500 cycles, the membrane completely failed when the hydrogen crossover rate exceeded the threshold of 15 $mAcm^{-2}$, which is consistent with a precipitous decrease in OCV.

(3) The appearance of the through-membrane cracks has been confirmed in the SEM images of degraded CCM.

(4) In addition, even though the hydrogen crossover is a sensitive and reliable pointer for checking membrane health, OCV is more feasible and realistic in the fuel cell vehicle. In order to combine the advantages of these two methods, an empirical model with a novel approach was applied to clarify the correlation between OCV drop and the hydrogen crossover rate. As a result, the model's prediction agrees quantitatively with the experimental results, indicating that this model can be used as a practical diagnostic tool for checking the integrity of membranes in PEMFC applications, such as FCVs. However, the validation of the current model needs to be consolidated by further study.

2.5. References

1. Matthew M. Mench. 2008. Polymer Electrolyte Fuel Cells. Fuel cell engines, pp. 285-379. John Wiley & Sons, Inc. https://doi.org/10.1002/9780470209769.ch6.

2. Mathias, Mark F., et al. “Two Fuel Cell Cars in Every Garage?” The Electrochemical Society Interface, vol. 14, no. 3, 1 Sept. 2005, pp. 24–35, 10.1149/2.f05053if.

3. Kreitmeier, Stefan, et al. “Investigation of Membrane Degradation in Polymer Electrolyte Fuel Cells Using Local Gas Permeation Analysis.” Journal of Power Sources, vol. 212, Aug. 2012, pp. 139–147, 10.1016/j.jpowsour.2012.03.071.

4. Lakshmanan, Balasubramanian, et al. “Polyetheretherketone Membranes for Elevated Temperature PEMFCs.” Electrochemical and Solid-State Letters, vol. 6, no. 12, 2003, p. A282, 10.1149/1.1619647.

5. A. B. LaConti, M. Hamdan, and R. C. McDonald. “Handbook of Fuel Cells: Fundamentals, Technology, and Applications, Vol. 3.” W. Vielstich, A. Lamm, and H. A. Gasteiger, Editors, Wiley, New York, 2003.

6. Francia, Carlotta, et al. “Estimation of Hydrogen Crossover through Nafion® Membranes in PEMFCs.” Journal of Power Sources, vol. 196, no. 4, Feb. 2011, pp. 1833–1839, 10.1016/j.jpowsour.2010.09.058.

7. Vilekar, Saurabh A., and Ravindra Datta. “The Effect of Hydrogen Crossover on Open-Circuit Voltage in Polymer Electrolyte Membrane Fuel Cells.” Journal of Power Sources, vol. 195, no. 8, Apr. 2010, pp. 2241–2247, 10.1016/j.jpowsour.2009.10.023

8. Inaba, Minoru, et al. “Gas Crossover and Membrane Degradation in Polymer Electrolyte Fuel Cells.” Electrochimica Acta, vol. 51, no. 26, Aug. 2006, pp. 5746–5753, 10.1016/j.electacta.2006.03.008

9. DuPont, Product Information Sheets, 2008. http://www.dupont.com/fuelcells/pdf/extrusion_cast.pdf.

10. ZHANG, S, et al. “A Review of Accelerated Stress Tests of MEA Durability in PEM Fuel Cells.” International Journal of Hydrogen Energy, vol. 34, no. 1, Jan. 2009, pp. 388–404, 10.1016/j.ijhydene.2008.10.012.

11. US Department of Energy, DOE cell component accelerated stress test protocols for PEM fuel cells, (2007). https://www1.eere.energy.gov/hydrogenandfuelcells/fuelcells/pdfs/component_durability_profile.pdf.

12. Lai, Yeh-Hung, et al. “Viscoelastic Stress Analysis of Constrained Proton Exchange Membranes under Humidity Cycling.” Journal of Fuel Cell Science and Technology, vol. 6, no. 2, 20 Feb. 2009, 10.1115/1.2971045.

13. Kusoglu, Ahmet, et al. “Aspects of Fatigue Failure Mechanisms in Polymer Fuel Cell Membranes.” Journal of Polymer Science Part B: Polymer Physics, vol. 49, no. 21, 17 Aug. 2011, pp. 1506–1517, 10.1002/polb.22336.

14. Kusoglu, Ahmet, and Adam Z. Weber. “New Insights into Perfluorinated Sulfonic-Acid Ionomers.” Chemical Reviews, vol. 117, no. 3, 23 Jan. 2017, pp. 987–1104, 10.1021/acs.chemrev.6b00159.

15. Kai, Yusuke, et al. “Crack Formation on Membrane Electrode Assembly (MEA) under Static and Cyclic Loadings.” ASME 2012 10th International Conference on Fuel Cell Science, Engineering and Technology, 23 July 2012, 10.1115/fuelcell2012-91164.

16. Vengatesan, S., et al. “Diagnosis of MEA Degradation under Accelerated Relative Humidity Cycling.” Journal of Power Sources, vol. 196, no. 11, June 2011, pp. 5045–5052, 10.1016/j.jpowsour.2011.01.088.

17. Kreitmeier, Stefan, et al. “Investigation of Membrane Degradation in Polymer Electrolyte Fuel Cells Using Local Gas Permeation Analysis.” Journal of Power Sources, vol. 212, Aug. 2012, pp. 139–147, 10.1016/j.jpowsour.2012.03.071.

18. Uribe, Francisco A., et al. “A Microelectrode Study of Oxygen Reduction at the Platinum/Recast-Nafion Film Interface.” Journal of the Electrochemical Society, vol. 139, no. 3, 1 Mar. 1992, pp. 765–773, 10.1149/1.2069299.

19. Kang, Jungtak, and Junbom Kim. “Membrane Electrode Assembly Degradation by Dry/Wet Gas on a PEM Fuel Cell.” International Journal of Hydrogen Energy, vol. 35, no. 23, Dec. 2010, pp. 13125–13130, 10.1016/j.ijhydene.2010.04.077.

20. Bernardi, Dawn M., and Mark W. Verbrugge. “A Mathematical Model of the Solid-Polymer-Electrolyte Fuel Cell.” Journal of the Electrochemical Society, vol. 139, no. 9, 1 Sept. 1992, pp. 2477–2491, 10.1149/1.2221251.

21. Sompalli, Bhaskar, et al. “Membrane Degradation at Catalyst Layer Edges in PEMFC MEAs.” Journal of the Electrochemical Society, vol. 154, no. 12, 2007, p. B1349, 10.1149/1.2789791.

22. Lü, Weizhong, et al. “The Effects of Pinholes on Proton Exchange Membrane Fuel Cell Performance.” International Journal of Energy Research, vol. 35, no. 1, 28 Dec. 2010, pp. 24–30, 10.1002/er.1728.

23. Spinelli, P., et al. “Semi-Empirical Evaluation of PEMFC Electro-Catalytic Activity.” Journal of Power Sources, vol. 178, no. 2, Apr. 2008, pp. 517–524, 10.1016/j.jpowsour.2007.10.040

24. Neyerlin, K. C., et al. “Determination of Catalyst Unique Parameters for the Oxygen Reduction Reaction in a PEMFC.” Journal of the Electrochemical Society, vol. 153, no. 10, 2006, p. A1955, 10.1149/1.2266294.

25. C. Song, J. Zhang, in: J. Zhang (Ed.), PEM Fuel Cell Electrocatalysts and Catalyst Layers, Springer, New York, NY, 2008.

26. Kocha, Shyam S., et al. “Characterization of Gas Crossover and Its Implications in PEM Fuel Cells.” AIChE Journal, vol. 52, no. 5, 2006, pp. 1916–1925, 10.1002/aic.10780.

27. Damjanovic, A. “Temperature Dependence of Symmetry Factors and the Significance of Experimental Activation Energies.” Journal of Electroanalytical Chemistry, vol. 355, no. 1-2, Aug. 1993, pp. 57–77, 10.1016/0022-0728(93)80354-k.

28. Song, Chaojie, et al. “PEM Fuel Cell Reaction Kinetics in the Temperature Range of 23–120°C.” Electrochimica Acta, vol. 52, no. 7, Feb. 2007, pp. 2552–2561, 10.1016/j.electacta.2006.09.008.

29. Khorasany, R.M.H., et al. “In-Situ Simulation of Membrane Fatigue in Polymer Electrolyte Fuel Cells.” International Journal of Hydrogen Energy, vol. 42, no. 16, Apr. 2017, pp. 11838–11844, 10.1016/j.ijhydene.2017.01.173.

Chapter 3

Investigation of in-situ catalytic combustion in PEMFCs during a combined chemical and mechanical stress test

Abstract

This chapter 3 is focused on elucidating the catalytic combustion phenomenon in proton- exchange membrane fuel cells. A visualization cell and an infrared (IR) camera are used to capture the thermal behavior in situ under combined chemical and mechanical accelerated stress conditions. A catalyst-coated membrane (CCM) embedded in the cell is subjected to a relative humidity (RH) cycling test under the open-circuit voltage (OCV) condition. In the current durability test, hydrogen gas and air are fed into the anode and cathode compartments, respectively, which differ from the durability test in Chapter 2, where nitrogen gas is supplied into both sides of the cell. Whereas, operation pressure and cell temperature in Chapter 3 are same with those in Chapter 2 (atmospheric pressure and 80 ℃). The temperature distribution on the gas diffusion layer surface at the cathode is captured through a high-transmittance glass window (ZnS window). Continuous IR imaging revealed a hot spot at ca. 1,600 RH cycles, suggesting the existence of pinholes and cracks in the degraded CCM and the occurrence of catalytic combustion there. The occurrence of the hot spot coincides with the time at which the electrochemical indicators (i.e., hydrogen crossover rate and OCV) detect membrane failure. Furthermore, a post-mortem analysis revealed several pinholes, the position of which matched that of the hot spot. These pinholes are responsible for the rapid increase in the hydrogen crossover rate as well as the significant decrease in the OCV at 1,600 RH cycles until the end of the durability test. A one-dimensional heat transfer model has been developed to predict the temperature rise of the cathode's GDL induced by combustion. The model estimates fairly well the change in GDL temperature according to the hydrogen crossover rate, thus being able to track the transition of the combustion process from a moderate to accidental scale of combustion. Additionally, according to this model, the membrane decomposes thermally during the durability test when the combustion heat flux exceeds the maximum dissipated heat flux of the cell (approximately 2.0 Wcm^{-2}).

3.1. Introduction

Hydrogen fuel cell vehicles (HFCVs) are a promising substitute for internal combustion engine vehicles (ICEVs) in the near future owing to their advantages, such as high energy conversion efficiency, no harmful gas emission during operation, and sustainability. Although HFCVs have been commercialized by several automakers, the number of HFCVs manufactured is far behind that of ICEVs. In 2020, there were only 25,926 light-passenger fuel-cell cars in stock [1]. In addition to the lack of hydrogen refueling stations, the production costs and longevity of the fuel cell stack are the two main obstacles to the popularity of HFCVs. In order to replace traditional vehicles, HFCVs must satisfy certain price (30–40 $\$kW^{-1}$) and lifespan targets (5,000 h equivalent to 150,000 miles of driving by 2020, and the ultimate goal is 8,000 h) [2].

Perfluorinated sulfonic acid (PFSA) membranes, which have been widely used in fuel cell vehicles, must be super thin to satisfy the power density demand. The trend of membrane development is to reduce their thickness to reduce costs and increase the power density while ensuring a durability target [3]. Therefore, improving the membrane durability is one of the top priorities for proton-exchange-membrane fuel-cell (PEMFC) vehicles.

Under the actual operating conditions of fuel cell vehicles, the membrane suffers under various harsh conditions, such as load variation, start/shutdown cycles, sub-zero- temperature start-up, and idling conditions at a high open-circuit voltage (OCV). Detrimental effects due to the above conditions over time result in the performance loss of the vehicle as well as shorten the durability of the components in the fuel cell assembly in general and especially the electrolyte membrane. The factors affecting the durability of the membrane can be widely divided into two main mechanisms: chemical and mechanical degradation.

Chemical degradation is the main cause of membrane thinning and pinhole formation. Reactive chemical species, including •OH and •OOH [4,5], and carbon radicals (–COOH) [6] chemically attack and decompose PFSA membranes [7,8]. A high operating temperature and pressure and low humidity can intensify the chemical membrane degradation [9]. To investigate the chemical stability of membranes, Fenton's test is widely applied as ex-situ accelerated stress test [10-13], while holding PEMFCs under OCV conditions is an in situ chemical durability test [14-16]. Under OCV conditions, the concentration gradients of the reactant gases are the highest, thus resulting in a large amount of fuel and air crossing through the membrane, which facilitates the generation of hydrogen peroxide (H_2O_2) at both electrodes via the two-electron oxygen reduction reaction ($O_2 + 2H^+ + 2e^- \rightarrow H_2O_2$, $E_0 = 0.695$ V versus standard hydrogen electrode (75 °C)). Although H_2O_2 is a weak oxidizer, it promotes the formation of stronger free radicals, i.e., •OH and •OOH [5, 17], in the presence of metal cations (Fe^{2+} or Fe^{3+} and Cu^{2+}), thus resulting in the decomposition of the membrane. This is an example of how chemical degradation begins and occurs. Furthermore, the high voltage at the OCV results in the dissolution of platinum particles from the catalyst layers, and the dissolved platinum particles diffuse into the membrane, resulting in the formation of a platinum band. This platinum band could trigger the generation of H_2O_2 [18-20]. Although this is thought to be as the second example of how the chemical

degradation starts, other researchers reported that dispersed platinum particles in the membrane could not only act as radical scavengers [21,22], but also help to decrease gas reactant crossover from one electrode to the other electrode [23], thereby mitigating the formation of H_2O_2 at electrodes, resulting in the suppression of chemical degradation. Thus, the chemical degradation mechanism in the PEMFCs is thought to be rather complicated. This issue will be discussed again in Chapter 4 of this dissertation.

In the case of mechanical membrane degradation, common defects were reported, such as cracks in the membrane and delamination between the membrane and catalyst layers. The dimensional change in the constrained membrane in the fuel cell owing to water content and temperature variations results in the development of residual stresses. However, the impact of the former is more dominant. These stresses behave like fatigue loads and accelerate the deterioration of the membrane over time. The relative humidity (RH) cycling test is the most popular accelerated stress test (AST) that has been applied extensively to investigate the mechanical durability of membranes. In the RH cycling test, inert gases (N_2 or Ar) or air [3,24,25] are fed into both the cathode and anode to eliminate the chemical effect. The mechanical membrane degradation mechanism was investigated in Chapter 2 of this dissertation.

In practical PEMFCs where hydrogen and air are fed to the anode and cathode channels, respectively, hydrogen inevitably crosses through the membrane and causes moderate combustion with oxygen in the air stream owing to the presence of platinum in the cathode catalyst. In the intact membrane, the heat released from moderate combustion is sufficiently dissipated through the gas diffusion layer (GDL) and coolant medium and does not cause any significant increase in cell temperature. Over the long operation period of FCVs, serious defects such as micro-cracks and thinning may appear in the degraded membrane owing to the simultaneous impacts of mechanical and chemical stresses. As a result, the amount of hydrogen crossing through the membrane increases significantly. The higher the hydrogen crossover rate, the greater the amount of heat that is released from combustion. In the worst case or in an accidental combustion, wherein the released heat rate is much higher than the maximum heat dissipation flux of the cell, hot spots are formed, possibly resulting in a pinhole formation in the membrane at these hot spots owing to thermal polymer decomposition [5,26]. The formation of pinholes in the membrane can cause the entire cell stack to collapse, resulting in the instant death of the fuel cell [27]. Thermal polymer decomposition is a dangerous degradation process. However, it is difficult to clarify when, where, and how hydrogen combustion in fuel cells changes from a moderate to an accidental scale. Therefore, measuring and understanding the transient process from a moderate to accidental scale of combustion is extremely important for developing practical tools for diagnosing the cell state and for developing durable membranes.

Till date, few studies have been focused on investigating catalytic combustion in PEMFCs. Lu et al. [28] estimated a 4 °C temperature rise at the center of a 140-μm-diameter artificial pinhole owing to combustion by modelling the thermal behavior in a PEMFC. Kreitmeier et al. [26] employed thermochromic pigments as temperature indicators after perforating a membrane with artificial pinholes. The greatest temperature escalation in the center of a 300-μm-diameter pinhole was approximately

140 °C according to the researchers. The accuracy of the outcome, however, is primarily determined by the size of the color pigments and the relative humidity of the reactant gases. Other researchers using dumb cells have investigated the temperature distribution on damaged membranes obtained from accelerated stress testing. The hotspots in these deteriorated cells reached temperatures of 2.1 °C [29] and 50 °C [30], respectively, which are greater than the working temperature. This difference in the temperature rise could be due to the different degrees of membrane degradation that originated from different experimental conditions. Although several researchers figured out the combustion in PEMFC, they relied on some artificial pinholes and utilized some ex-situ techniques.

The main objective of this chapter is to elucidate the transient process of catalytic combustion from moderate to accidental levels in an in-situ manner. As indicated above, accidental combustion is supposed to occur in the presence of fatal defects in the membrane, such as micro-crack formation and membrane thinning. In this study, the anode RH cycling test is employed under the OCV condition for a single PEMFC with embedded high-transmittance glass (ZnS glass) at the cathode side. This harsh endurance test, which can impose chemical and mechanical stresses on the membrane simultaneously is expected to accelerate the degradation of the membrane and the consequent formation of serious defects. Simultaneously, an infrared (IR) camera captures the temperature distribution on the surface of the cathode GDL at every 200 RH cycles and is expected to detect hot spots due to large-scale combustion. In addition, electrochemical measurements, such as the hydrogen crossover rate and OCV, which indicate the degree of membrane degradation, are also performed. Thus, a correlation between the membrane integrity and temperature change due to catalytic combustion can be obtained. Moreover, a post mortem analysis is also conducted to investigate the morphological changes in the degraded catalyst coated membrane (CCM). Finally, the discussion on the obtained correlation then contributes to elucidating the transient process and proposing diagnostic methods to detect the signs of accidental combustion.

3.2. Experimental

3.2.1. Experimental apparatus and durability testing protocol

Fig. 3.1a presents the flow diagram of the experimental system, which is designed to conduct both accelerated stress tests and periodic electrochemical evaluations for the visualization cell. A rectangular CCM with a 10-mm width and a 34-mm length was formed in the center of the membrane with a platinum loading of 0.5 mg cm^{-2} at both electrodes. The CCM fabrication procedure has been indicated in section 2.2 in Chapter 2. As be seen in Fig. 3.1b, a square window of 52 × 52 mm is perforated in the clamp plate of the cathode. Then, a high-transmissivity glass (ZnS glass) of 40 mm diameter and 2 mm thickness is installed on a composite frame placed between the clamp plate and flow field. This structure allows the IR camera to accurately observe the temperature distribution on the surface of the GDL.

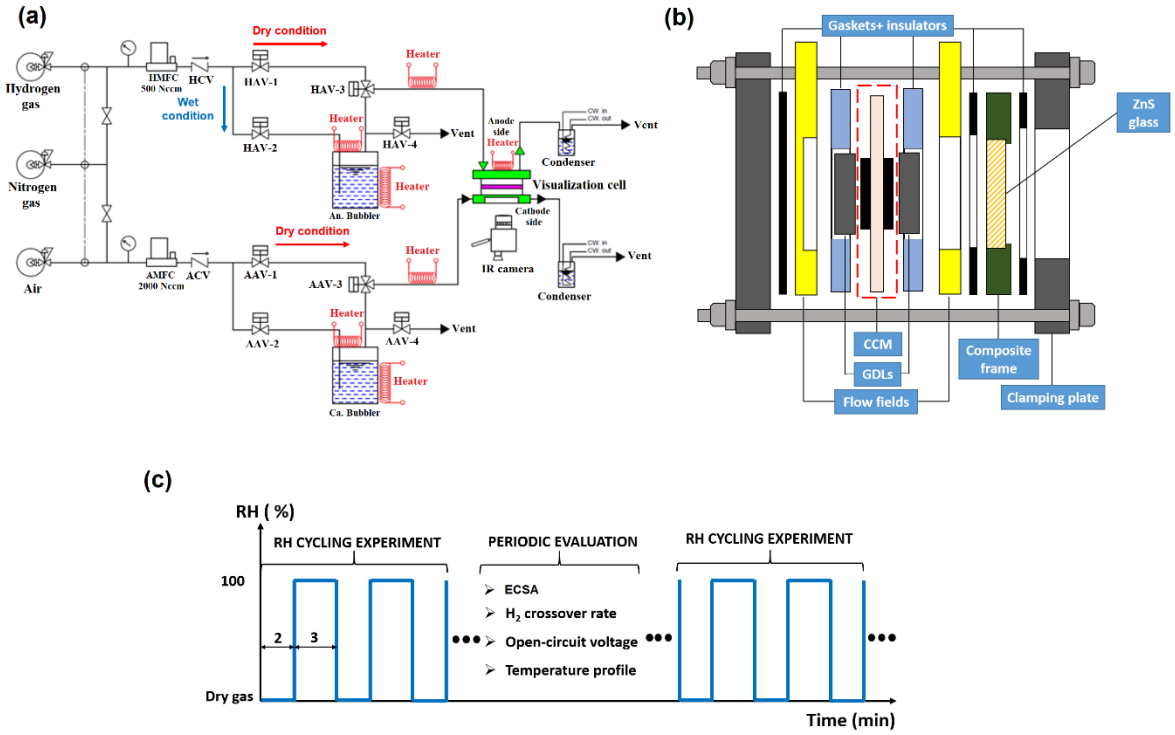

Fig. 3. 1. (a) Experimental apparatus, (b) schematic cross-sectional cell structure, and (c) experimental procedure.

Fig. 3.1c illustrates the durability testing procedure. Prior to the durability test, the cell was incubated with 100% RH nitrogen gas (only on the anode side) for 24 h at a cell temperature (T_{cell}) of 80 °C to ensure that the membrane could be hydrated completely. During the RH cycling test, the cell was maintained under OCV conditions at T_{cell} = 80 °C and at atmospheric pressure. For the anode compartment, hydrogen gas was fed at a flow rate of 200-Nccm (normal cm^3 min^{-1}), and the humidity was alternately changed between the dry (2 min) and wet portions (100% RH in 3 min) by switching three valves (HAV-1, HAV-2, and HAV-3), as shown in Fig. 3.1a. Meanwhile, dry air at a flow rate of 100-Nccm was continuously fed into the cathode compartment. The dry air helps prevent water droplets from attaching to the ZnS glass. Because water absorbs IR rays, the temperature measurement would thus be inaccurate. The membrane resistance and OCV were measured using a high-frequency resistance device (Tsuruga, 3566) and then recorded using a data logger (Graphtec Corporation, GL840) every 1 s during the durability test. The electrochemical active surface area (ECSA), hydrogen crossover rate, and OCV were measured every 200 RH cycles. Besides, the temperature distribution on the surface of the cathode's GDL was captured with an IR camera during OCV measurements to investigate catalytic combustion of the leaked gases.

3.2.2. Details of electrochemical and thermal imaging measurements

In the evaluation period presented in Fig. 3.1c, electrochemical (including the ECSA, hydrogen crossover rate, OCVs) and thermal imaging measurements are conducted. Cyclic voltammetry (CV) and

linear sweep voltammetry (LSV) are performed to measure the cathode's ECSA and hydrogen crossover rate through the membrane, respectively, using a voltammetry system (SP300, BioLogic Science Instruments). The crossover rate and ECSA are the important indicators for evaluating membrane degradation and catalyst decay, correspondingly. A flow rate of 150-Nccm of fully humidified hydrogen is fed into the anode side, which serves as both the counter and reference electrode, and 200-Nccm of dry nitrogen gas is fed into the cathode side, which is operated as the working electrode. The cell temperature is kept at 80°C and nitrogen gas is stopped right before starting CV measurements. Hydrogen desorption area at the cathode electrode is a measure of ECSA. The applied potential ranges from 0.05 V to 0.9 V vs. NHE (Normal Hydrogen Electrode (H_2/H^+) with a scan rate of 50 mVs^{-1}.

Meanwhile, the LSV technique can reveal the hydrogen crossover rate, which is represented in the units of current density. The applied potential is swept from 0.05 to 0.5 V versus NHE, with a scan rate of 0.5 mV s^{-1}. The crossover current density is then obtained at an applied potential of 0.4 V versus NHE, at which the leaked hydrogen gas from the anode is oxidized completely on the cathode's catalyst [5]. When the fatal defects appear in the membrane, the hydrogen crossover rate increases and fluctuates vigorously as confirmed in Chapter 2, and the current density saturation in the potential from 0.4 to 0.5 V corresponds to the crossover current density. The hydrogen crossover rate is measured under two pressure conditions:

(a) Atmospheric pressure for both anode and cathode compartments, and

(b) Application of 20-kPa backpressure only in the anode compartment.

In the following, conditions (a) and (b) are denoted as "atmospheric pressure" and "20-kPa anode backpressure," respectively.

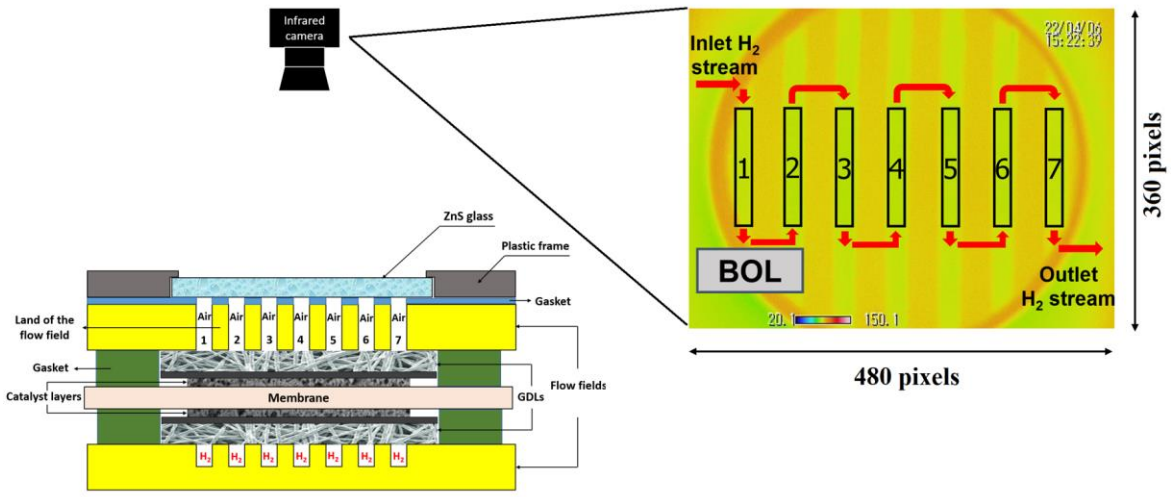

Fig. 3. 2. Schematic figure showing how to capture the cathode's GDL IR images.

Similar to the case of the hydrogen crossover rate, the OCV is measured under the same and differential pressure conditions between the anode and cathode. Although the differential pressure condition, as noted above, comprises a differential pressure of only 20-kPa, it helps to highlight the

existence of severe defects in the membrane, such as pinholes or through-membrane cracks.

Thermographs (IR images) of the GDL surface are captured via an IR camera (NEC Avio, R450) through a high-transmittance glass (ZnS) window embedded at the cathode under the OCV state at T_{cell} = 80 °C, as shown in Fig.3.2. The spectral range of the IR camera is from 8 to 14 μm, and measuring range from -40 to 650 °C with the accuracy of ± 1 °C (when the environment temperature is from 20 to 30 °C). In order to accurately measure the GDL surface temperature, camera emissivity is calibrated according to the cell temperature on the cathode side. It is noted that a thermocouple is embedded in the cathode separator to confirm the cell temperature on the cathode side and to make this calibration. As a result, a substantial emissivity was determined to be 0.68 under the condition that the cell temperature is 80 °C while N_2 was fed to both the cathode and anode sides. Each IR image has a standard size of 480 pixels in width and 360 pixels in height. The (standard) space and time resolution are 330 pixels per inch (PPI) and 5 frames per second (or 5 Hertz), respectively. The GDL temperature was obtained from the IR images by using the InfreC Analyzer (NS9500 standard).

In the postmortem analysis, a scanning electron microscope (Helios Nanolab 600i) is employed to examine the microstructural changes in the degraded CCM. Any specific damage is compared with the hotspots observed in the IR imaging.

3.3. Results and discussion

3.3.1. Membrane degradation evaluation

3.3.1.1. Changes in OCV and membrane resistance during the durability test

Fig. 3.3a presents variations of membrane resistance and OCV during the durability test. The membrane resistance fluctuated repeatedly during the test, ranging from 60 to 196 mΩcm^2, revealing the change in membrane water content indirectly. In-plane stresses will be formed by the repeated dimensional change in the constrained membrane as the water content changes. These stresses act as a fatigue load, causing the membrane to mechanically degrade over time.

To calculate the in-plane stresses, the hygral strain based on the membrane water content needs to be calculated. An extra experiment was performed to determine the relationship between the membrane resistance and the RH of the reactant gases. Moreover, an empirical equation exists showing the correlation between RH and the water content of the Nafion membrane [31]. Hence, the membrane water content can be estimated using the membrane resistance. Consequently, the cyclic variation in the membrane water content can be estimated to be between 5.61 and 13.1 (Fig. 3.3b), corresponding to membrane resistances of 60 and 196 mΩcm^2, respectively. There is an approximate equation that represents the correlation between the hygral strain (ε) and water content change ($(\lambda_i - \lambda_{average})$ of the membrane (Eq. (3.1) [31]).

$$\varepsilon = \beta_{swe}(\lambda_i - \lambda_{average}) \quad (3.1)$$

where $\beta_{swe} = 0.009$ is is an experimental hygral expansion coefficient; λ_i and $\lambda_{average}$ are the water content of the membrane at time t and average membrane water content during the RH cycling test, respectively.

The in-plane stresses generated in the membrane can then be estimated using Eq. (3.2):

$$\bar{\sigma} = \varepsilon \bar{E} \quad (3.2)$$

where E is the average Young's modulus. The average Young's modulus of NRE211 at 80 °C is approximately 100 MPa [32]. Consequently, variations of water content and the in-plane stress have been calculated and shown in Fig. 3.3b and Table 3.1. The average fatigue stress induced by the durability test is predicted to be 6.74 MPa or the stress amplitude (Δσ/2) of 3.37 MPa.

Table 3. 1 Prediction of water content and the stress range induced by the durability test

Testing conditions	Average water content, λ_{mean}	Minimum water content, λ_{min}	Maximum water content, λ_{max}	Average stress range, $\Delta\sigma$ (MPa)
RH cycling at OCV condition	9.2	5.61	13.1	6.74

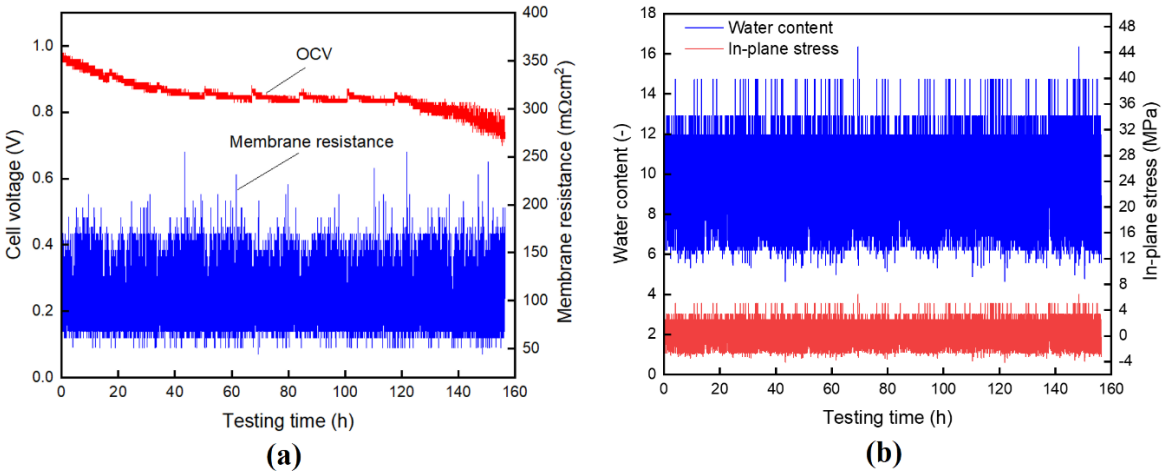

Fig.3. 3. (a) Variations of membrane resistance and cell voltage and (b) the prediction of water content and in-plane stresses formed in the membrane during the RH cycling test.

Membrane has an important role in separating react gases from forming the combustible mixture. However, non-desired electrochemical reactions of the leaked hydrogen at the cathode and the leaked oxygen at the anode occur at the electrodes during the durability tests, causing an increase potential at anode side and a reduction potential in the cathode side, resulting in the OCV reduction. Furthermore, leaking of reactant gases can initiate to the formation of hydrogen peroxide (H_2O_2), then triggering the formation of free radicals, leading to chemical membrane decomposition, as mentioned in Section 3.1.

Although the H_2O_2 formation mechanism is still controversial, three possible formation mechanisms for H_2O_2 can be proposed. As for the first one, H_2O_2 formation at the cathode is suggested, where a 2-electron oxygen reduction reaction (Eq. (3.3) [33]) takes place.

$$O_2 + 2H^+ + 2e^- \rightarrow H_2O_2 \qquad E^0 = 0.695 \text{ V vs SHE} \quad (3.3)$$

As for the second mechanism, H_2O_2 can be formed at the Pt band inside the membrane through the reaction in Eq. (3.3). Oxygen gas permeated from cathode meets the proton conducted from anode at the Pt band and forms H_2O_2. Pt band is often yielded under some degradation processes as follows. The Pt band formed close to the cathode is another source of H_2O_2 production inside the membrane. The Pt particles are dissolved from the cathode catalyst and repositioned in the membrane when the cell experiences a potential cycle [34] or is held in the OCV condition [18], resulting in the formation of the Pt band. The generation rate of H_2O_2 depends on the potential at the Pt band location in the membrane [18]. Regarding the third mechanism, the anode's low potential makes it simple for H_2O_2 to be produced via Eq. (3.3).

Fluoride generated through reactions related to H_2O_2 is an important indicator to determine the place where H_2O_2 is formed. The presence of fluoride was detected in the cathode and anode drainage [5, 30], indicating H_2O_2 formation on both sides of the cell. In addition, the H_2O_2 formation rate depends on several factors, such as the potential, catalytic activity, RH, temperature, and crossover rate of reactant gases.

Sethuraman et al. [35] expressed the H_2O_2 formation rate at the anode side ($\dot{Q}_{H_2O_2,An}$) using an empirical relation.

$$\dot{Q}_{H_2O_2,An} = \chi_{H_2O_2} \dot{Q}_{O_2} \quad (3.4)$$

where $\chi_{H_2O_2}$ is the fraction of O_2 that is converted to H_2O_2 and is dependent on the water activity of the membrane, a_w, as follows:

$$\chi_{H_2O_2} = 0.2081 - 0.1208 \times a_w - 0.072 \times {a_w}^2 - 2.132 \times 10^{-14} {a_w}^3 \quad (3.5)$$

It can be seen that $\chi_{H_2O_2}$ increases with a decrease in water activity in the membrane (or decreased RH). Thus, during the RH cycling tests, $\chi_{H_2O_2}$ in the dry portion is higher than that in the wet portion. $\dot{Q}_{O_2}$ is the oxygen crossing rate from the cathode to the anode through the membrane ($mols^{-1}cm^{-2}$), which is calculated using Fick's law of diffusion in Eq. (3.6) as follows

$$\dot{Q}_{O_2} = D_{O_2-PEM} \frac{p'_{O_{2,Ca}} - p_{O_{2,An}}}{H_{O_2-PEM} L_{PEM}} \approx D_{O_2-PEM} \frac{p'_{O_{2,Ca}}}{H_{O_2-PEM} L_{PEM}} \quad (3.6)$$

where $D_{O_2\text{-PEM}}$ (cm^2s^{-1}) and $H_{O_2\text{-PEM}}$ ($atmcm^3mol^{-1}$) are diffusion coefficients and Henry's constants of oxygen diffusion through Nafion membrane, respectively (cm^2s^{-1}); L_{PEM} is thickness of the membrane (cm); and $p'_{O_{2,Ca}}$ and $p_{O_{2,An}}$ are the actual partial pressure of oxygen at the cathode and anode, respectively

(atm). Assuming that oxygen will react completely at the anode, the concentration of oxygen at the cathode is considered negligible (or $p_{O_{2,An}} \approx 0$).

In addition, Sethuraman et al. [35] derived the H_2O_2 formation rate at the cathode-membrane interface ($\dot{Q}_{H_2O_2,Ca}$), as follows:

$$\dot{Q}_{H_2O_2,Ca} = k_f \left(C_{O_2}\right)^1 (C_{H^+})^2 \quad (3.7)$$

where k_f is the rate constant for H_2O_2 formation ($mol^2\ cm^{-5}\ s^{-1}$) and C_{O_2} and C_{H^+} are the dissolved oxygen concentration in the bulk of the electrolyte and proton concentration, respectively ($molcm^{-3}$). It should be noted that Eq. (3.7) is valid for H_2O_2 formation at the cathode-membrane interface when the potential is lower than 0.695 V, which is the equilibrium potential of Eq. (3.3).

Although several mechanisms of H_2O_2 formation have been proposed to date, H_2O_2 formation only at the anode side has been discussed as for the main mechanism in this study. The H_2O_2 formation mechanism initiated by the Pt band seems improbable at the beginning of life (BOL) because the Pt band was not observed in the FIB-SEM analysis (in sector post- mortem analysis). In addition, because the cathode potentials in the three testing conditions at the BOL are higher than 0.695 V, H_2O_2 formation at the cathode side is less likely. Thus, the formation of H_2O_2 at the anode was the most plausible mechanism in this study. This assumption is consistent with the findings of Liu and Zuckerbrod [36] that H_2O_2 is predominantly produced on the anode side by oxygen reduction. The estimated formation rates of H_2O_2, based on Eq. (3.4), under the RH cycling test in wet and dry conditions are summarized at the last column in Table 3.2. The formation rate of H_2O_2 at the anode depends on the oxygen crossover rate.

Table 3. 2. H_2O_2 formation rate at the anode electrode

Properties	**Value**	
Current density, i (Acm^{-2})	0	
Cell voltage, V_{cell} (V)	0.96	
Inlet oxygen partial pressure, $p_{O_{2,Ca}}$ (atm)	0.2099	
The fraction of O_2 reducing to H_2O_2 [35], $\chi_{H_2O_2}$ (-)	Under wet condition	0.0153
	Under dry condition	0.2081
Diffusion coefficients of oxygen through Nafion membrane [35],	Under wet condition	1.01×10^{-4}

$D_{O_2\text{-PEM}} = 9.78 \times 10^{-8} + 3.5 \times 10^{-9}T + 10^{-9}a_w$ (cm^2s^{-1}) where T =353 K, and a_w is water activity of the membrane.	Under dry condition	1.33×10^{-6}
Henry's constants of oxygen diffusing into the Nafion membrane [37], $H_{O_2\text{-PEM}} = \exp(\frac{-666}{T}+14.1)$ (atm cm^3mol^{-1})	20,1615	
Membrane thickness, L_{PEM} (cm)	0.0025	
The oxygen crossing rate through the membrane from the cathode to anode (Eq. (3.6)), $\dot{Q}_{O_2}$ ($molcm^{-2}s^{-1}$)	Under wet condition	4.22×10^{-8}
	Under dry condition	5.55×10^{-10}
The H_2O_2 generation rate at the anode (Eq. (3.4)), $\dot{Q}_{H_2O_2,An}$ (mol $cm^{-2}s^{-1}$)	Under wet condition	6.45×10^{-10}
	Under dry condition	1.16×10^{-10}

As shown in Fig. 3.3, the average OCV decay rate during the test is quite high, at 1.43 mVh^{-1} or 0.11 $mVcycle^{-1}$, which is approximately 72 times faster than the purely chemical stress test [3], in which the cell was kept under OCV conditions at 80 °C for 2,000 hours. The OCV in PEMFCs is determined by the Nernst equation and by the crossover rate of hydrogen through the membrane. Under the durability test, the membrane is degraded with the increase in RH cycling numbers, resulting in an increase in the hydrogen crossover rate and, eventually, a decrease in the OCV. In Chapter 2, it was mentioned that there was a correlation between OCV and the hydrogen crossover rate. Thus the OCV decrease indirectly indicates a decay in the integrity of the membrane. Furthermore, catalyst degradation is responsible for the OCV decline when the cell voltage varies repeatedly at a high value.

According to Fig. 3.3a, the OCV decays at the different rates during the durability test. Due to ECSA reduction caused on by carbon oxidation and variations in cell voltage, OCV rapidly declines during the first three testing periods from BOL to after 600 RH cycles (50 h of testing time), follows by a slight decline in the middle of the durability test and a sharp decline in the final two testing periods as a result of increased gas leakage through the failed membrane. The OCV begins to drop significantly and varies with a larger amplitude at the last testing periods, indicating the existence of catastrophic defects in the membrane. This is because these defects not only greatly increase the amount of hydrogen gas that leaks through the membrane, but also vary the leakage rate significantly owing to the change in the hydrogen partial pressure at the anode during the durability test, resulting in a vigorous fluctuation

in the OCV. The abrupt decrease in the OCV could be an early important signal for transient hydrogen combustion from a moderate to an accidental scale, thus resulting in the formation of a pinhole due to thermal polymer degradation.

3.3.1.2. The changes of hydrogen crossover rate and OCV during the durability test

Figs. 3.4a and 3.4b present the LSVs at atmospheric pressure and a 20-kPa anode backpressure, respectively, after different numbers of RH cycles. The current density obtained in the figures corresponds to the hydrogen crossover rate. In the case of the 1,600, 1,800 and 2,000 RH cycles in Fig. 3.4a and b, the LSVs (crossover current density) significantly fluctuate. The water blockage in the flow channel and its drainage as through-membrane cracks emerge in the deteriorated membrane have been explained as the cause of this phenomena, which first appeared in Chapter 2. Once again, the fluctuation of the LSVs is a signal indicating the formation of serious defects in the membrane induced by the durability test. Furthermore, it poses a difficulty in obtaining an accurate hydrogen crossover rate through the degraded membrane. Although the LSV profiles exhibit fluctuation as the RH cycle progresses, they suggest that increase in the number of RH cycles increased the hydrogen crossover rate. Furthermore, according to the y-axis range, the hydrogen crossover rate under the 20-kPa anode backpressure condition presented in Fig. 3.4b is much higher than that under atmospheric pressure conditions (in Fig. 3.4a) after the LSVs fluctuate strongly. This result agrees with a physical intuition, wherein a higher pressure at the anode (20-kPa anode backpressure) increases the crossover rate for the same degraded membrane.

The variations with increasing the number of RH cycles in the crossover rates obtained from the LSVs are summarized in Fig. 3.4c. After enduring 1,600 RH cycles, the crossover rate increases significantly and exceeds the membrane failure criterion of 15 $mAcm^{-2}$ [4]. With a 20-kPa anode backpressure, this is more apparent as the crossover current density increases sharply to 62.4 $mAcm^{-2}$ when the number of RH cycles reaches 1,600 (or 134 h). This abrupt increase in the crossover rate suggests the appearance of serious physical defects in the membrane, such as pinholes or through-membrane cracks.

After 1,600 RH cycles, until the end of the durability test, the crossover rate continues to increase, possibly owing to the increase in the size of the pinholes and cracks or an increase in the number of these defects. The crossover current density increases precipitously in the case of a 20-kPa anode backpressure and is approximately 5.6–8.8 fold higher than in the same case at atmospheric pressure. This indicates that hydrogen gas leakage through the degraded membrane is dominated by the gas convection mechanism in the presence of pinholes or through-membrane cracks. It should be noted that, if no pinholes and cracks exist, the hydrogen crossover progresses in a diffusion manner, and the crossover rate in the case of the 20-kPa anode backpressure (120-kPa hydrogen pressure) is estimated to be 1.2 fold higher than that in the case of atmospheric pressure (100-kPa hydrogen pressure).

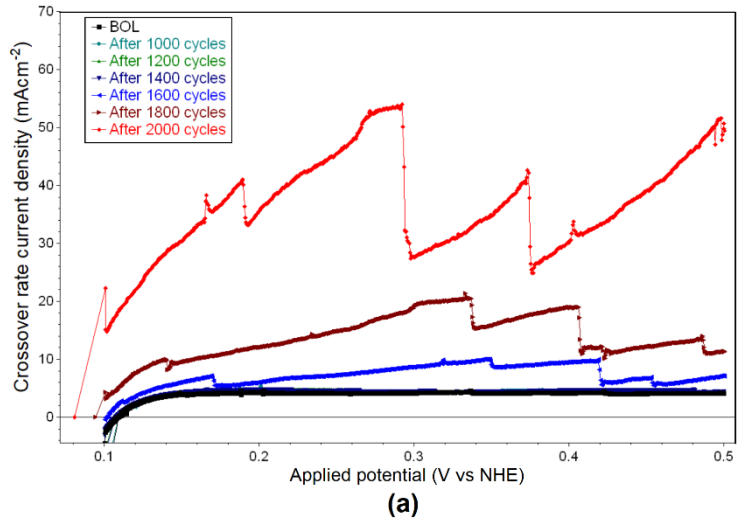

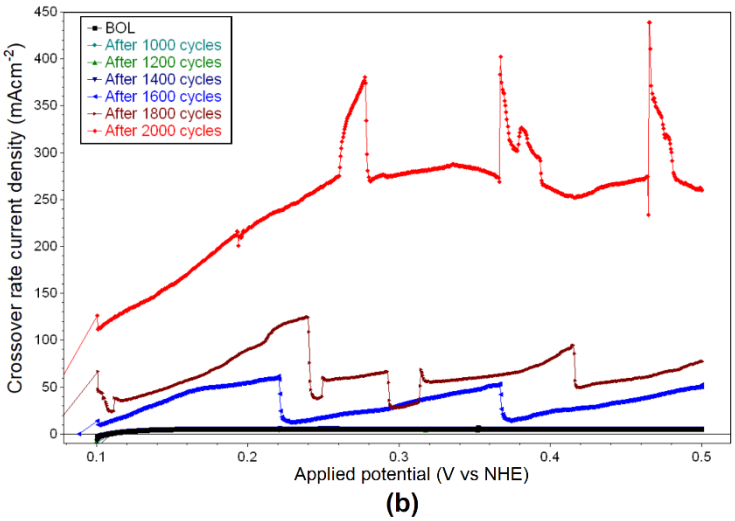

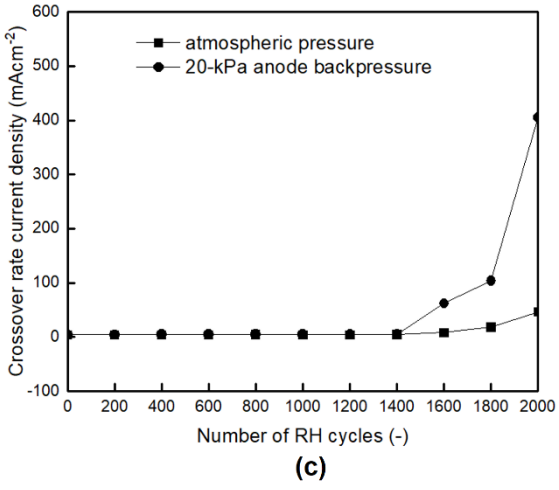

Fig. 3. 4. Linear sweep voltammograms for H_2/N_2 cell after different numbers of RH cycles (a) at atmospheric pressure, (b) at 20-kPa anode backpressure, and (c) variation of the hydrogen crossover current density through the membrane after different numbers of RH cycles.

The OCV is an important parameter of PEMFCs. It is well known that there is a correlation between

the OCV and hydrogen crossover rates. Particularly, a mixed potential is created by the oxidation of leaky hydrogen at the cathode and the reduction of oxygen at the anode, which lowers the OCV [5,38,39]. Hence, the OCV has also been considered as a practical and reliable diagnostic indicator for verifying the integrity of polymer membranes [40].

Figure 3.5 presents the decline of OCVs at atmospheric pressure and 20-kPa anode pressure at different numbers of RH cycles, which is in correlation with the ECSA change. The OCV shows two drastic drops under both pressure conditions. The first decline in OCV appeared from the beginning of life (BOL) to about 800 RH cycles which is thought to be caused by the reduction of ECSA. During the RH cycle test, the cell voltage fluctuates (Fig. 3.3a), even for the OCV condition, when the hydrogen stream at the anode is switched from a dry to humidified state and vice versa. This unfavorable situation is thought to lead to the oxidation of the carbon-black support and the dissolution of Pt in the cathode catalyst [41-43]. This results in the drop of ECSA, and consequently the gradual decrease in OCV. The second sharp decline in OCV appeared just after 1,600 RH cycles, especially under a 20-kPa anode backpressure. The second decline of OCV agrees with the detection of the hydrogen crossover rate in Fig.3.4c. From this point to the end of the durability test, the increase in hydrogen crossover rate dominates the decrease in OCV. The reducing tendency of the OCV in Fig. 3.5 is consistent with the continuous decline of OCV that is measured during the durability test, as shown in Fig. 3.3a. After 1,600 RH cycles until the end of the durability test, the OCVs continued to decrease with a higher decay rate owing to the increase in the hydrogen crossover rate through the degraded membrane, which is caused by the increase in the number as well as defect's size. In particular, with an anode backpressure of 20-kPa, the OCV exhibits a precipitous decrease and eventually reaches a very low value of 0.61 V, corresponding to the hydrogen crossover rate of 0.406 Acm^{-2} at the end of the durability test.

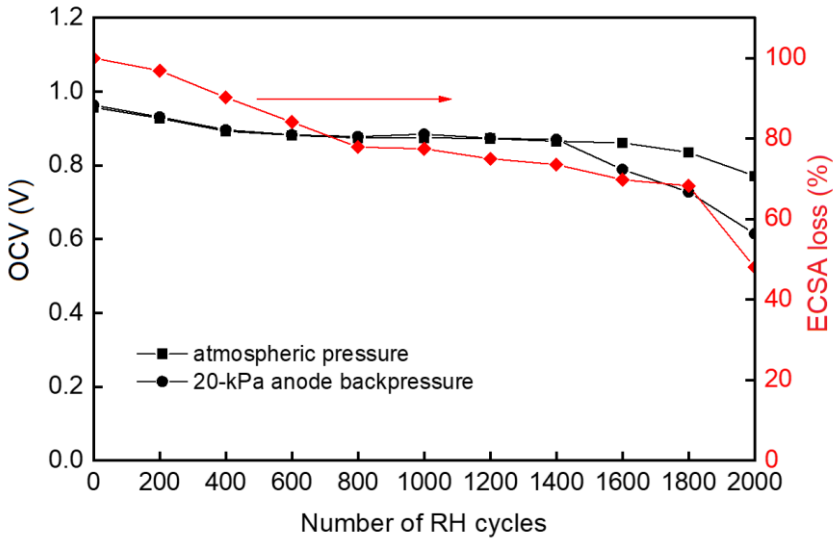

Fig. 3. 5. The correlation between cathode's ECSA and OCVs after different numbers of RH cycles.

The electrochemical measurement results and the discussion presented in the above sections

indicate that the membrane completely fails after enduring 1,600 RH cycles, which is equivalent to approximately 134 h of testing. Other membrane mechanical durability tests reveal a similar tendency, but the membrane fails more slowly. A Nafion membrane of thickness 25 μm, which is subjected to the RH cycling test using air for both compartment of the cell, fails after thousands of RH cycles depending on the testing conditions, e.g., 4,000 RH cycles (or 267 h of testing) [3] and 4,500 RH cycles (or 300 h of testing) [25]. In Chapter 2, the membrane, which was experienced the purely mechanical stress, failed after 12,500 RH cycles (or over 1,041 h of testing). The membrane under the combined chemical and mechanical stress test in this chapter failed approximately 7.8 times faster than of in the mechanical stress only (see in Fig.3.6). The faster failure of the membrane in this study is a result of the simultaneous impact of chemical and mechanical degradation. Specifically, the OCV conditions and the formation of cracks triggered by mechanical stresses intensify the generation of H_2O_2, which is a chemical precursor that promotes the formation of free radicals, such as HO· and HOO·. These radicals are primarily responsible for the mechanical and chemical stability deterioration of the PFSA membranes. Sadeghi Alavijeh et al. [44] reported that chemical degradation could result in a reduction in the tensile strength and consequent toughness fracture, as well as a decrease in the crack propagation resistance of PFSA membranes. Chemical degradation, in turn, accelerates mechanical degradation. Moreover, the OCV and low humidity conditions in the current study can facilitate the attack of radicals on the PSFA membrane structure, in both the backbone main chain and side groups [9].

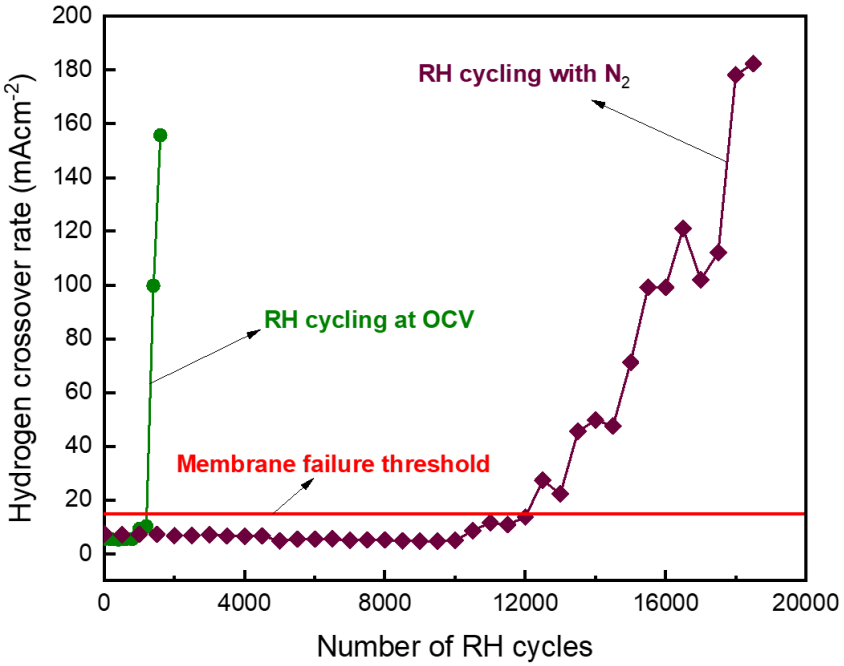

Fig. 3. 6. The hydrogen crossover rate vs. number of RH cycles under purely mechanical stress (result from Chapter 2) and in the current chapter's combined chemical and mechanical stress test. The red, horizontal line represents the membrane failure criterion of the hydrogen crossover rate of 15 mAcm^{-2}.

3.3.2. Temperature change during durability test

Figs. 3.7a and 3.7b present the IR images of the cathode compartment at the beginning – of – life (BOL) and after different RH cycles under the OCV condition, at atmospheric pressure and at 20-kPa anode backpressure, respectively. The regions denoted by seven black rectangles at BOL, wherein the GDL surface is visible, are the subject of the investigation into the temperature change caused by catalytic combustion during OCV measurement. The obtained crossover current and simple calculation can estimate the volumetric concentration of hydrogen gas at the cathode side, and it is summarized in Table 3.3 to specifically consider the thermal behavior captured by the IR camera.

Table 3. 3. Hydrogen crossover rates and the volumetric hydrogen concentration on cathode side at different numbers of RH cycles

Number of RH cycles		**BOL**	**200**	**400**	**600**	**800**	**1000**	**1200**	**1400**	**1600**	**1800**	**2000**
Crossover current density, mAcm^{-2}	At atmospheric pressure	4.24	4.39	4.29	4.38	4.59	4.48	4.46	4.52	8.41	18.6	46.3
	At 20-kPa anode backpressure	4.76	4.86	4.97	5.14	5.25	5.33	5.35	5.37	62.4	104	406

Hydrogen concentration, vol%	At atmospheric pressure	0.07	0.07	0.07	0.07	0.07	0.07	0.07	0.07	0.13	0.29	0.71
	At 20-kPa anode backpressure	0.07	0.07	0.08	0.08	0.08	0.08	0.08	0.08	0.95	1.57	5.86

Under OCV conditions, as no load is applied to the cell, the temperature elevation of the surface of the GDL must originate from the combustion of the leakage hydrogen from the anode with oxygen gas in the cathode. Although, in the BOL (intact CCM) case, hydrogen permeates the membrane marginally, and the concentration of hydrogen gas on the cathode side is low (0.07–0.08 vol%), catalytic combustion occurred due to the presence of platinum. Thus, even at the BOL, the temperature increases as compared to the case wherein nitrogen gas is supplied to both the anode and cathode. According to Fig. 3.8, the average temperature increments vary between 5 °C and 6 °C at both pressure conditions. After 1,600 RH cycles (or after 134 h of testing), several hot spots are observed only during measuring OCV at 20-kPa anode backpressure (highlighted by the red circles) in channels 1, 2, and 7, as shown in Fig. 3.7b. Hotspots in channels 1 and 7 can reach maximum temperature increases of 9.3 and 10.4 °C, respectively, which is higher than the 8.5 °C in channel 2. The appearance of the hot area after 1,600 RH cycles is consistent with the development of fatal flaws (pinholes or through-membrane cracks), which are indicated by the aforementioned hydrogen crossover rate and OCV data. As some hydrogen gas flows through a pinhole, a hydrogen gas mixture with air is formed, and catalytic combustion occurs in a large scale, thus resulting in the appearance of a hot spot. Because of the presence of a pinhole after 1,600 RH cycles, the hot-spot temperature continues to increase with the increase in the number of RH cycles owing to the appreciable increase in the hydrogen crossover rate. With a 20-kPa anode backpressure, the hydrogen crossover rate increases owing to the dominance of gas convection, thus resulting in a dramatic increase in the GDL temperature, as shown in Fig. 3.8b. At atmospheric pressure, the hotspot with a temperature of 90.3 °C appears at channel 1 until after 2,000 RH cycles when the hydrogen crossover rate reaches 46.3 $mAcm^{-2}$ (corresponding to the hydrogen concentration of 0.71 vol% as shown in Table 3.3).

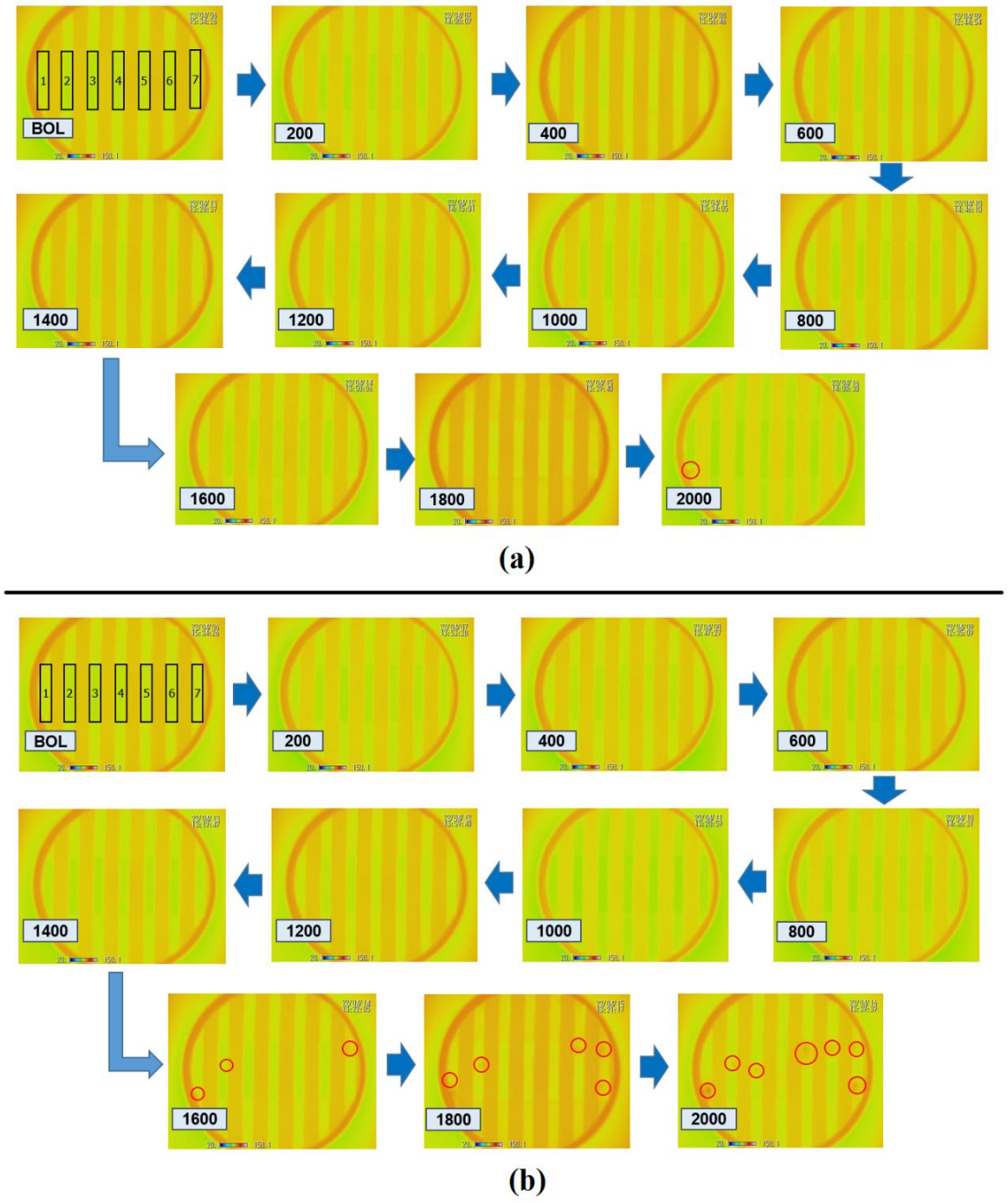

Fig. 3. 7. IR images of the cathode's GDL surface (a) at the atmospheric pressure and (b) at 20-kPa anode backpressure after different numbers of RH cycles. The red circles represent the initial position of the hotspot. The seven black rectangles, which are numbered from 1 to 7, are the GDL surface under the channel region of the flow field. And, the red circles indicate the hotspot locations. The temperature range is from 20.1 to 150.1 °C.

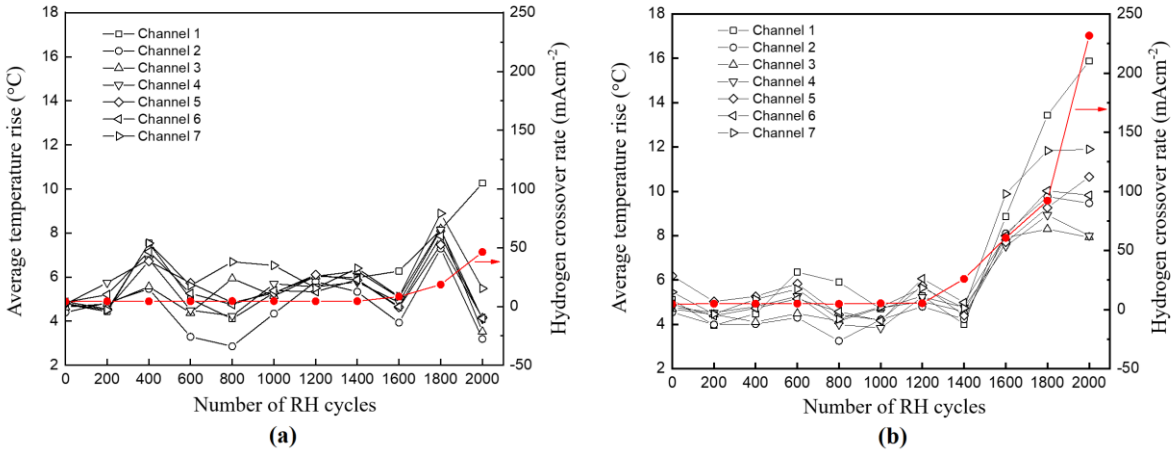

Fig. 3. 8. Correlation between maximum temperature rise and hydrogen crossover rate (a) at atmospheric pressure and (b) at 20-kPa anode backpressure.

Furthermore, despite the abnormally high hydrogen crossover rate and hydrogen concentration on the cathode side at the end of the durability test, the temperature increase is not on an accidental scale. As shown in Table 3.3, the hydrogen crossover current density at the end of the durability test reaches approximately 406 $mAcm^{-2}$, which is 27 times beyond that of the membrane failure criterion (15 $mA\ cm^{-2}$ [4]). This high crossover and simple mass balance calculation in the cathode channel suggest a volumetric hydrogen concentration of 5.86 vol%, which is beyond the lowest concentration (4 vol%) that could possibly induce an explosion. However, the highest temperature of 96 °C (a 16 °C temperature increase) is recorded in channel 1 in the case of a 20-kPa anode backpressure (see Fig. 3.8b). This temperature increase is less than that when accidental combustion occurs.

The small temperature increase is possible because the heat released from the catalytic combustion with the hydrogen gas mixture generated quickly dissipates into the environment through the cell components as shown in Fig. 3.9. The hydrogen gas crossover rate in the worst case, which is shown at the end of the durability test in Fig. 3.8b, is approximately 406 $mAcm^{-2}$ owing to the presence of pinholes and cracks in the membrane. Assuming that the crossover hydrogen gas burns completely, the maximum heat formation (q''_{Com}) can be calculated as follows.

$$q''_{\mathrm{Com}} = \frac{i_{\mathrm{cross}} \times \Delta H_{\mathrm{f}}}{2\mathrm{F}} = \frac{0.406 \times 241 \times 10^{3}}{2 \times 96485} = 0.507\ \mathrm{Wcm^{-2}} \qquad (3.8)$$

where $\Delta H_{\mathrm{f}} = 241\ \mathrm{kJmol^{-1}}$ is the heat of hydrogen combustion at 25 °C (water vapor); F = 96,485 $\mathrm{Cmol^{-1}}$ is Faraday's constant; and i_{cross} = 0.406 $\mathrm{Acm^{-2}}$ is the hydrogen crossover current density. If this combustion heat of $q''_{\mathrm{com}} = 0.507\ \mathrm{Wcm^{-2}}$ is applied to the Nafion membrane, it can ignite the membrane within 15s [45]. However, the CCM in this study is surrounded by the GDL, separator channel, and visualization window, and the gas flows in the channel. Thus, the heat released from hydrogen combustion at the cathode's catalyst layer can be dissipated efficiently to the environment through convection and conduction through the gas stream and visualization window. Therefore, a maximum

temperature increase of 16 °C (or hotspot temperature of 96 °C), as shown in Fig. 3.8b, is plausible. In the case of the fuel cell stack, owning to the cooling system, the heat produced in the cell is dissipated in a more efficient manner than that in this study.

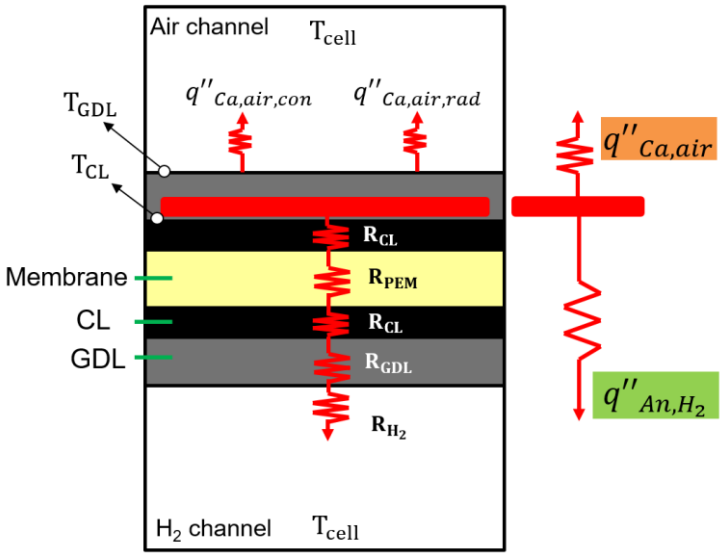

Fig. 3. 9. Combustion heat is dissipated via anode and cathode sides.

A one-dimensional heat transfer model was proposed to predict the cathode's GDL surface induced by combustion, which is based on the hydrogen crossover rate data with 20-kPa anode backpressure. The heat released from combustion of q''_{com} will be transferred in two directions: anode ($q''_{An,\,H_2}$) and cathode ($q''_{Ca,\,air}$) sides, as described in Fig. 3.9. This calculation has some assumptions as follows: (i) Combustion of the gas mixture (H_2 and air) occurs on the cathode's catalyst layer; (ii) A stable heat transfer progress in the through-plane direction; (iii) Thermal radiation heat from the anode GDL to the hydrogen stream is negligible; (iv) The emissivity (ε) of the cathode's GDL is 1; (v) the thermal contact resistances between cell components are negligible. The calculation procedure is shown in Fig. 3.10. The details of the seven-step iteration calculation will be indicated in Appendix A of this dissertation.

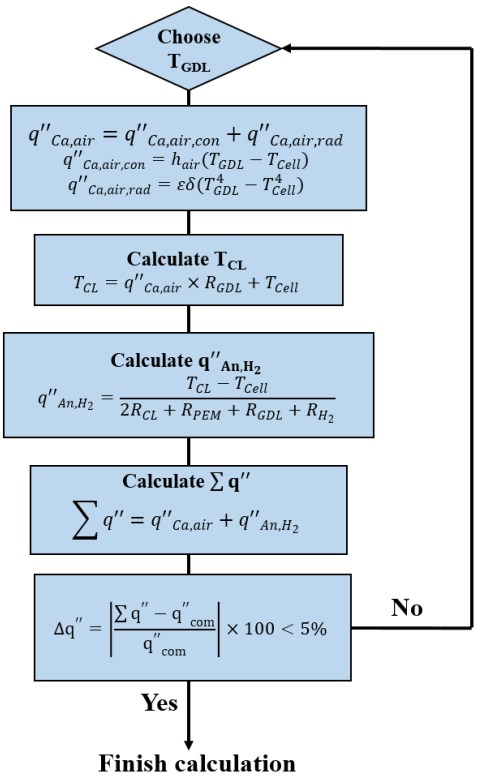

Fig. 3. 10. Calculation procedure for prediction the GDL temperature rise due to combustion.

As can be seen in Fig. 3.11, even though the current heat transfer calculation is simplified with many assumptions, it can predict fairly well the change in GDL temperature induced by combustion in comparison with experimental results. The calculation is slightly underestimated compared to the experimental results prior to membrane failure (1,600 RH cycles). Considering the accuracy of the IR camera is ±1 °C, the small deviation between calculation and experiment is minor, and the current calculation show good agreement with the measurement. Then, after 1,600 RH cycles to the end of the durability test, the calculation can follow the increasing temperature trend with the experimental data but with a relatively larger deviation. This is probably because, in the calculation, the hydrogen crossover rate is assumed to be uniform so that heat dissipation progresses in a one-dimensional manner (through plane direction). In contrast, the defects appeared locally in the degraded membrane, where hotspots appear. In this case, the heat from the combustion will be dissipated efficiently in three dimensions, resulting in a lower GDL temperature in the experiment.

According to the calculation, in addition, the heat dissipates mainly through the anode side, at which the heat transfer resistance is much smaller than that of the cathode path. For instance, in the case after 2,000 RH cycles, the heat flux from the combustion spot was transferred via the anode and cathode sides, which were $q''_{Ca,\,air} = 0.096$ W cm^{-2} and $q''_{An,\,H_2} = 0.410$ Wcm^{-2}, respectively. Due to the higher thermal conductivity of hydrogen gas than air at the same temperature (e.g., over 7 times at 80 °C), the convective heat transfer coefficient from GDL to the hydrogen stream is greater than that of its counterpart to the air stream, as shown in Table 3.4. Thus, the heat transfer resistance from the GDL to the air stream is

over 5 times greater than the convection heat resistance from the GDL to the hydrogen stream.

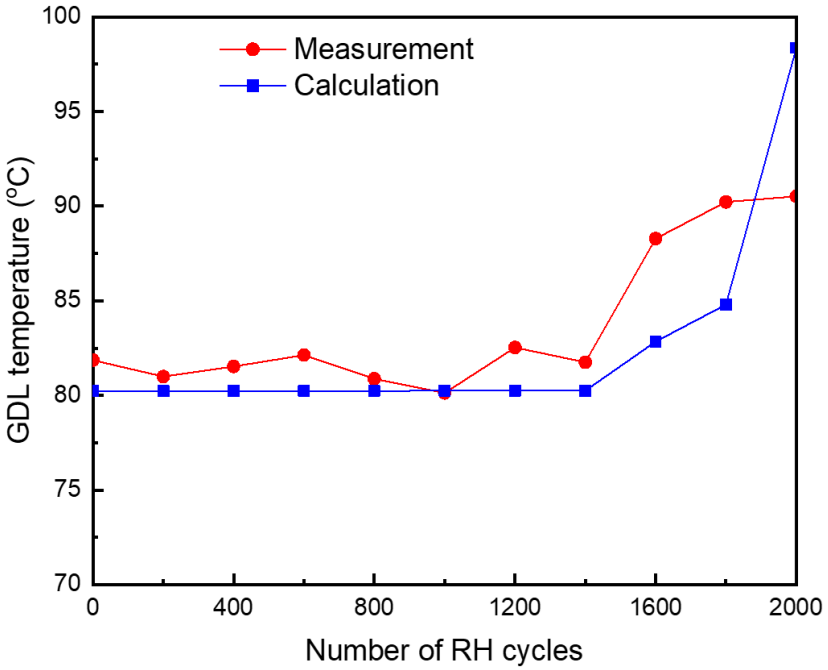

Fig. 3. 11. Comparison between the calculation and experiment of the average GDL temperature rise due to combustion at the case 20-kPa anode backpressure.

The maximum dissipated heat flux ($q''_{\text{dissipated,max}}$) is defined that the maximum heat flux released from combustion can be transferred by the cell structure corresponding to the auto-ignition temperature of the membrane, as calculated via Eq.(3.9). When the combustion heat flux exceeds this threshold, membrane will burn and be thermally decomposed, resulting in the formation of pinholes.

$$q''_{\text{dissipated,max}} = \mathrm{K_{Cell}}\left(\mathbf{T_{ig}} - \mathbf{T_{Cell}}\right) \quad (3.9)$$

where the cell temperature (T_{cell}) is 80 °C; The auto-ignition temperature (T_{ig}) of the NRE211 membrane is 300 °C [45]; $\mathrm{K_{cell}}$ is the overall heat transfer coefficient of the cell ($\mathrm{Wcm^{-2}K^{-1}}$) and can be calculated via Eq.(3.10).

$$K_{\text{Cell}} = K_{\text{Ca}} + K_{\text{An}} = \frac{1}{R_{\text{GDL}} + R_{\text{air}}} + \frac{1}{2R_{\text{CL}} + R_{\text{PEM}} + R_{\text{GDL}} + R_{\text{H}_2}} \quad (3.10)$$

where R_{CL}, R_{PEM}, R_{GDL}, R_{air}, and R_{H_2} are the thermal conduction resistances of the CL, the membrane, the GDL and the convection heat resistances from the GDL to the air and hydrogen streams, respectively. It can be seen that the maximum dissipated heat flux or the self-cooling heat flux depends mainly on the overall heat transfer coefficient of the cell (K_{cell}) and the cell temperature (T_{cell}) according to Eq. (3.9). The K_{cell} is a function of the cell components (or the cell structure), the reactant gas flow condition, and is almost constant. Based on Eq. (3.9), the maximum dissipated heat flux is estimated to be around 2.0

Wcm^{-2} ($q''_{dissipated,max}$ = 2.0 Wcm^{-2}**)**. This value is recognized as a maximum allowable heat flux. Within the testing conditions and cell geometry in this study, the combustion heat of $q''_{com} = 0.507$ Wcm^{-2} shown above is lower than the maximum allowable heat flux. Therefore, the emergence of hotspots in the IR images indicates that the combustion process is on the transition scale, where the combustion heat is lower than the maximum dissipated heat flux ($q''_{com} < q''_{dissipated,max}$).

At hotspot locations, the membrane not only experiences the combined effect of the chemical and mechanical mechanisms but also the thermal stress induced by combustion. This is because the combustion occurs at the catalyst-GDL interface, and the thermal conductivity of the membrane and catalyst layer is lower than that of the GDL. When the GDL temperature at hot spots is in the 90–100 °C range, the membrane temperature will be higher due to thermal resistance and reach close to its glass transient temperature (100–150 °C) [46]. For instance, based on the above heat transfer calculation, when the cathode's GDL surface temperature is 98.4 °C after the membrane endures 2,000 RH cycles, the average temperature of the membrane is predicted to be 98.8 °C. As a result, Nafion membranes would creep and thin under mechanical stress, particularly in dry conditions, hence accelerating membrane deterioration faster.

3.3.3 Post mortem analysis

In order to investigate the morphology of the deteriorated membrane after finishing the durability test, a specimen from the degraded CCMs in channel 1, where a hot spot was visible in Fig. 3.7, is cut and examined under high magnification. The specimen has a width of 3 mm and length of 11 mm, which allow it to cover the entire active area of channel 1. The observation results are then compared to the morphology of the fresh CCM, as shown in Fig. 3.12a and 3.12b.

Apparently, three large pinholes have been found in the selected specimen, with diameters ranging from 12 to 16.4 μm (see Fig. 3.12c). These pinholes are located in the outlet region of channel 1 (outlet of the air stream and inlet of the hydrogen stream), where the mechanical stress concentration and hydrogen concentration gradient are the highest. Owing to the combined impact of the mechanical and chemical stresses that are induced by the RH cycling test in the OCV condition, membrane is thinned locally or deteriorated mechanically leading to the formation of cracks. The hydrogen crossover rate through these locations is high as compared to the rate regulated by membrane permeability. The leaked hydrogen gas combusts with oxygen at the cathode's catalyst, releasing heat flux at a rate greater than the maximum dissipated heat flux of the cell of approximately 2.0 Wcm^{-2} ($q''_{com} > q''_{dissipated,max}$) during the durability test, and then burning, instantly and temporarily, the membrane and ionomer component in the catalyst layer, eventually resulting in the pinhole formation. Noticeably, three pinholes line up in a groove without the catalyst. The catalyst material might have been blown up due to the flashback of hydrogen combustion at the cathode and re-located on both sides of this groove, exposing the membrane (highlighted by the dark colored area in Fig. 3.12c). The formation of these pinholes is thought to be

responsible for the abrupt increase in the hydrogen crossover rate as well as the sudden drop of OCV after 1,600 RH cycles.

According to the cross-sectional image in Fig. 3.12d, the membrane thickness in the region close to these pinholes has also drastically decreased from 23 μm at BOL to roughly 13.7 μm at the end of life (EOL). This observation confirms the impact of chemical stress on the membrane in the current combined chemical and mechanical degradation stress test. The reduction in membrane thickness is caused by the attack of free radicals, which are formed during the test. Therefore, this location is favorable for the formation of pinholes due to the increase in the hydrogen crossover rate through the thin membrane.

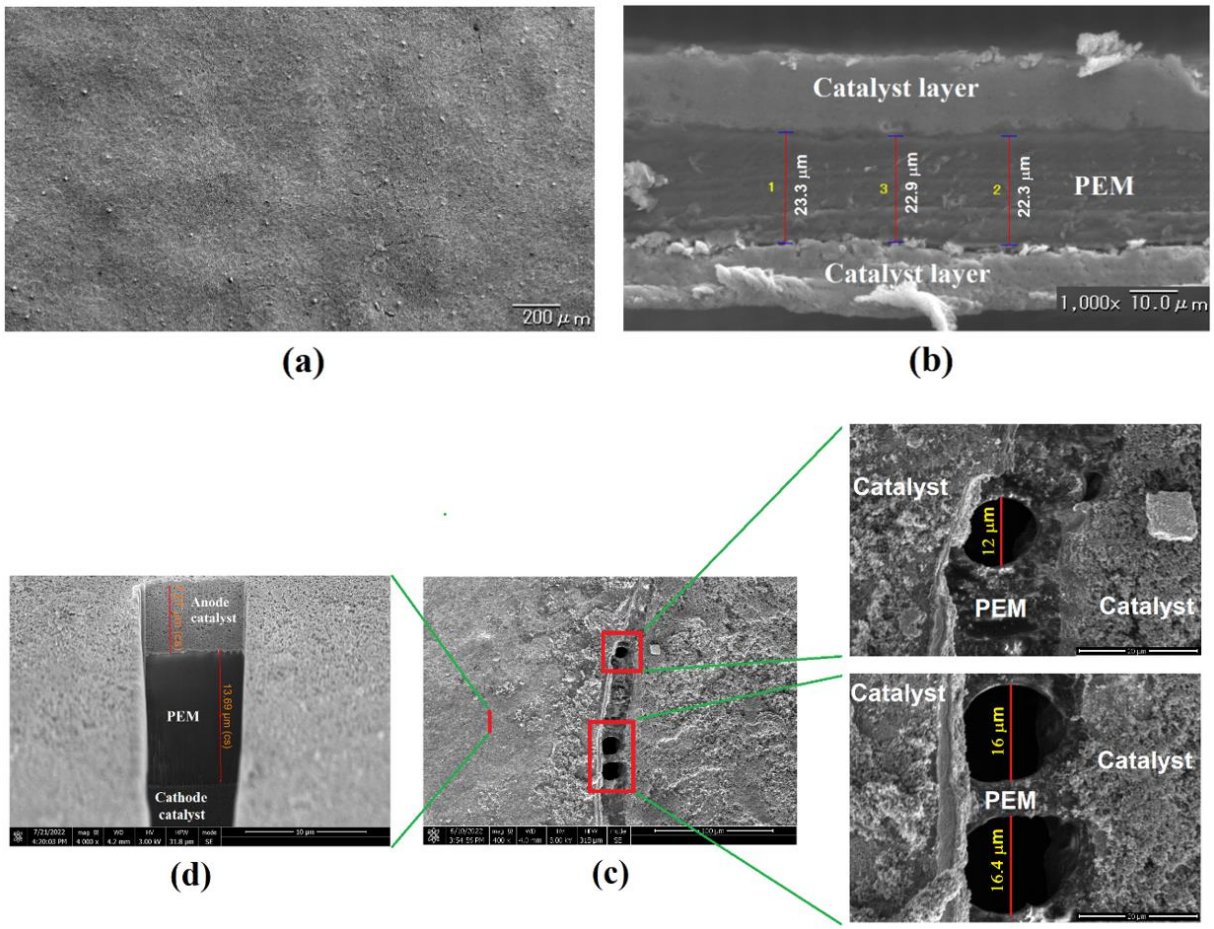

Fig. 3. 12. High-magnification images of (a) surface, and (b) cross section of the fresh CCM, (c) three pinholes, and (d) a cross section around the pinholes on the degraded CCM in channel 1 observed from the anode side.

3.4. Conclusions

Thermal imaging and electrochemical analyses clarified the cell degradation process and catalytic combustion in an in situ manner during a combined chemical and mechanical stress test as follows

(1) Even in the BOL, the temperature of the surface of the GDL under OCV conditions is increased by several degrees Celsius owing to catalytic combustion at the cathode catalyst

layer with a low hydrogen-gas leakage-rate-regulated membrane permeability.

(2) The harsh accelerated stress test with RH cycling under the OCV condition results in a synergistic effect of both chemical and mechanical degradation on the membrane. Consequently, membrane failure occurs over 7.8 times earlier compared to the case of mechanical stress test, wherein the RH cycle is imposed under nitrogen gas conditions in Chapter 2.

(3) The IR imaging technique comprising the use of a visualization cell embedded with a ZnS glass window can be a powerful diagnostic tool for detecting the formation of pinholes in accelerated stress tests of PEMFCs. The hot spot(s) captured via the imaging indicates pinhole formation in a straightforward manner. In addition, IR imaging can capture degradation processes, such as increases in the number of pinholes and/or accidental situations, by capturing many hot spots and/or wider hot regions.

(4) Every sign of membrane degradation captured via imaging is synchronized with the changes in the hydrogen crossover rate, OCV, and membrane resistance measured via the electrochemical method. This suggests that OCV measurement, which is possible in practical PEMFCs, is a good tool for determining the state of the membrane.

(5) In the current combined chemical and mechanical durability test, each degradation mechanism enhances the other, resulting in rapid membrane degradation and the formation of fatal defects. Once fatal defects, including pinholes and cracks, form, the degradation progresses in an accelerated manner, wherein both the hydrogen crossover rate and catalyst layer temperature abruptly increase as the number of RH cycles increases. However, even in worse-case scenario, the temperature increase is limited to 10–16 °C higher than the operating temperature of 80 °C, at most. Heat conduction and convection effectively transfer the heat from catalytic combustion to the surrounding environment.

(6) Furthermore, the heat transfer model has been developed to predict the GDL temperature rise based on the hydrogen crossover rate data. The model can track the combustion process as it transitions from a moderate to an accidental scale. Besides, combustion heat at the cathode is predominantly transferred to the hydrogen stream. Based on the model, the formation of pinholes clearly indicates that, during the durability test, the combustion heat flux exceeded the maximum dissipated heat flux of the cell locally.

3.5 References

1. IEA, Fuel cell electric vehicles stock by region and by mode, 2020, IEA, Paris, https://www.iea.org/data-and-statistics/charts/fuel-cell-electric-vehicles-stock-by-region-and-by-mode-2020 . Accessed 10 November 2021.

2. Department of Energy of the United States, Fuel Cell Technologies Office Multi-Year Research, Development, and Demonstration Plan. https://www.energy.gov/sites/prod/files/2017/05/f34/fcto _

myrdd _ fuel _ cells.pdf.

3. Mathias, Mark F., et al. “Two Fuel Cell Cars in Every Garage?” The Electrochemical Society Interface, vol. 14, no. 3, 1 Sept. 2005, pp. 24–35, 10.1149/2.f05053if.

4. A.B. LaConti, M. Hamdan, and R.C. McDonald, Handbook of Fuel Cells: Fundamentals, Technology, and Applications, Vol. 3, W. Vielstich, A. Lamm, and H. A. Gasteiger, Editors, Wiley, New York (2003).

5. Inaba, Minoru, et al. “Gas Crossover and Membrane Degradation in Polymer Electrolyte Fuel Cells.” Electrochimica Acta, vol. 51, no. 26, Aug. 2006, pp. 5746–5753, 10.1016/j.electacta.2006.03.008.

6. Endoh, Eiji, et al. “Degradation Study of MEA for PEMFCs under Low Humidity Conditions.” Electrochemical and Solid-State Letters, vol. 7, no. 7, 2004, p. A209, 10.1149/1.1739314.

7. Zatoń, M., et al. “Current Understanding of Chemical Degradation Mechanisms of Perfluorosulfonic Acid Membranes and Their Mitigation Strategies: A Review.” Sustainable Energy & Fuels, vol. 1, no. 3, 2017, pp. 409–438, 10.1039/c7se00038c.

8. Ghassemzadeh, Lida, et al. “Chemical Degradation of Nafion Membranes under Mimic Fuel Cell Conditions as Investigated by Solid-State NMR Spectroscopy.” The Journal of Physical Chemistry C, vol. 114, no. 34, 5 Aug. 2010, pp. 14635–14645, 10.1021/jp102533v.

9. Endoh, Eiji. “Development of Highly Durable PFSA Membrane and MEA for PEMFC under High Temperature and Low Humidity Conditions.” ECS Transactions, vol. 16, no. 2, 3 Oct. 2008, pp. 1229–1240, 10.1149/1.2981964.

10. Mittal, Vishal O., et al. “Is H_2O_2 Involved in the Membrane Degradation Mechanism in PEMFC?” Electrochemical and Solid-State Letters, vol. 9, no. 6, 2006, p. A299, 10.1149/1.2192696.

11. Robert, Mylène, et al. “Time-Resolved Monitoring of Composite NafionTM XL Membrane Degradation Induced by Fenton’s Reaction.” Journal of Membrane Science, vol. 621, Mar. 2021, p. 118977, 10.1016/j.memsci.2020.118977.

12. Healy, J., et al. “Aspects of the Chemical Degradation of PFSA Ionomers Used in PEM Fuel Cells.” Fuel Cells, vol. 5, no. 2, Apr. 2005, pp. 302–308, 10.1002/fuce.200400050.

13. Robert, Mylène, et al. “Effects of Conjoint Mechanical and Chemical Stress on Perfluorosulfonic-Acid Membranes for Fuel Cells.” Journal of Power Sources, vol. 476, Nov. 2020, p. 228662, 10.1016/j.jpowsour.2020.228662.

14. Mukundan, Rangachary, et al. “Membrane Accelerated Stress Test Development for Polymer Electrolyte Fuel Cell Durability Validated Using Field and Drive Cycle Testing.” Journal of the Electrochemical Society, vol. 165, no. 6, 2018, pp. F3085–F3093, 10.1149/2.0101806jes.

15. ZHANG, S, et al. “A Review of Accelerated Stress Tests of MEA Durability in PEM Fuel Cells.” International Journal of Hydrogen Energy, vol. 34, no. 1, Jan. 2009, pp. 388–404, 10.1016/j.ijhydene.2008.10.012.

16. Rodgers, Marianne P., et al. “Perfluorinated Sulfonic Acid Membrane and Membrane Electrode Assembly Degradation Correlating Accelerated Stress Testing and Lifetime Testing.” ECS Transactions, vol. 58, no. 1, 31 Aug. 2013, pp. 129–148, 10.1149/05801.0129ecst.
17. W.C. Schumb, C.N. Satterfield, R.L. Wentworth, Reinhold Pub. Co., New York, 1955, p. 492.
18. Ohma, Atsushi, et al. “Phenomenon Analysis of PEFC for Automotive Use (1) Membrane Degradation Behavior during OCV Hold Test.” ECS Transactions, vol. 3, no. 1, 21 Dec. 2019, pp. 519–529, 10.1149/1.2356173.
19. Burlatsky, Sergei F., et al. “Aspects of PEMFC Degradation.” ECS Transactions, vol. 1, no. 8, 28 June 2006, pp. 239–246, 10.1149/1.2214557.
20. Zhao, D., et al. “The Effect of Platinum in a Nafion Membrane on the Durability of the Membrane under Fuel Cell Conditions.” Journal of Power Sources, vol. 195, no. 15, Aug. 2010, pp. 4606–4612, 10.1016/j.jpowsour.2010.02.043.
21. Macauley, N., et al. “Pt Band Formation Enhances the Stability of Fuel Cell Membranes.” ECS Electrochemistry Letters, vol. 2, no. 4, 5 Feb. 2013, pp. F33–F35, 10.1149/2.007304eel.
22. Endoh, Eiji, et al. “Degradation Mechanism of the PFSA Membrane and Influence of Deposited Pt in the Membrane.” ECS Transactions, vol. 11, no. 1, 28 Sept. 2007, pp. 1083–1091, 10.1149/1.2781021.
23. Watanabe, Masahiro, et al. “Self-Humidifying Polymer Electrolyte Membranes for Fuel Cells.” Journal of the Electrochemical Society, vol. 143, no. 12, 1 Dec. 1996, pp. 3847–3852, 10.1149/1.1837307.
24. Alavijeh, Alireza Sadeghi, et al. “Microstructural and Mechanical Characterization of Catalyst Coated Membranes Subjected to in Situ Hygrothermal Fatigue.” Journal of the Electrochemical Society, vol. 162, no. 14, 2015, pp. F1461–F1469, 10.1149/2.0471514jes.
25. Lai, Yeh-Hung, et al. “Viscoelastic Stress Analysis of Constrained Proton Exchange Membranes under Humidity Cycling.” Journal of Fuel Cell Science and Technology, vol. 6, no. 2, 20 Feb. 2009, 10.1115/1.2971045
26. Kreitmeier, Stefan, et al. “Polymer Electrolyte Membrane Durability -Local Degradation at Pinholes.” ECS Transactions, vol. 50, no. 2, 15 Mar. 2013, pp. 927–933, 10.1149/05002.0927ecst.
27. Lakshmanan, Balasubramanian, et al. “Polyetheretherketone Membranes for Elevated Temperature PEMFCs.” Electrochemical and Solid-State Letters, vol. 6, no. 12, 2003, p. A282, 10.1149/1.1619647.
28. Lü, Weizhong, et al. “The Effects of Pinholes on Proton Exchange Membrane Fuel Cell Performance.” International Journal of Energy Research, vol. 35, no. 1, 28 Dec. 2010, pp. 24–30, 10.1002/er.1728.
29. Zhang, Shengsheng, et al. “Effects of Open-Circuit Operation on Membrane and Catalyst Layer Degradation in Proton Exchange Membrane Fuel Cells.” Journal of Power Sources, vol. 195, no. 4, 15 Feb. 2010, pp. 1142–1148, 10.1016/j.jpowsour.2009.08.070.

30. Vengatesan, S., et al. “Diagnosis of MEA Degradation under Accelerated Relative Humidity Cycling.” Journal of Power Sources, vol. 196, no. 11, June 2011, pp. 5045–5052, 10.1016/j.jpowsour.2011.01.088.

31. Kusoglu, Ahmet, and Adam Z. Weber. “New Insights into Perfluorinated Sulfonic-Acid Ionomers.” Chemical Reviews, vol. 117, no. 3, 23 Jan. 2017, pp. 987–1104, 10.1021/acs.chemrev.6b00159.

32. Kai, Yusuke, et al. “Crack Formation in Membrane Electrode Assembly under Static and Cyclic Loadings.” Journal of Fuel Cell Science and Technology, vol. 10, no. 2, 25 Mar. 2013, 10.1115/1.4023878.

33. M.R. Tarasevich, A. Sadkowski, E. Yeager, B.E. Conway, J. O’M. Bockris,in: E. Yeager, S.U.M. Khan, R.E. White (Eds.), Comprehensive Treatise of Electrochemistry, vol. 7, Plenum Press, New York, 1983, p.301.

34. D.L. Damron (2016). “Improved Characterization and Movement of the Platinum Band in a Proton Exchange Membrane Fuel Cell.” Electronic Theses and Dissertations (ETDs) 2008+. T, University of British Columbia. Doi:http://dx.doi.org/10.14288/1.0228789.

35. Sethuraman, Vijay A., et al. “Hydrogen Peroxide Formation Rates in a PEMFC Anode and Cathode.” Journal of the Electrochemical Society, vol. 155, no. 1, 2008, p. B50, 10.1149/1.2801980.

36. Liu, Wen, and David Zuckerbrod. “In Situ Detection of Hydrogen Peroxide in PEM Fuel Cells.” Journal of the Electrochemical Society, vol. 152, no. 6, 2005, p. A1165, 10.1149/1.1904988

37. Bernardi, Dawn M., and Mark W. Verbrugge. “Mathematical Model of a Gas Diffusion Electrode Bonded to a Polymer Electrolyte.” AIChE Journal, vol. 37, no. 8, Aug. 1991, pp. 1151–1163, 10.1002/aic.690370805

38. Francia, Carlotta, et al. “Estimation of Hydrogen Crossover through Nafion® Membranes in PEMFCs.” Journal of Power Sources, vol. 196, no. 4, Feb. 2011, pp. 1833–1839, 10.1016/j.jpowsour.2010.09.058.

39. Vilekar, Saurabh A., and Ravindra Datta. “The Effect of Hydrogen Crossover on Open-Circuit Voltage in Polymer Electrolyte Membrane Fuel Cells.” Journal of Power Sources, vol. 195, no. 8, Apr. 2010, pp. 2241–2247, 10.1016/j.jpowsour.2009.10.023.

40. Sompalli, Bhaskar, et al. “Membrane Degradation at Catalyst Layer Edges in PEMFC MEAs.” Journal of the Electrochemical Society, vol. 154, no. 12, 2007, p. B1349, 10.1149/1.2789791.

41. Schlögl, Katrin, et al. “Identical-Location TEM Investigations of Pt/c Electrocatalyst Degradation at Elevated Temperatures.” Journal of Electroanalytical Chemistry, vol. 662, no. 2, Nov. 2011, pp. 355–360, 10.1016/j.jelechem.2011.09.003;

42. Yu, Yi, et al. “A Review on Performance Degradation of Proton Exchange Membrane Fuel Cells during Startup and Shutdown Processes: Causes, Consequences, and Mitigation Strategies.” Journal

of Power Sources, vol. 205, May 2012, pp. 10–23, 10.1016/j.jpowsour.2012.01.059;

43. Moore, Michael, et al. “A Numerical Study on the Impact of Cathode Catalyst Layer Loading on the Open Circuit Voltage in a Proton Exchange Membrane Fuel Cell.” Journal of the Electrochemical Society, vol. 168, no. 4, 1 Apr. 2021, p. 044519, 10.1149/1945-7111/abf50c.

44. Sadeghi Alavijeh, A., et al. “Decay in Mechanical Properties of Catalyst Coated Membranes Subjected to Combined Chemical and Mechanical Membrane Degradation.” Fuel Cells, vol. 15, no. 1, 28 Nov. 2014, pp. 204–213, 10.1002/fuce.201400040.

45. Stanic, Vesna. “Mechanism of Pinhole Formation in Membrane Electrode Assemblies for PEM Fuel Cells.” ECS Proceedings Volumes, vol. 2004-21, no. 1, Jan. 2004, pp. 391–401, 10.1149/200421.0391pv.

46. Kundu, Sumit, et al. “Mechanical Properties of NafionTM Electrolyte Membranes under Hydrated Conditions.” Polymer, vol. 46, no. 25, 28 Nov. 2005, pp. 11707–11715, www.sciencedirect.com/science/article/abs/pii/S0032386105013674, 10.1016/j.polymer.2005.09.059.

Chapter 4

Effect of current density on membrane degradation under the combined chemical and mechanical stress test in the PEMFCs

Abstract

This chapter elucidates the effects of current density on membrane degradation under combined mechanical and chemical stress tests. Relative humidity (RH) cycling tests using hydrogen gas and air are conducted on a polymer electrolyte membrane fuel cell based membrane NRE211 at the open circuit voltage (OCV), 0.05 and 0.3 Acm^{-2} conditions. The different current density conditions result in different in-plane membrane stresses and H_2O_2 formation rates during the test. After every 200 RH cycles, membrane integrity is assessed via the hydrogen crossover rate and OCV. Furthermore, catalytic combustion is analyzed during OCV measurement using the thermal imaging method employing a high-transmittance glass at the cathode side. The membrane fails after 1,600, 1,800, and 2,200 RH cycles under the OCV condition, 0.05 and 0.3 Acm^{-2}, respectively. The vigorous membrane degradation under OCV conditions can be attributed to the higher mechanical stress and H_2O_2 formation rate. Hotspots created due to the combustion between the crossover hydrogen and air are successfully captured, with a maximum temperature rise ranging from 15 to 16 °C compared with a given cell temperature of 80 °C. A one-dimensional heat transfer model can fairly well predict the change in gas diffusion layer (GDL) temperature induced by catalytic combustion. The combustion heat is transferred predominantly to the hydrogen stream owing to the high convective heat transfer coefficient from GDL to hydrogen stream. Moreover, a post-mortem analysis (SEM imaging) revealed the presence of pinholes, through-membrane cracks, and membrane thinning at the hotspot locations.

4.1. Introduction

Green hydrogen generated from renewable sources and fuel cell technology can serve as the foundation for achieving net-zero emissions by the year 2050 [1, 2]. Presently, internal combustion engines (ICEs) are being employed in the transportation sector (including rail, road, aviation, and shipping), accounting for 60% of the global oil demand [3]. In addition, the burning of oil-derived fuels in ICEs releases CO_2, SO_2, NO_x, and particulate matter, which cause serious environmental problems, such as global warming, climate change, acid rain, and local air pollution. According to the International Energy Agency (IEA), CO_2 emissions from the transport sector comprise 24% of total global emissions [4]. The use of green hydrogen in polymer electrolyte membrane fuel cell-driven vehicles is an appropriate solution for reducing emissions and the dependence on oil-derived fuels in transportation. Polymer electrolyte

membrane fuel cell-driven vehicles offer distinct advantages [5, 6], including no emissions (only water is produced during operation), quick start-up at sub-zero temperature (-30 °C), high power density, high energy conversion efficiency, long cruising range, short refueling duration (< 3 min), and quiet operation.

Membrane durability is the key to the success of polymer electrolyte membrane fuel cell (PEMFC) applications, especially in the transportation sector, where higher durability, such as 150,000 miles (light duty vehicles), 500,000 miles (bus), and 1 million miles (heavy duty vehicles), is expected for PEMFC [7]. In the PEMFC applications on the transportation sector, the membrane is ultra-thin (for example, a 10.5 μm membrane in the Toyota Mirai fuel cell vehicle [7]) to get higher output and easier water management. Moreover, the membrane experiences harsh operating conditions such as load cycles [8], idle conditions [9], shutdown/start-up cycles [10 ,11], and freezing starts [12].

These impacts are categorized into two membrane degradation mechanisms: chemical and mechanical. Mechanical stresses on the constrained membrane in PEMFCs result from dimensional changes in the membrane due to the dynamic fluctuations in its temperature and water content [13 -16], leading to the formation of cracks on the membrane and delamination between the membrane and catalyst layers. Meanwhile, chemical stress decomposes perfluorosulfonic acid (PFSA) membranes. A small amount of hydrogen peroxide (H_2O_2) is formed, and the presence of contaminant cations (Fe^{2+}, Fe^{3+}, Cu^{2+}, Ti^{3+}, Mg^{2+}, Na^{+}) yields free radicals, such as •OH, ••OOH, and •H. These radicals, then, are responsible for the chemical decomposition of the PFSA membrane structure e.g., scissoring the main chain of the structure, unzipping the side chain, and terminating groups, which reduce the membrane thickness and increase the proton conducting resistance [17-19]. Many strategies have been proposed to mitigate these stresses (mechanical and chemical) for prolonged membrane lifetimes. Two viable approaches for improving the chemical and mechanical durability of the membrane include doping radical scavengers, such as Ce^{3+} or Mn^{2+}, into the ionomer to prevent radical generation [20,21] and reinforcing the membrane with an e-PTEE layer [22, 23].

To understand each mechanism, membranes have often been investigated separately using accelerated stress tests. However, in the actual operation of fuel cell vehicles, both chemical and mechanical mechanisms have a simultaneous synergistic effect on the membrane. In particular, the increase in leakage of reactant gases through cracks caused by mechanical stress promotes the generation of hydrogen peroxide, consequently enhancing chemical degradation. Reactive species decompose the membrane, reducing its tensile strength [24,25] and hastening mechanical membrane degradation. Therefore, to fully understand membrane degradation and establish appropriate mitigation strategies for extending membrane lifetime, it is essential to investigate the degradation process using a relevant combined mechanical and chemical stress test that resembles fuel cell operation.

In addition to the mechanical and chemical degradation mentioned above, thermal degradation should also be considered to increase the durability of PEMFCs. Although the membrane's function as a

gas separator in PEMFCs, unavoidable crossover through the mechanically and chemically degraded membrane leads to the formation of a combustible mixture at the electrodes. The mixture then combusts in the presence of platinum in the catalyst layers, which results in exothermic heat release, consequently heating up the membrane and resulting in a thermal decomposition on the membrane. The increase in the membrane temperature is determined by the correlation between the heat generation rate (due to combustion) and heat transfer characteristics in the cell. The self-cooling capability primarily depends on the cell structure (components) and coolant flowing next to each cell. For instance, the GDL overlapping catalyst is regarded as a high-heat conductor [26]. The crossover rate and catalytic activity determine the amount of heat emitted during the combustion.

When the membrane is intact, the crossover rate is low for an intact membrane, and the amount of combustible mixture and combustion heat rate are minimal. In a previous study, the combustion heat rate was estimated to be 7.4 $mWcm^{-2}$, corresponding to a hydrogen crossover rate of approximately 5 $mAcm^{-2}$ through a fresh 25 μm membrane [27]. The estimated combustion heat was less than that in a conventional fuel cell operation (electricity generation). Thus, when the membrane is intact, the combustion heat originating from the low crossover rate can be released to the outside and does not cause an abnormal temperature increase.

In contrast, problems arise when the membrane degrades (chemically and/or mechanically), and thinning and localized cracks are formed. In this case, a higher hydrogen crossover rate causes a considerable increase in hydrogen concentration in the mixture with air at the cathode. The heat production rate from the catalytic combustion of the gas mixture can be significantly higher than the cell's capacity for cooling or the self-dissipation of the cell, ultimately increasing the membrane temperature. In an accidental scenario, when the combustion heat flux exceeds the maximum dissipated heat flux of the cell, the membrane could thermally decompose, eventually leading to an abrupt collapse of the cell. Few reports have been published about fatal membrane damage caused by accidental combustion in PEMFCs [26, 28, 29] and polymer electrolyte membrane water electrolyzers (PEMWEs) [30]. Thermal decomposition of the membrane, owing to accidental combustion, is a secondary and dangerous degradation mechanism. The previous chapter (Chapter 3) showed some thermal decomposition due to accidental combustion when the mechanical and chemical degradation progressed. However, the current density in Chapter 3 was adjusted to zero to simplify the phenomena in the cell when mechanical, chemical, and thermal degradation progress. It is noted that, once the current is applied, the cell voltage decreases and water forms as a product of an electrochemical reaction in the cell. The decreased cell voltage changes the production rate of hydrogen peroxide. The produced water and its phase change (latent heat) influence the heat balance in the cell.

Therefore, this Chapter 4 aims to investigate the effects of current density on membrane durability and elucidate the catalytic combustion phenomenon in PEMFCs under combined mechanical and chemical stress tests. At a worse case, some thermal decomposition is superimposed. RH cycling durability tests using hydrogen gas and air were carried out under the open circuit voltage (OCV) condition and at current

densities of 0.05 and 0.3 Acm^{-2}. Comparing the results under the three testing conditions figures out the effect of different current densities on the degree of mechanical, chemical, and thermal degradation processes. In particular, this chapter is dedicated to answering the following questions:

(1) Does the large amount of water produced by higher current density operation moderate the wet and dry situation established by the RH cycle and mitigate the in-plane stresses, resulting in the suppression of mechanical degradation?

(2) Does lowering the cell voltage by higher current density operation moderate the formation rate of hydrogen peroxide (H_2O_2) at the anode side [31], resulting in the suppression of chemical degradation?

After every 200 RH cycles, the membrane integrity is evaluated and compared for the above experimental conditions via important indicators, including the hydrogen crossover rate and OCVs. Moreover, IR imaging with a visualization cell is used to capture the temperature rise of the GDL induced by the catalytic combustion of leaked hydrogen gas through the membrane in the cathode compartment. In the postmortem analysis, SEM, assisted by the thermal imaging results, helps to reveal the distribution of defects forming in the degraded membrane. Cracking and membrane thinning are mainly caused by the simultaneous impacts of chemical and mechanical degradation. Meanwhile, the thermal decomposition of the membrane causes pinhole formation when the combustion heat reaches the maximum dissipated heat flux of the cell structure or the combustion process transitions to the accidental scale. As a result, the SEM observation also aids in the detection of pinholes in the degraded membrane, confirming the occurrence of thermal decomposition caused by accidental combustion.

4.2. Experimental

4.2.1. Experimental apparatus

Figure 4.1a shows the flow diagram of the experimental system, designed to conduct accelerated stress tests and periodic electrochemical evaluations for the visualization cell. Dry or humidified hydrogen gas was supplied to the anode side of the cell at a regulated flow rate. Meanwhile, dry air or nitrogen gas was introduced to the cathode side to prevent water from changing the ZnS glass characteristics. An IR camera was placed next to the cell to capture the temperature change in the cathode GDL caused by combustion.

Figure 4.1b shows a schematic cross-section of the cell where the catalyst-coated membrane (CCM) is sandwiched between two GDLs (Sigracet 34BC, thickness of 315 mm), two co-current serpentine (stainless steel gold-plated) flow fields with 2 mm-wide channels and 3 mm lands, and two SS316 clamping plates. The CCM was fabricated using the method described in chapter 3 and a prior paper [27]. A 52 mm × 52 mm square window was perforated in the cathode's clamping plate. A high-transmissivity glass (ZnS glass), 40 mm in diameter and 2 mm thick, was installed on a composite frame placed between the clamp

plate and the flow field. This structure allowed the IR camera to accurately observe the temperature distribution on the surface of the GDL.

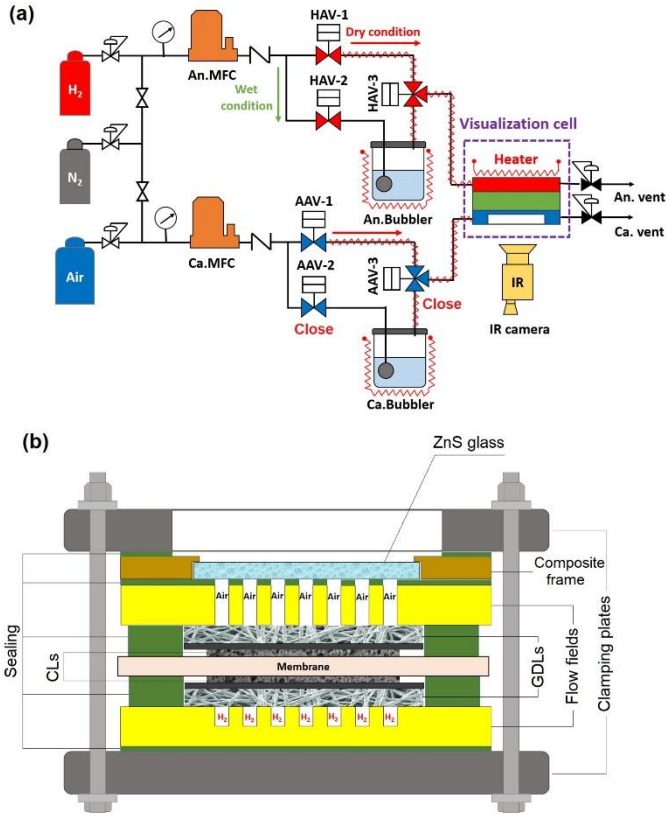

Fig. 4. 1. (a) Experimental apparatus, (b) schematic of cross-sectional cell structure.

Figure 4.2 illustrates the durability-testing procedure. To ensure the complete hydration of the membrane prior to the durability test, the cells were incubated with 100%RH nitrogen gas (just on the anode side) for a day at a cell temperature of 80 °C. During the RH cycling test, hydrogen gas was fed to the anode side at a flow rate of 200 Nccm (normal cm^3 min^{-1}), and the humidity was alternately changed between the dry (2 min) and wet portions (100%RH for 3 min) by controlling valves HAV-1, HAV-2, and HAV-3, as shown in Fig.4a. Meanwhile, 100 Nccm of dry air was continuously fed into the cathode compartment. Dry air prevented the formation of water droplets. It should be noted that water droplets absorb IR rays and degrade ZnS glass color, leading to inaccurate temperature measurements. During the RH cycling test, the membrane resistance and cell voltage were measured using a high-frequency resistance device (Tsuruga, 3566) and then recorded using a data logger (Graphtec Corporation, GL840) every 1 s. For every 200 RH cycles, there was a periodic evaluation in which electrochemical parameters, including the electrochemical surface area (ECSA), hydrogen crossover rate, and OCVs, were measured. In addition, the IR camera captured the temperature distribution on the surface of the GDL through the ZnS-glass window during OCV measurements. When the hydrogen crossover rate exceeded the lowest explosion level (4vol. % in the mixture with 100 Nccm air at the cathode side), the RH cycling test was stopped for

safety. Before the periodic evaluation, the cell was stabilized with 100%RH nitrogen gas on the anode side and dry nitrogen gas on the cathode side for 30 min at a cell temperature of 80 °C.

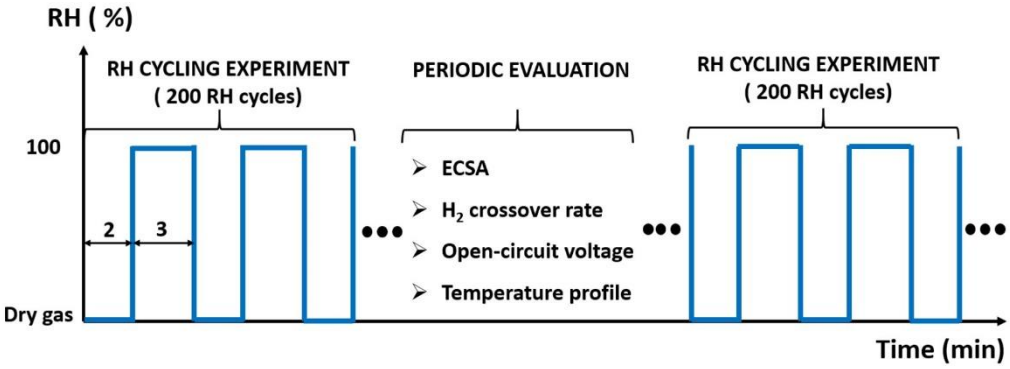

Fig. 4. 2. Experimental procedure for durability testing.

The three experimental conditions for different current densities are listed in Table 4.1. As mentioned in the introduction section, these conditions provide insight into the effect of different current densities on mechanical and chemical stresses on the membrane. The current densities were selected based on the actual operation of the FCVs. OCV and 0.05 Acm^{-2} represent the idle condition, while 0.3 Acm^{-2} may stand for the running mode.

Table 4. 1. Experimental conditions

Anode/Cathode reactant gas	Relative humidity	Current density (Acm^{-2})	Anode/Cathode gas flow rate (Nccm)	Anode/cathode outlet pressure
H_2/Air	Anode: 2 min dry/3 min 100%RH Cathode: Dry air	0	200/100	Atmospheric pressure
H_2/Air	Anode: 2 min dry/3 min 100%RH Cathode: Dry air	0.05	200/100	Atmospheric pressure
H_2/Air	Anode: 2 min dry/3 min 100%RH Cathode: Dry air	0.3	200/100	Atmospheric pressure

4.2.2. Electrochemical and thermal imaging measurements

A periodic evaluation was conducted for every 200 RH cycles, as shown in Fig. 4.2. Electrochemical (including ECSA, hydrogen crossover rate, and OCVs) and thermal imaging measurements were conducted. Cyclic voltammetry (CV) and linear sweep voltammetry (LSV) were performed using a voltammetry system (SP300, BioLogic Science Instruments) to measure the ECSA of the cathode and hydrogen crossover rate through the membrane, respectively. The crossover rate and ECSA are important indicators for evaluating membrane degradation and catalyst decay. During the crossover rate and ECSA measurements, fully humidified hydrogen gas (150 Nccm) was fed into the anode side (counter and reference electrode), and dry nitrogen gas (200 Nccm) was fed into the cathode side (working electrode).

The cell temperature was maintained at 80°C, and nitrogen gas was stopped immediately before starting the CV measurements. The hydrogen desorption area at the cathode electrode is a measure of the ECSA. The applied potential ranges from 0.05 V to 0.9 V vs. NHE (Normal Hydrogen Electrode (H_2/H^+) with a scan rate of 50 mVs^{-1}. Meanwhile, the LSV technique can reveal the hydrogen crossover rate, expressed in units of the current density. The applied potential is swept from 0.05 to 0.5 V versus NHE, with a scan rate of 0.5 mV s^{-1}. The crossover current density is then calculated at an applied potential of 0.4 V versus NHE, at which the leaked hydrogen gas from the anode gets completely oxidized on the cathode catalyst [32]. When the fatal defects appear in the membrane, the hydrogen crossover rate increases, and the current density saturation in the potential from 0.4 to 0.5 V corresponds to the crossover current density. Two different pressure cases were used to measure the hydrogen crossover rate: (a) atmospheric pressure in the anode and cathode compartments and (b) the introduction of 20-kPa backpressure alone in the anode compartment. The "20-kPa anode backpressure," despite having a differential pressure of only 20-kPa, facilitates the early detection of serious membrane defects, such as pinholes and through-thickness cracks.

During the periodic evaluation, OCV measurements were also performed after measuring the hydrogen crossover rate. The operating conditions in the OCV state were as follows: fully humidified H_2 at a flow rate of 150 Nccm and dry air at a flow rate of 200 Nccm fed into the anode and cathode compartments, respectively. The cell temperature was maintained at 80 °C. The OCVs were measured at atmospheric pressure and anode backpressure of 20-kPa, which are similar to the pressure conditions used for the measurements of the hydrogen crossover rate. During OCV measurement, thermographs (IR images) of the GDL surface were captured using an IR camera (NEC Avio, R450) through a high-transmittance glass (ZnS) window embedded at the cathode at a cell temperature of 80 °C. The IR camera's spectral range is 8 to 14 μm, and the measuring range is -40 to 650 °C with an accuracy of ±1 °C (when the ambient temperature is in the range from 20 to 30 °C). In order to accurately measure the GDL surface temperature, camera emissivity is calibrated according to the cell temperature on the cathode side. As a result, a substantial emissivity was determined to be 0.68 under the condition that the cell temperature is 80 °C while N_2 was fed to both the cathode and anode sides. Each IR image has a standard size of 480 pixels in width and 360 pixels in height. The (standard) space and time resolution are 330 pixels per inch (PPI) and 5 frames per second (or 5 Hertz), respectively. The GDL temperature was obtained from the IR images by using the InfreC Analyzer (NS9500 standard).

4.2.3. Postmortem analysis

The microstructural changes in the degraded CCMs were examined using a focused ion beam-scanning electron microscope (FIB-SEM; Helios Nanolab 600i, FEI) once the durability tests were complete. The samples were selected from the deteriorated CCMs where the hotspots appeared clearly in the IR images.

4.3. Results and discussion

4.3.1. Changes in membrane resistance and cell voltage during durability tests

Figure 4.3a, b, and c describe the changes in membrane resistance and cell voltage during the RH cycling tests at OCV and current densities of 0.05, and 0.3 Acm^{-2}, respectively. Cell voltage (red-colored line) follows a general characteristic, where higher current density decreases cell voltage. The cell voltage synchronizes with the RH cycle (the alternative change of dry and wet states in the hydrogen stream at the anode). It is because the RH cycle changes the membrane resistance (blue-colored line) and ohmic overvoltage, resulting in the change in cell voltage.

As shown in Fig. 4.3a, b, and c, the membrane resistance synchronizes with the RH cycle. Resistance oscillates within different ranges depending on the testing conditions, for example, 136 $m\Omega cm^2$ (in the OCV condition), 137 $m\Omega cm^2$ (in the condition of 0.05 Acm^{-2}) and 87 $m\Omega cm^2$ (in the condition of 0.3 Acm^{-2}). Resistances at OCV and 0.05 Acm^{-2} are similar because the amount of water generated at low current density was considerably small. In contrast, higher water production at 0.3 Acm^{-2} considerably narrows the resistance change compared to other conditions. Because the resistance of the membrane depends mainly on its water content, the variation in the resistance during the RH cycling test indicates a change in the membrane water content. In a PEMFC, the change in water content leads to expansion and shrinkage of the constrained membrane, resulting in the formation of in-plane stresses. These stresses act as fatigue loads, causing the mechanical degradation of the membrane over time. However, a wider membrane resistance range induced by a durability test results in a greater variance in water content, ultimately leading to a higher membrane fatigue stress.

To investigate the effect of mechanical stress on membrane durability, the in-plane stresses formed in the membrane under three different testing conditions were calculated. The details of the in-plane stress computation were indicated in Chapters 2 and 3 of this dissertation. Figures 4.4a, b, and c are the estimated value of water content and corresponding in-plane stress formed in the membrane during the durability tests at three testing conditions. For quantitative analysis, the average values of the membrane water content and stress range were calculated (from Figs. 4.4a, b, and c) and summarized in Table 4.2. During the RH cycling test, membrane water content fluctuates around the average value ($\lambda_{average}$) in a range ($\Delta\lambda$). Under the average ($\lambda_{average} - \Delta\lambda/2 < \lambda_i < \lambda_{average}$), the membrane shrinks, and tensile stress is induced. Contrarily, the membrane expands, and compressed stress is induced when the water content is higher than the average ($\lambda_{average} < \lambda_i < \lambda_{average} + \Delta\lambda/2$). The stress range ($\Delta\sigma$) is one of the most important indicators of mechanical stress in a membrane. With a higher stress range, mechanical membrane deterioration is more severe. Based on data in Table 4.2, the stress range is highest at 6.74 MPa in the RH cycling at OCV condition and reduces with increasing applied current density due to water generation at the cathode and hydration of membrane. The magnitude of the stress range indicates faster membrane deterioration with the RH cycling at the OCV condition.

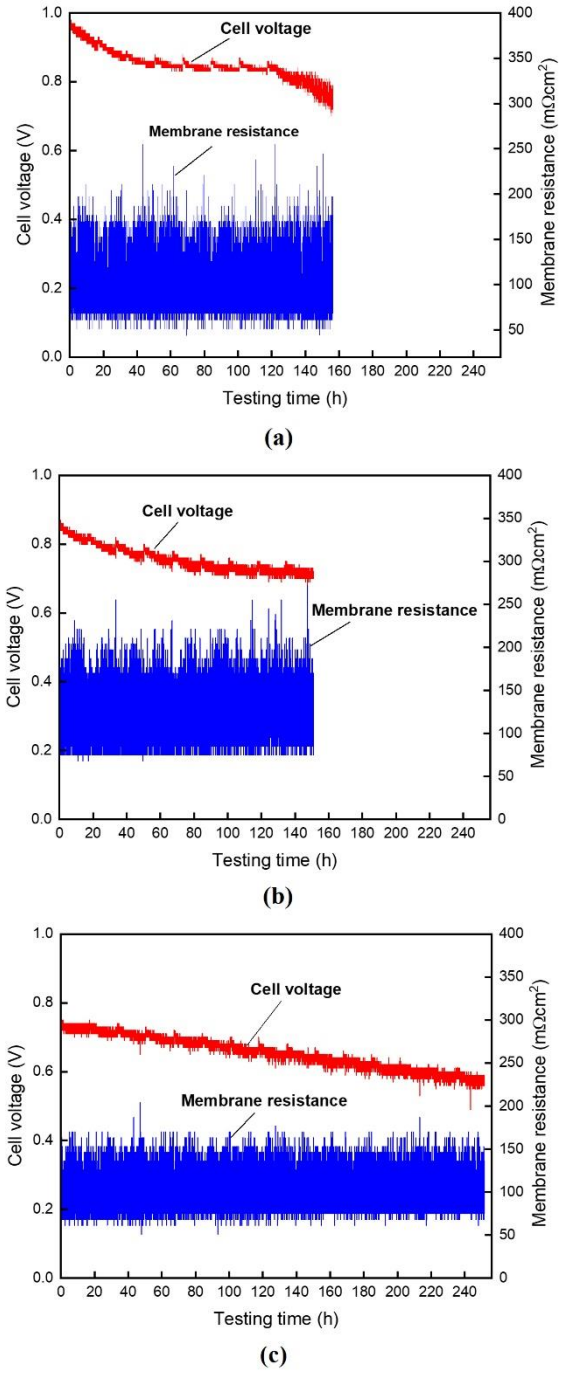

Fig. 4. 3. Variations in membrane resistance and cell voltage during the RH cycling tests at (a) OCV condition, (b) 0.05 Acm^{-2}, and (c) at 0.3 Acm^{-2}.

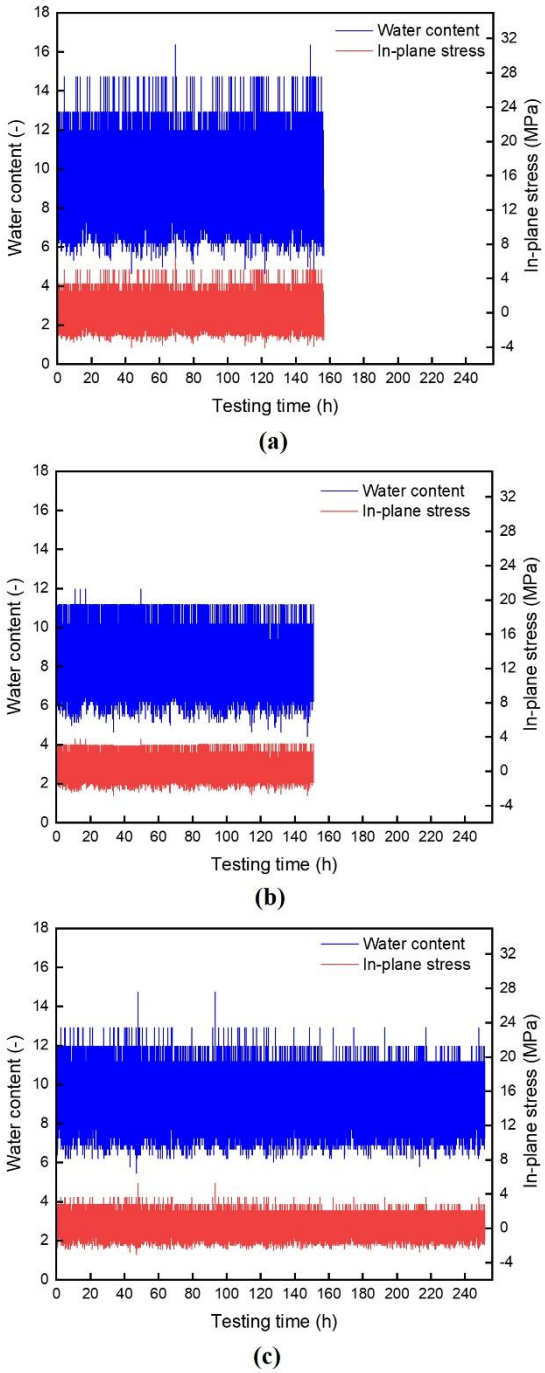

Fig. 4. 4. Predictions of the water content and in-plane stress formation in the membrane during the RH cycling tests at (a) OCV condition, (b) 0.05 Acm^{-2}, and (c) at 0.3 Acm^{-2}.

Table 4. 2. Summary of the prediction of water content variation and corresponding stress range at different testing conditions based on the membrane resistance data.

Testing conditions	**Average membrane resistance change, ΔR_{PEM} (mΩcm^2)**	**Average water content change, $\Delta\lambda$**	**Average stress range, $\Delta\sigma$ (MPa)**
RH cycling at OCV condition	136	7.49	6.74
RH cycling at 0.05 Acm^{-2}	137	5.72	5.13
RH cycling at 0.3 Acm^{-2}	87	5.06	4.67

The hydrogen peroxide (H_2O_2) formed in a cell can trigger the formation of free radicals, leading to chemical membrane decomposition, as mentioned in Section 4.1. In order to evaluate the chemical stress on the membrane, the formation rate of H_2O_2 is calculated according to the procedure mentioned in Chapter 3. Theoretically, H_2O_2 can be formed at the cathode (when the potential is under 0.695 V), inside the membrane where the Pt band exists and at the anode. However, the cathode potentials in the three testing conditions at the BOL are higher than 0.695 V, H_2O_2 formation at the cathode side is less likely. In addition, the H_2O_2 formation mechanism initiated by the Pt band seems improbable at the beginning of life (BOL) because the Pt band is only formed under some degradation processes. Thus, the formation of H_2O_2 at the anode is the most plausible mechanism. This assumption is consistent with the findings of Liu and Zuckerbrod [33] that H_2O_2 is predominantly produced on the anode side by oxygen reduction. The estimated formation rates of H_2O_2 under the three testing conditions in wet and dry conditions (the number indicated inside the round brackets), were calculated via the empirical Equation (4.1) [31] and summarized in Table 4.3.

The H_2O_2 formation rate at the anode-membrane interface ($\dot{Q}_{H_2O_2,An}$) using an empirical relation as follows:

$$\dot{Q}_{H_2O_2,An} = \chi_{H_2O_2}\dot{Q}_{O_2}, \qquad (4.1)$$

where $\chi_{H_2O_2}$ is the fraction of O_2 that is converted to H_2O_2 and is dependent on the water activity of the membrane, a_w, as follows:

$$\chi_{H_2O_2} = 0.2081 - 0.1208\times a_w - 0.072\times a_w^2 - 2.132\times 10^{-14} a_w^3 \qquad (4.2)$$

It can be seen Fig.4.5a that $\chi_{H_2O_2}$ increases with a decrease in water activity in the membrane (or decreased RH). Thus, during the RH cycling tests, $\chi_{H_2O_2}$ in the dry portion is higher than that in the wet portion. $\dot{Q}_{O_2}$ is the oxygen crossing rate from the cathode to the anode through the membrane (molcm^{-2}s^{-1}), which is calculated using Fick's law of diffusion in Eq. (4.3) as follows

$$\dot{Q}_{O_2} = D_{O_2\text{-PEM}} \frac{p'_{O_2,Ca} - p_{O_2,An}}{H_{O_2\text{-PEM}} L_{PEM}} \approx D_{O_2\text{-PEM}} \frac{p'_{O_2,Ca}}{H_{O_2\text{-PEM}} L_{PEM}} \quad (4.3)$$

where $D_{O_2\text{-PEM}}$ and $H_{O_2\text{-PEM}}$ are diffusion coefficients and Henry's constants of oxygen diffusion through Nafion membrane, respectively (cm^{2}s^{-1}); L_{PEM} is thickness of the membrane (cm); and $p'_{O_2,Ca}$ and $p_{O_2,An}$ are the actual partial pressure of oxygen at the cathode and anode, respectively (atm). Assuming that oxygen will react completely at the anode, the concentration of oxygen at the cathode is considered negligible (or $p_{O_2,An} \approx 0$). As a result, $\dot{Q}_{O_2}$ increases linearly with increasing RH and is higher with lower applied current density due to higher actual oxygen partial pressure ($p_{O_2,Ca}$), as shown in Fig. 4.5a.

Table 4. 3. H_2O_2 formation rate at the anode-membrane interface

Properties	**Value**		
Current density, i (Acm^{-2})	0	0.05	0.3
Cell voltage at BOL, V_{cell} (V)	0.96	0.86	0.74
Inlet oxygen partial pressure (in the dry air stream), $p_{O_2,Ca}$ (atm)	0.2099		
Actual partial pressure of oxygen at the cathode, $p'_{O_2,Ca}$(atm)	0.2099	0.2023	0.1640
Diffusion coefficients of oxygen through Nafion membrane [31], $D_{O_2\text{-PEM}} = 9.78 \times 10^{-8} + 3.5 \times 10^{-9}T + 10^{-9}a_w$ (cm^{2}s^{-1}) where T =353 K, a_w is water activity of the membrane.	1.01×10^{-4} (1.33×10^{-6})		
Henry's constants of oxygen diffusing through the Nafion membrane [34], $H_{O_2\text{-PEM}} = exp(\frac{-666}{T} + 14.1)$ (atm cm^{3}mol^{-1}) where T =353 K.	201615		
Membrane thickness, L_{PEM} (cm)	0.0025		

Oxygen crossing rate through the membrane from the cathode to anode (Eq. (4.3)), $\dot{Q}_{O_2}$ (molcm^{-2}s^{-1})	4.22×10^{-8} (5.55×10^{-10})	4.07×10^{-8} (5.35×10^{-10})	3.3×10^{-8} (4.34×10^{-10})
O_2 fraction reducing to H_2O_2 (Eq. (4.2)) [31], $\chi_{H_2O_2}$ (-)	0.0153 (0.2081)		
H_2O_2 generation rate ($\dot{Q}_{H_2O_2,An}$) at the anode (Eq. (4.1)), (molcm^{-2}s^{-1})	6.46×10^{-10} (1.16×10^{-10})	6.22×10^{-10} (1.11×10^{-10})	5.04×10^{-10} (0.90×10^{-10})

Table 4.3 and Fig. 4.5b suggest that a lower current density promote H_2O_2 formation at the anode. The H_2O_2 formation rate at OCV condition is 1.04 and 1.28 times higher than that at 0.05 and 0.3 Acm^{-2}, respectively. Furthermore, as can be seen in Fig.4.5b, the formation rate of H_2O_2 increases with RH until reaching a peak at around 60% RH and then decreases with RH. Because the dry and wet portions are kept at 2 and 3 min, respectively, in the RH cycling tests, the difference in H_2O_2 formation rates between the dry and wet portions is compared and shown in Table 4.3. Apparently, the formation rate of H_2O_2 at the anode is primarily determined by the oxygen crossing rate, and it is approximately six times higher in the wet portion than in the dry portion. The chemical stress on the membrane induced by the RH cycling test was harsher at lower current densities and wet operating conditions, which accelerated the chemical deterioration of the membrane. Furthermore, the above calculation was conducted using the BOL CCM. However, under the RH cycling tests, the crossover rate of oxygen increased owing to membrane degradation, resulting in an increase in the H_2O_2 formation rate at the anode. Additionally, the cathode potential in the condition of 0.3 Acm^{-2} tended to fall below 0.695 V after 68 h of testing (see Fig. 4.3c), indicating H_2O_2 generation on the cathode side [35].

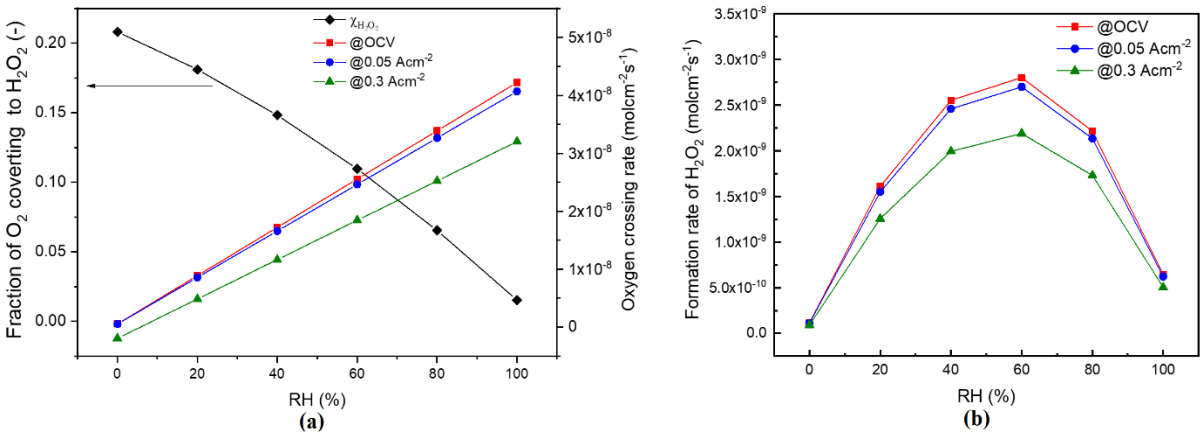

Fig. 4. 5. The dependence of (a) the fraction of O_2 converting to H_2O_2 and the oxygen crossing rate, and (b) the H_2O_2 formation rate on the relative humidity at three testing conditions.

Furthermore, Figs. 4.3a, b, and c show the decrement in the cell voltage during the RH cycling tests at three conditions. By fitting the voltage data, the decay rates of the voltage are 1.43 (0.11), 0.87

(0.07), and 0.60 (0.05) mVh^{-1} ($mVcycle^{-1}$) in the RH cycling tests at OCV, 0.05, and 0.3 Acm^{-2}, respectively. Apparently, the voltage drop rate is the lowest at the applied current density of 0.3 Acm^{-2}. The relatively high current density of 0.3 Acm^{-2} can mitigate catalyst layer deterioration. In particular, the cell voltage is relatively low (less than 0.74 V according to the data in Table 3), leading to less carbon oxidation, less Pt dissolution, and a smaller reduction in ECSA. Therefore, the case with a current density of 0.3 Acm^{-2} has the lowest voltage drop rate.

In addition, the voltage decay tendency is consistent with the results from the above residual stress prediction and H_2O_2 formation rate calculations, where lower current densities intensify the mechanical and chemical stresses on the membrane. Due to the synergistic effects of the chemical and mechanical stresses on the membrane in the current durability tests, the voltages decay at a significant rate of mVh^{-1}. In particular, mechanical stress initiates the formation of cracks in the membrane, leading to an increase in reactant gases crossing through the membrane and promoting the formation of H_2O_2 and free radicals. The free radicals are triggered by the H_2O_2 formation, which in turn, makes the membrane thinner and weakens the mechanical strength, shortens the time for cracks to propagate through the membrane and eventually leads to the creation of micro-leaked path for reactant gases. The chemical decomposition with the radicals reduces the mechanical strength of the membrane, resulting in crack initiation and propagation [25]. Whereas a more practical and long-term operation test of the PEMFC vehicles [36] shows an appreciably slower voltage decay rate (on the order of μVh^{-1}). Although the membrane in the practical test also experiences the combined effects of mechanical and chemical stress, the mechanical stress induced by the load cycle is less severe than its counterpart in this study, wherein the membrane can endure the cyclic variation of the RH. As a result, the voltage decay in the current study exhibits a higher rate than in the practical case.

4.3.2. Degradation evaluation

The variations in the hydrogen crossover rate concerning the stress ranges in the three current density conditions under atmospheric pressure and 20-kPa anode backpressure after every 200 RH cycles are shown in Fig. 4.6a. A marginal difference in the hydrogen crossover rate was observed for the two pressure conditions. For the OCV condition, after 1,600 cycles (or 134 h of testing), the hydrogen crossover rate under the 20-kPa anode backpressure had a higher increment than that under atmospheric pressure, exceeding the membrane failure threshold of 15 $mAcm^{-2}$ [37]. Similar trends were observed for 0.05 Acm^{-2} after 1,800 cycles (or 150 h of testing) and 0.3 Acm^{-2} after 2,200 cycles (or 184 h of testing). The abrupt increase in the hydrogen crossover rates revealed fatal damage to the membrane structure, resulting in the development of pinholes and membrane-through cracks. For the 0.3 Acm^{-2} condition, the increase in hydrogen crossover rate is at a lower rate compared with OCV and 0.05 Acm^{-2} conditions, indicating the gradual membrane degradation under this testing condition. When the membrane is exposed to higher mechanical and chemical stresses, it fails in a shorter time with a faster rate of deterioration. This trend agrees well with the calculated results of the formation rate of H_2O_2 and range of stress in Section 4.3.1.

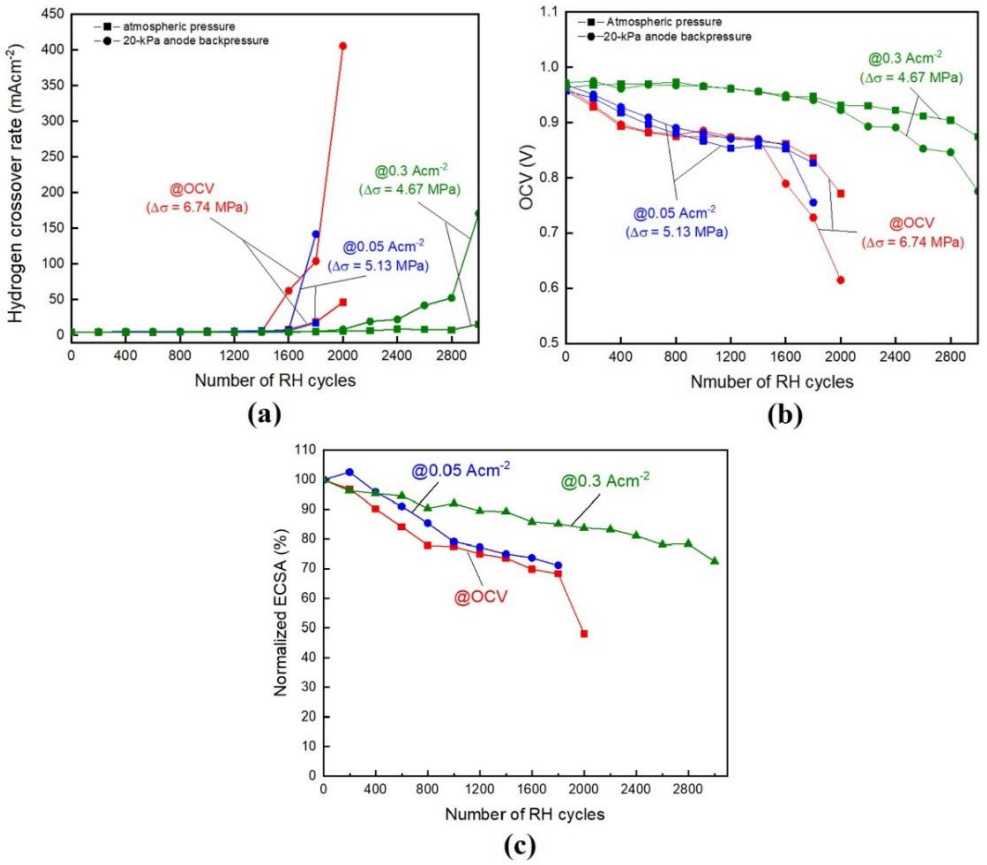

Fig. 4. 6. Variations in (a) hydrogen crossover rate, (b) OCVs, and (c) normalized ECSA after different RH cycles in three testing conditions. $\Delta\sigma$ is the stress range.

The variations in the OCV under the three experimental conditions for both the pressure cases are shown in Fig. 4.6b after every 200 RH cycles. It is well known that the oxidation of leaked hydrogen at the cathode and the reduction of leaked oxygen at the anode lead to a drop in the OCV. Hence, OCV is considered a practical and reliable indicator for examining membrane integrity [38-40]. Furthermore, the reduction of the ECSA in the cathode catalyst layer also contributes to the decline in the OCV.

Fig. 4.6 shows that the membrane degradation process can be divided into two regions. In the first region or prior to membrane failure, from the beginning to a specific number of RH cycles, because the hydrogen crossover rate through the membrane follows the law of diffusion and is very small (approximately 5 $mAcm^{-2}$) regardless of the anode backpressure, cathode catalyst degradation causes a drop in ECSA and, as a result, a gradual decrease in OCV. During the RH cycle test, the cell voltage fluctuates (Fig. 4.3), even for the given constant current density condition, when the hydrogen stream at the anode is switched from a dry to humidified state and vice versa. This unfavorable situation, which is particularly enhanced by the lower current density conditions (OCV and 0.05 Acm-2) is thought to lead to the oxidation of the carbon-black support and the dissolution of Pt in the cathode catalyst [41-43], resulting in ECSA reduction. Furthermore, the fluctuation of the cathode's potential (from 0.05 to 0.9 V) during the electrochemical measurements can degrade the cathode's catalyst. However, carbon-black support

oxidation caused by high cathode potential during the durability test appears to be more dominant because the testing time is longer than the duration for electrochemical measurements and the variation of cell voltage during the durability tests was small. In the second region, or after membrane failure, cracks and pinholes are formed, the hydrogen crossover rate abruptly increases, and the mixture gas resulting from the large amount of crossover significantly decreases the OCV. The transition point from the first to the second region depends on the applied current density. The more unfavorable the testing conditions are (lower applied current densities), the faster the membrane degradation. The transition point (number of RH cycles) is earliest under the OCV condition, followed by the RH cycling at 0.05 Acm^{-2} and delayed much longer under the 0.3 Acm^{-2} condition.

The decrease in the OCV in Fig. 4.6b indicates the degradation level of the membrane. The average OCV decay rates in the OCV condition are 2.09 and 1.11 mVh^{-1} at 20-kPa anode backpressure and atmospheric pressure, respectively. The decay rates are higher than those of the 0.05 Acm^{-2} condition at 1.42 and 0.87 mVh^{-1} and the 0.3 Acm^{-2} condition at 0.79 and 0.35 mVh^{-1}. In addition, the current results depict the severity of the testing conditions in the order of OCV, 0.05 Acm^{-2}, and 0.3 Acm^{-2}.

In summary, some critical findings can be derived from the above discussion. Fig. 4.7 is a summary of Chapters 2, 3, and 4. Firstly, the membranes in the cases exposed to mechanical and chemical degradation have failed rapidly compared with those exposed to the purely mechanical durability test in Chapter 2. The RH cycling test using H_2/air with lower applied current densities will accelerate membrane degradation faster, leading to more early failure by approximately 5.7–7.8 times compared with that using H_2/air. Secondly, the OCV can monitor the deterioration of the cathode catalyst and assess the membrane integrity. The OCV exhibited a notable decline in the considerable rise of the hydrogen crossover rate (in addition to the noticeable degradation of the ECSA).

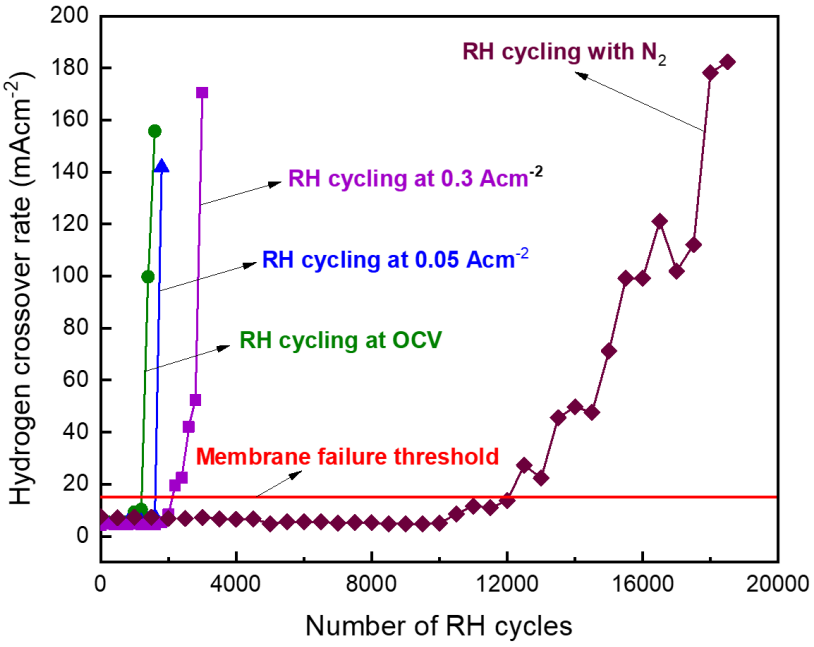

Fig. 4. 7. The hydrogen crossover rate versa number of RH cycles under purely mechanical stress (data from Chapter 2), and in the combined chemical and mechanical stress tests at OCV, 0.05 and 0.3 Acm^{-2} conditions. The red, horizontal line represents hydrogen crossover rate of 15 $mAcm^{-2}$ which is defined as the membrane failure threshold.

4.3.3. Investigation of in situ catalytic combustion of leaked hydrogen gas with air at the cathode

Figure 4.8 shows IR images of the cathode side recorded at 20-kPa anode backpressure during the OCV measurements in the RH cycling tests. The possible imaging areas of the cathode GDL surface in the channel region are highlighted using the seven black rectangles. When hydrogen leaks from the anode and combusts catalytically with oxygen in the air on the cathode side, a temperature rise of the GDL surface can be observed in the IR image. As evident in Fig.4.9, when the membrane is still intact, the temperature increase due to catalytic combustion of the leaked hydrogen solely follows solely Fick's law of diffusion and varies approximately between 4 and 7 °C within the seven channels.

When the membrane has defects, hotspots (highlighted by the red circles in Fig. 4.8) appear on some channels with an abrupt increase in the hydrogen crossover rate and abrupt decrease in OCVs. In particular, hotspots started to emerge after 1,600 cycles in channels 2 and 7 under the OCV condition (Fig. 4.8a), resulting in an increase the GDL temperature (Fig. 4.9a). Consistently, the hydrogen crossover rate and OCV change significantly after 1,600 cycles. For the 0.05 Acm^{-2} condition, the appearance of hotspots in channels 4, 5, and 7 (Fig. 4.8b and Fig. 4.9b) at 1,800 cycles is consistent with the hydrogen crossover rate and OCV. In contrast, for 0.3 Acm^{-2}, a hotspot appears later at channel 4 at 2,400 cycles, as displayed in Fig. 4.7c, after the crossover rate rises at 2,200 cycles, as shown in Fig. 4.9c. Further, the maximum temperature rise in the condition of 0.3 Acm^{-2} is relatively gradual compared with other conditions.

Although there is a slight difference amongst the conditions, the appearance of hotspots synchronizes with membrane failure, as indicated by the abrupt changes in the hydrogen crossover rate and OCV.

Figure 4.8 suggests that the hotspots reach the maximum temperature at the end of the durability tests, when the crossover rate is the highest. As shown in Fig. 4.9, the highest temperature rise for the OCV condition was 16 °C at the hotspot in Channel 1, 15 °C for 0.05 Acm^{-2} condition in channel 7, and 16 °C for 0.3 Acm^{-2} condition in channel 3. Given that the reference temperature (the temperature at which no gas is supplied at BOL) is 80 °C, the maximum temperature at hotspots is 95 to 96 °C. Although a simple calculation estimated a high hydrogen concentration on the cathode side (e.g., 5.86 vol% in the OCV case in Table 4.3), the maximum temperature at the hotspots was not very high (less than 100 °C). The good thermal conductivity of the GDL [26] helped in the transmission of the exothermal heat from hotspot locations to the environment. However, in practical cases, the membrane temperature is possibly close to the glass transient temperature (100–150 °C [44]) because of inadequate heat conduction, which would significantly reduce the mechanical strength of the membrane and lead to premature membrane failure.

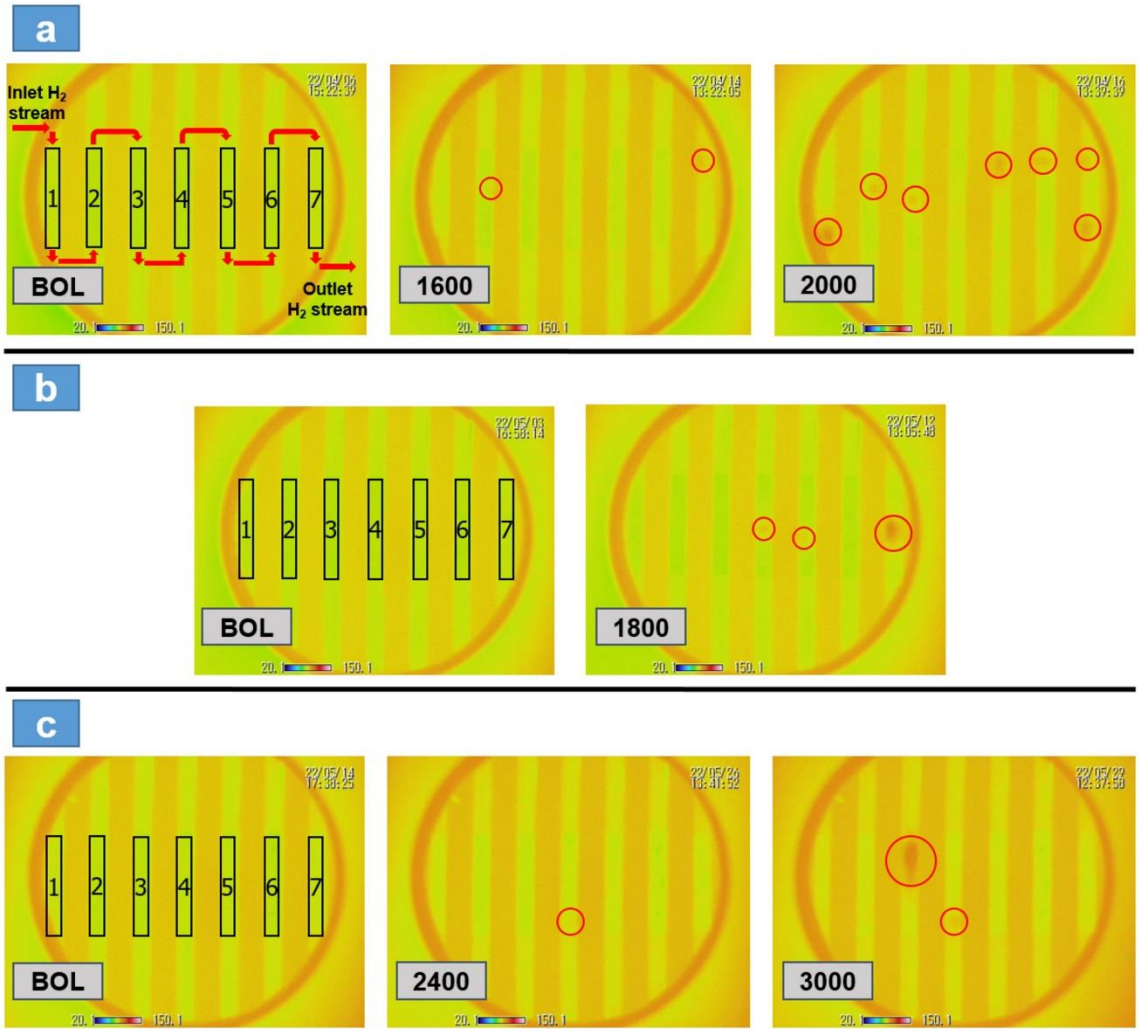

Fig. 4. 8. IR images of the cathode side recorded under 20-kPa anode backpressure case during periodic OCV measurements in the RH cycling test in (a) the OCV condition, (b) 0.05 Acm^{-2} condition, and (c) 0.3 Acm^{-2} condition. Red circles show hotspots caused by combustion. 150 Nccm of fully humidified hydrogen gas and 200 Nccm of dry air were fed into the anode and cathode sides, respectively, at a cell temperature of 80 °C. The temperature range is from 20.1 to 150.1 °C.

The appearance of hotspots depends predominantly on the magnitude of the hydrogen crossover rate and hydrogen concentration in air on the cathode side. Table 4.3 shows an estimation of the volumetric concentration of hydrogen crossing through the membrane in the mixture with 200 Nccm airflow during periodic OCV measurements at a 20-kPa anode backpressure condition. In this calculation, the hydrogen crossover rate data were obtained at anode backpressure of 20-kPa, as shown in Fig. 4.6a. A hotspot emerged when the hydrogen concentration reached 0.34%, which corresponds to the crossover over rate of 22.4 $mAcm^{-2}$ in the condition of 0.3 Acm^{-2}. This is the lowest concentration among the three experimental conditions at which the heat flux is released from catalytic combustion beyond the self-cooling flux of the cell, resulting in the emergence of a hotspot in IR imaging. The hydrogen concentration calculation assumes that hydrogen leaks uniformly through the membrane in all channels. However, the leakage of hydrogen

gas through specific cracks in the degraded membrane can yield a locally high hydrogen concentration, eventually forming local hotspots. Therefore, maintaining a high rate of airflow is recommended to dilute hydrogen leakage across the membrane, consequently preventing thermal decomposition of the membrane.

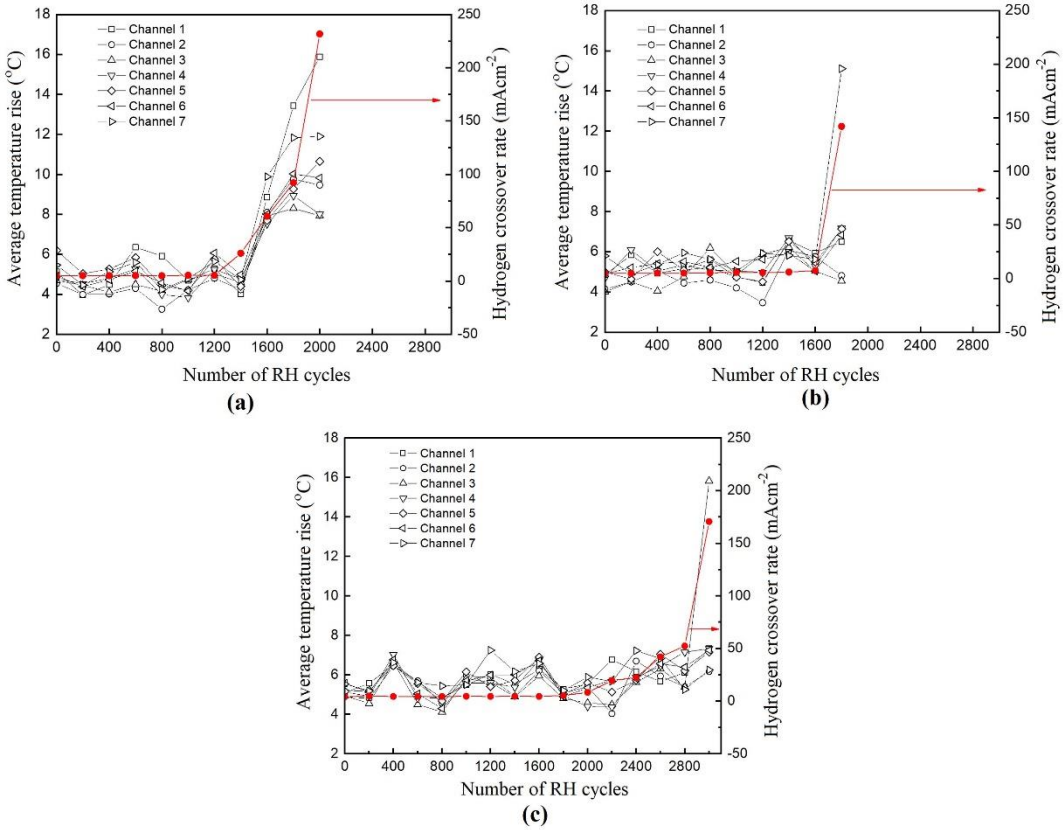

Fig. 4. 9. Correlation between the hydrogen crossover rate and average temperature in the region of each channel during the durability tests under the (a) OCV, (b) 0.05 Acm^{-2}, and (c) 0.3 Acm^{-2} conditions. The average temperature was extracted from IR imaging.

IR imaging reveals that hotspots tend to be located at (1) the entrance and exit regions of the CCM and (2) the separator's channel and land boundary. The results contribute to the understanding of distribution of defects (e.g., cracks, locally thinning membrane, and pinholes) in the degraded membrane. According to the stress calculation in Section 4.3.1, mechanical stress depends predominantly on the magnitude of the membrane water content oscillation. Owing to the co-current serpentine pattern of the anode flow field, as displayed in Fig. 4.8a at BOL, the membrane experiences a significant change of water content at the entrance and exit of the CCM compared to the middle part during the RH cycling test. Thus, the membrane endures a higher stress range at these locations, enabling the formation and propagation of cracks throughout the membrane. This tendency can be confirmed in the conditions of OCV and 0.05 Acm^{-2}(Figs. 4.8a and b), where the defects appeared as hot spots in IR imaging concentrated at the inlet and outlet. Meanwhile, higher amount of water production in the 0.3 Acm^{-2} condition mitigated the water content difference at the inlet and outlet of the CCM. Hence, the location of hotspots, which suggests defects in Fig. 4.8c, differs from the other conditions. Furthermore, the formation rate of H_2O_2 at the anode

and membrane interface is proportional to the oxygen crossing rate. At the entrance of the airstream, the air pressure is slightly higher than at the exit of the cell, so consequently more H_2O_2 will be produced and correspondingly more free radicals will be formed. Thus, the membrane at the entrance of the airstream can deteriorate chemically more severely than other regions, leading to membrane thinning and an increase in the hydrogen crossover rate. Therefore, hotspots were mainly distributed in entrance region of the airstream, apparently at OCV and 0.05 Acm^{-2} conditions. The distribution of hotspots is consistent with the OCV holding test, which is indicated in the Appendix B of this dissertation.

In addition, the edges in the channels and under the land (or ribs) tend to have defects. Because the water content variation of the membrane under land is much narrower than that under the channel regions during the RH cycling test due to the limitation of water transportation, the in-plane tensile stress in the channel regions is expected to have a higher amplitude. The in-plane stress formed in the channel regions is interrupted near the land edge. As a result, the stress concentration in the membrane under the edge between the channel and land is particularly high in comparison to that under the channel and land [45, 46], facilitating the formation and development of cracks.

Subsequently, the synergistic effect of mechanical and chemical stresses can be identified. Once cracks induced by mechanical stress appear, the crossover rate increases; chemical degradation, such as membrane thinning is accelerated; and the mechanical strength of the membrane is weakened. Therefore, under chemical and mechanical stress, lethal defects, for example, through-membrane cracks and pinholes, are possibly formed at the edge and near the inlet and outlet of the channel.

Furthermore, the different conditions lead to different defect locations, resulting in varied locations of the maximum temperature rise, as shown in Fig. 4.9. The maximum temperature is observed in channel 1 in the condition of OCV and channels 7 and 3 in the conditions of 0.05 and 0.3 Acm^{-2}, respectively.

In addition, the number of hotspots indirectly indicated the extent of membrane deterioration for all three testing conditions. The IR image of the OCV condition (Fig. 4.8a) suggests six hotspots at the end-of-life (EOL) (at 2,000 RH cycles). On the other hand, the condition of 0.05 Acm^{-2} (Fig. 4.8b) and 0.3 Acm^{-2} (Fig. 4.8c) shows 3 and 2 hotspots, respectively. Thus, the number of hotspots can also reveal the significance of the degradation. Thus, the IR imaging introduced in this study is useful for capturing the heterogeneous defects in membranes.

Table 4. 4. Volumetric concentration of hydrogen in the mixture of 200 Nccm airflow in cathode side during the periodic OCV measurements at 20-kPa anode backpressure condition

Number of RH cycles		BOL	1400	1600	1800	2000	2200	2400	2600	2800	3000
OCV	$i_{H_2,20kPa}$	4.76	5.37	62.4	104	405					

	($mAcm^{-2}$)										
	$C_{H_2,20kPa}$ (%)	0.07	0.08	0.95	1.57	5.86					
0.05 Acm^{-2}	$i_{H_2,20kPa}$ ($mAcm^{-2}$)	4.87	6.05	7.47	142						
	$C_{H_2,20kPa}$ (%)	0.07	0.09	0.11	2.13						
0.3 Acm^{-2}	$i_{H_2,20kPa}$ ($mAcm^{-2}$)	4.31	4.59	4.58	5.37	8.34	19.5	22.4	42.1	52.4	170
	$C_{H_2,20kPa}$ (%)	0.07	0.07	0.07	0.08	0.13	0.30	0.34	0.64	0.80	2.55

The temperature rises of the cathode's GDL surface during measuring OCVs caused by combustion in three testing conditions are examined with numerical calculation using a one-dimensional heat transfer model, as described in Section 3.3.2 of Chapter 3. The combustion heat flux in the calculation is based on the hydrogen crossover rate data in the case of 20-kPa anode backpressure in Table 4.4. The measured GDL temperature rise in Fig. 4.10 means the average temperature considering all seven channels (1, 2, 3, 4, 5, 6, and 7). Fig. 4.10 shows the comparison between the calculation and measurement of the GDL temperature rises in the three testing conditions. The calculation validates the increase in GDL temperature, which is proportional to the hydrogen crossover rates, by showing a reasonably good agreement with the experimental data. Prior to membrane failure, there is a slight under-prediction in the calculation; this deviation is reasonable owing to the accuracy of the IR camera (±1 °C). The calculation result shares the same increasing trend of the GDL temperature as the experimental data from the beginning of the membrane failure to the end of the durability test. Although the calculation qualitatively agrees with the experiment, there is a large deviation after membrane failure due to the inhomogeneity of the hydrogen rate crossing through the degraded membranes. The heat transfer calculation, in particular, assumes that the hydrogen crossover rate is uniform. However, cracks and membrane thinning appear locally in degraded membranes, and the combustion process occurs there, causing the temperature rise to be heterogeneous.

Both the calculation and the experimental results indicate that the GDL temperature increase is under 100 °C, even though the hydrogen crossover rate was abnormally high at the end of the durability test. Apparently, this temperature rise is quite lower than the melting point and auto-ignition temperatures of the Nafion membrane (around 300 °C). The maximum dissipated heat flux of the cell of around 2 Wcm^{-}

^{2} (maximum allowable heat flux shown at Section 3.3.2 of Chapter 3) is appreciably higher than the combustion heat flux. Therefore, the combustion heat could be transferred efficiently to the environment, preventing the membrane from melting or burning.

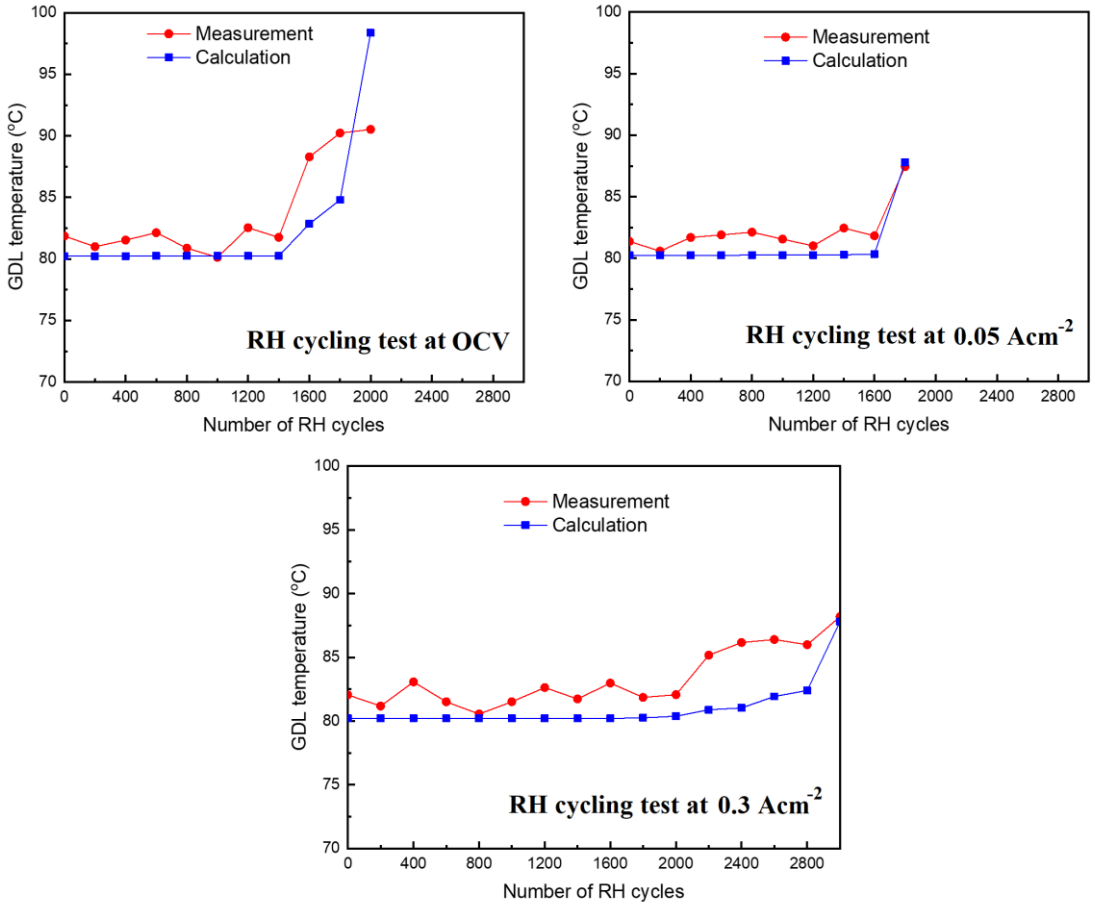

Fig. 4. 10. Comparison of the calculation and measured GDL temperature rises induced by combustion in three testing conditions.

4.3.4. Post mortem analysis

Hydrogen gas crossing through pinholes and fatal cracks in the membrane forms a combustible mixture with air and is burned in the presence of Pt, resulting in the formation of hotspots, as suggested by the IR images. Therefore, three samples from the hotspot containing deteriorated CCMs were cut at the end of the durability tests, corresponding to three testing conditions. The cut samples enclosed the hotspot location with a width of 3 mm and length of 11 mm. These samples were then observed from the anode side using SEM to examine the presence of pinholes and cracks. The morphological changes in the degraded CCM samples were compared with the surface and cross-sectional images of the fresh CCM, as shown in Fig. 4.11a. Cracks, pinholes, and membrane thinning can be observed in the SEM images in Figs. 4.11b, c, and d.

Figure 4.11b displays the SEM image of the anode surface of the sample from channel 1 after the durability test under OCV condition, at which the hotspot emerged in the IR image (see Fig. 4.8a). Three pinholes with an average diameter (ϕ) ranging from 12 to 16.4 μm were noticed. At a specific time in the durability test, there was noticeable hydrogen crossover via thinning or cracked membranes, which combusted with oxygen at the cathode catalyst and produced heat at a rate higher than the self-cooling heat flux of the cell (approximately 2.0 Wcm^{-2}). This results in burning of the membrane when the membrane temperature exceeds the ignition temperature of approximately 300 °C [29], eventually creating pinholes. Noticeably, the three pinholes were lined up in a groove without the catalyst. The catalyst material at the anode might have blown up because of the flashback of hydrogen combustion at the cathode. Catalyst material was, then, located on both sides of this groove, thereby exposing the membrane (highlighted by the dark-colored area in Fig. 4.11b). The formation of these pinholes was responsible for the abrupt increase in the hydrogen crossover rate, as well as the sudden drop in the OCV after 1,600 RH cycles. Furthermore, compared to the BOL membrane, the membrane thickness in the cross-section around these pinholes (Fig. 4.11b) drastically reduced by 40% (from approximately 23 to 13.7 μm). This membrane thinning is a clear evidence of chemical degradation, where membrane decomposition progresses in the current combined chemical and mechanical stress tests.

Figures 11c and 11d show two big cracks appearing at channels 7 and 3 in the RH cycling tests at 0.05 and 0.3 Acm^{-2}, respectively. Based on the cross-sectional images obtained using the focused ion beam, the cracks were fully developed through the membrane under both conditions, forming micro-gas leakage paths between the cathode and anode sides. The development of these catastrophic cracks accounts for the sudden change in hydrogen crossover and OCV, similar to pinholes in the OCV condition. Moreover, membrane thickness also decreased slightly from approximately 23 μm in the BOL (Fig. 4.11a) to 17 μm (in the condition of 0.05 Acm^{-2} in Fig. 4.11c) and 16 μm (in the condition of 0.3 Acm^{-2} in Fig. 4.11d). The emergence of through-membrane cracks at thin membrane locations indicates the synergistic effect of mechanical and chemical stresses on the membrane.

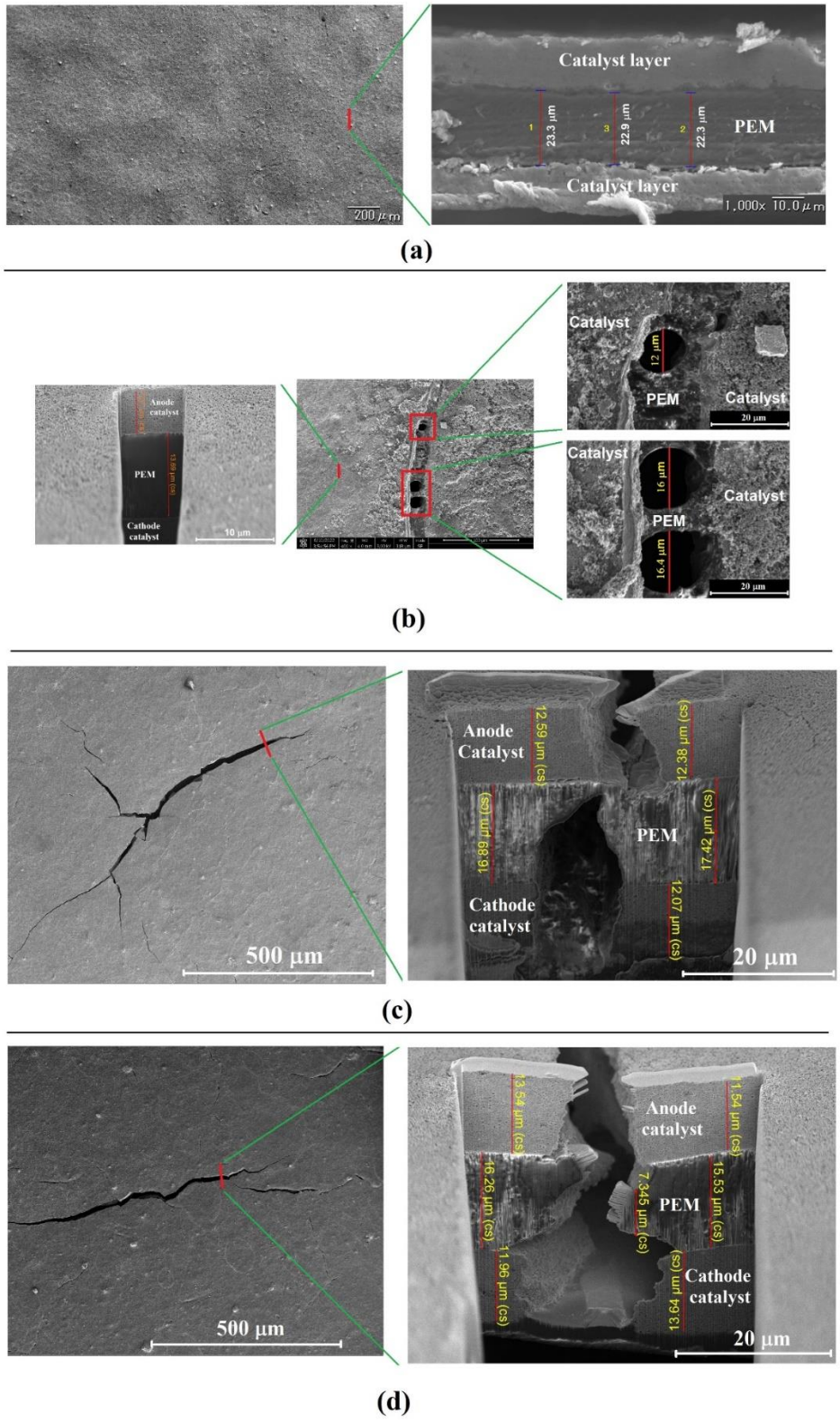

Fig. 4. 11. SEM images of (a) surface and cross section of the fresh CCM, (b) (c) and (d) surface and cross section of the degraded CCMs in the RH cycling at OCV condition, at 0.05 Acm^{-2}, and at 0.3 Acm^{-2}, respectively. PEM is the Nafion NRE211 membrane.

4.4. Conclusions

This chapter concentrated on the impact of current densities on membrane degradation. Combined chemical and mechanical stress tests were performed on a PEMFC. The membrane was subjected to an RH cycle by supplying air and hydrogen gas under different current densities. In addition to electrochemical measurements (hydrogen crossover rate and OCV), IR imaging during the test and SEM observation after the test clarified the following:

(1) A higher current density in the RH cycling tests causes higher amount of water production and less H_2O_2 formation, which mitigate mechanical stress and chemical stress on the membrane, respectively. This finding is supported by the quantitative analysis of the H_2O_2 formation rate and the residual stress range at different applied current densities in the RH cycling tests.

(2) The first appearance of hotspots observed by IR imaging synchronizes with an abrupt increase in hydrogen and a sudden decrease in OCV. This suggests the following:

- Repeated mechanical and continuous chemical stress, which gradually causes small cracks and thinning of the membrane in the RH cycle test, eventually reaches a critical level,
- Moderate combustion shifts to accidental combustion.
- The heat from the burning of the combustible mixture at the cathode catalyst exceeds, locally (at the positions where membrane thinning and cracks are formed), the self-cooling capability of the cell.
- Fatal defects, such as large through-membrane cracks and pinholes, are formed.

(3) The fatal cracks and pinholes suggested in the degradation test were observed in post-mortem analysis (SEM). The location of the fatal defects matches with that of the hotspots captured by IR imaging. Thus, IR imaging acts as a powerful diagnostic tool for detecting the locations of defects and evaluating the level of membrane degradation during accelerated stress tests.

(4) The rise in GDL temperature induced by combustion has been predicted using a one-dimensional heat transfer model. The model can track the transition of the combustion process from a moderate to accidental scale based on the hydrogen crossover rate data. Besides, combustion heat is transferred predominantly from the cathode's catalyst to the hydrogen stream. Despite that the high dissipated heat flux (maximum allowable heat flux) of the cell is estimated to be approximately 2.0 Wcm^{-2} (corresponding to a hydrogen crossover rate of 1.77 Acm^{-2}), the formation of pinholes in the OCV condition indicated that the local combustion heat flux exceeded this dissipated heat flux, resulting in the thermal decomposition of the membrane. It is worth mentioning that the thermal decomposition might have occurred shortly during the durability test, when the IR imaging did not perform.

(5) The maximum GDL temperature at the hotspots was observed to be under 100 °C during measuring OCVs; thus, the membrane temperature at these points possibly exceeded 100 °C but was much lower than the auto-ignition temperature (around 300 °C). This indicated that, even though pinholes (induced locally by accidental combustion during the durability test) and cracks had been formed and the hydrogen crossover rate through these defects was high, the corresponding combustion heat flux was still below the maximum dissipated heat flux. On the other hand, the combustion process was on a transient scale during the OCV measurement, and the membrane cannot be destroyed instantly by the thermal decomposition process. However, when the membrane operated close to its glass transient temperature, it became weaker, resulting in the enlargement of cracks and pinholes in the combined chemical and mechanical stress test.

4.5. References

1. Hydrogen Economy Outlook (BloombergNEF, 2020). https://data.bloomberglp.com/professional/sites/24/BNEF-Hydrogen-Economy-Outlook-Key-Messages-30-Mar-2020.pdf. (accessed 12 July 2022).

2. Hydrogen Roadmap Europe (Fuel Cells and Hydrogen Joint Undertaking, 2019). https://www.fch.europa.eu/. (accessed 12 July 2022). doi:10.2843/249013.

3. IEA (2021), Global Energy Review 2021, IEA, Paris. https://www.iea.org/reports/global-energy-review-2021. (accessed 12 July 2022).

4. IEA (2020), Tracking Transport 2020, IEA, Paris. https://www.iea.org/reports/tracking-transport-2020. (accessed 12 July 2022).

5. Alaswad, A., et al. “Developments in Fuel Cell Technologies in the Transport Sector.” International Journal of Hydrogen Energy, vol. 41, no. 37, Oct. 2016, pp. 16499–16508, 10.1016/j.ijhydene.2016.03.164

6. Yoshida, T., and K. Kojima. “Toyota MIRAI Fuel Cell Vehicle and Progress toward a Future Hydrogen Society.” Interface Magazine, vol. 24, no. 2, 1 Jan. 2015, pp. 45–49, 10.1149/2.f03152if.

7. Cullen, David A., et al. “New Roads and Challenges for Fuel Cells in Heavy-Duty Transportation.” Nature Energy, vol. 6, no. 5, 25 Mar. 2021, pp. 462–474, 10.1038/s41560-021-00775-z.

8. Lototskyy, Mykhaylo V., et al. “Performance of Electric Forklift with Low-Temperature Polymer Exchange Membrane Fuel Cell Power Module and Metal Hydride Hydrogen Storage Extension Tank.” Journal of Power Sources, vol. 316, June 2016, pp. 239–250, 10.1016/j.jpowsour.2016.03.058.

9. Wang, Guangjin, et al. “Degradation Behavior of a Proton Exchange Membrane Fuel Cell Stack under Dynamic Cycles between Idling and Rated Condition.” International Journal of Hydrogen Energy, vol. 43, no. 9, Mar. 2018, pp. 4471–4481, 10.1016/j.ijhydene.2018.01.020.

10. PEI, P, et al. “A Quick Evaluating Method for Automotive Fuel Cell Lifetime.” International Journal of Hydrogen Energy, vol. 33, no. 14, July 2008, pp. 3829–3836, 10.1016/j.ijhydene.2008.04.048

11. Yu, Yi, et al. “A Review on Performance Degradation of Proton Exchange Membrane Fuel Cells during Startup and Shutdown Processes: Causes, Consequences, and Mitigation Strategies.” Journal of Power Sources, vol. 205, May 2012, pp. 10–23, 10.1016/j.jpowsour.2012.01.059.

12. Wan, Zhongmin, et al. “A Review on Cold Start of Proton Exchange Membrane Fuel Cells.” Energies, vol. 7, no. 5, 13 May 2014, pp. 3179–3203, 10.3390/en7053179.

13. Aindow, T.T., and J. O’Neill. “Use of Mechanical Tests to Predict Durability of Polymer Fuel Cell Membranes under Humidity Cycling.” Journal of Power Sources, vol. 196, no. 8, Apr. 2011, pp. 3851–3854, 10.1016/j.jpowsour.2010.12.031

14. Mathias, Mark F., et al. “Two Fuel Cell Cars in Every Garage?” The Electrochemical Society Interface, vol. 14, no. 3, 1 Sept. 2005, pp. 24–35, 10.1149/2.f05053if..

15. Alavijeh, Alireza Sadeghi, et al. “Microstructural and Mechanical Characterization of Catalyst Coated Membranes Subjected to in Situ Hygrothermal Fatigue.” Journal of the Electrochemical Society, vol. 162, no. 14, 2015, pp. F1461–F1469, 10.1149/2.0471514jes.

16. Lai, Yeh-Hung, et al. “Viscoelastic Stress Analysis of Constrained Proton Exchange Membranes under Humidity Cycling.” Journal of Fuel Cell Science and Technology, vol. 6, no. 2, 20 Feb. 2009, 10.1115/1.2971045.

17. Gubler, Lorenz, et al. “Radical (HO•, H• and HOO•) Formation and Ionomer Degradation in Polymer Electrolyte Fuel Cells.” Journal of the Electrochemical Society, vol. 158, no. 7, 27 Apr. 2011, pp. B755–B769, 10.1149/1.3581040.

18. Zatoń, M., et al. “Current Understanding of Chemical Degradation Mechanisms of Perfluorosulfonic Acid Membranes and Their Mitigation Strategies: A Review.” Sustainable Energy & Fuels, vol. 1, no. 3, 2017, pp. 409–438, 10.1039/c7se00038c

19. Ghassemzadeh, Lida, et al. “Chemical Degradation of Nafion Membranes under Mimic Fuel Cell Conditions as Investigated by Solid-State NMR Spectroscopy.” The Journal of Physical Chemistry C, vol. 114, no. 34, 5 Aug. 2010, pp. 14635–14645, 10.1021/jp102533v.

20. G. Czapski, B.H. Bielski, N. Sutin, J. Phys. Chem. 67 (1963) 201–203.

21. Kusoglu, Ahmet, and Adam Z. Weber. "New Insights into Perfluorinated Sulfonic-Acid Ionomers." Chemical Reviews, vol. 117, no. 3, 23 Jan. 2017, pp. 987–1104, 10.1021/acs.chemrev.6b00159.

22. Mukundan, Rangachary, et al. "Membrane Accelerated Stress Test Development for Polymer Electrolyte Fuel Cell Durability Validated Using Field and Drive Cycle Testing." Journal of the Electrochemical Society, vol. 165, no. 6, 2018, pp. F3085–F3093, 10.1149/2.0101806jes

23. Gittleman, Craig S., et al. "Materials Research and Development Focus Areas for Low Cost Automotive Proton-Exchange Membrane Fuel Cells." Current Opinion in Electrochemistry, vol. 18, Dec. 2019, pp. 81–89, 10.1016/j.coelec.2019.10.009.

24. W.Liu, K. Ruth, and G. Rusch, J. New Mater. Electrochem. Syst., 4 (2001) 227-231.

25. Sadeghi Alavijeh, A., et al. "Decay in Mechanical Properties of Catalyst Coated Membranes Subjected to Combined Chemical and Mechanical Membrane Degradation." Fuel Cells, vol. 15, no. 1, 28 Nov. 2014, pp. 204–213, 10.1002/fuce.201400040.

26. Gunji, Hiroyuki, et al. "Gas-Leak-Induced Pinhole Formation at Polymer Electrolyte Membrane Fuel Cell Electrode Edges." International Journal of Hydrogen Energy, vol. 42, no. 1, Jan. 2017, pp. 562–574, 10.1016/j.ijhydene.2016.11.038.

27. Ngo, Phi Manh, et al. "Investigation of In-Situ Catalytic Combustion in Polymer-Electrolyte-Membrane Fuel Cell during Combined Chemical and Mechanical Stress Test." Journal of Power Sources, vol. 542, Sept. 2022, p. 231803, 10.1016/j.jpowsour.2022.231803.

28. Lakshmanan, Balasubramanian, et al. "Polyetheretherketone Membranes for Elevated Temperature PEMFCs." Electrochemical and Solid-State Letters, vol. 6, no. 12, 2003, p. A282, 10.1149/1.1619647.

29. Stanic, Vesna. "Mechanism of Pinhole Formation in Membrane Electrode Assemblies for PEM Fuel Cells." ECS Proceedings Volumes, vol. 2004-21, no. 1, Jan. 2004, pp. 391–401, 10.1149/200421.0391pv.

30. Millet, P., et al. "Cell Failure Mechanisms in PEM Water Electrolyzers." International Journal of Hydrogen Energy, vol. 37, no. 22, Nov. 2012, pp. 17478–17487, 10.1016/j.ijhydene.2012.06.017.

31. Sethuraman, Vijay A., et al. "Hydrogen Peroxide Formation Rates in a PEMFC Anode and Cathode." Journal of the Electrochemical Society, vol. 155, no. 1, 2008, p. B50, 10.1149/1.2801980

32. Inaba, Minoru, et al. "Gas Crossover and Membrane Degradation in Polymer Electrolyte Fuel Cells." Electrochimica Acta, vol. 51, no. 26, Aug. 2006, pp. 5746–5753, 10.1016/j.electacta.2006.03.008.

33. Liu, Wen, and David Zuckerbrod. “In Situ Detection of Hydrogen Peroxide in PEM Fuel Cells.” Journal of the Electrochemical Society, vol. 152, no. 6, 2005, p. A1165, 10.1149/1.1904988

34. Bernardi, Dawn M., and Mark W. Verbrugge. “Mathematical Model of a Gas Diffusion Electrode Bonded to a Polymer Electrolyte.” AIChE Journal, vol. 37, no. 8, Aug. 1991, pp. 1151–1163, 10.1002/aic.690370805.

35. Vengatesan, S., et al. “Diagnosis of MEA Degradation under Accelerated Relative Humidity Cycling.” Journal of Power Sources, vol. 196, no. 11, June 2011, pp. 5045–5052, 10.1016/j.jpowsour.2011.01.088.

36. Scholta, J., et al. “Longevity Test Results for Reformate Polymer Electrolyte Membrane Fuel Cell Stacks.” Journal of Power Sources, vol. 196, no. 12, June 2011, pp. 5264–5271, 10.1016/j.jpowsour.2010.08.113

37. A.B. LaConti, M. Hamdan, and R.C. McDonald, Handbook of Fuel Cells: Fundamentals, Technology, and Applications, Vol. 3, W. Vielstich, A. Lamm, and H. A. Gasteiger, Editors, Wiley, New York (2003).

38. Sompalli, Bhaskar, et al. “Membrane Degradation at Catalyst Layer Edges in PEMFC MEAs.” Journal of the Electrochemical Society, vol. 154, no. 12, 2007, p. B1349, 10.1149/1.2789791.

39. Lü, Weizhong, et al. “The Effects of Pinholes on Proton Exchange Membrane Fuel Cell Performance.” International Journal of Energy Research, vol. 35, no. 1, 28 Dec. 2010, pp. 24–30, 10.1002/er.1728

40. Spinelli, P., et al. “Semi-Empirical Evaluation of PEMFC Electro-Catalytic Activity.” Journal of Power Sources, vol. 178, no. 2, Apr. 2008, pp. 517–524, 10.1016/j.jpowsour.2007.10.040.

41. Schlögl, Katrin, et al. “Identical-Location TEM Investigations of Pt/c Electrocatalyst Degradation at Elevated Temperatures.” Journal of Electroanalytical Chemistry, vol. 662, no. 2, Nov. 2011, pp. 355–360, 10.1016/j.jelechem.2011.09.003.

42. Yu, Yi, et al. “A Review on Performance Degradation of Proton Exchange Membrane Fuel Cells during Startup and Shutdown Processes: Causes, Consequences, and Mitigation Strategies.” Journal of Power Sources, vol. 205, May 2012, pp. 10–23, 10.1016/j.jpowsour.2012.01.059.

43. Moore, Michael, et al. “A Numerical Study on the Impact of Cathode Catalyst Layer Loading on the Open Circuit Voltage in a Proton Exchange Membrane Fuel Cell.” Journal of the Electrochemical Society, vol. 168, no. 4, 1 Apr. 2021, p. 044519, 10.1149/1945-7111/abf50c.

44. Kundu, Sumit, et al. “Mechanical Properties of NafionTM Electrolyte Membranes under Hydrated Conditions.” Polymer, vol. 46, no. 25, 28 Nov. 2005, pp. 11707–11715, 10.1016/j.polymer.2005.09.059

45. Khorasany, R.M.H., et al. “In-Situ Simulation of Membrane Fatigue in Polymer Electrolyte Fuel Cells.” International Journal of Hydrogen Energy, vol. 42, no. 16, Apr. 2017, pp. 11838–11844, 10.1016/j.ijhydene.2017.01.173.

46. Singh, Yadvinder, et al. “Tracking the Evolution of Mechanical Degradation in Fuel Cell Membranes Using 4D in Situ Visualization.” Journal of Power Sources, vol. 412, Feb. 2019, pp. 224–237, 10.1016/j.jpowsour.2018.11.049.

Chapter 5

Overall conclusions, mitigation strategies and future prospects

This final chapter emphasizes important findings from the current study. Furthermore, based on these findings and consultation from the literature, primary strategies have been proposed to diagnose and mitigate mechanical, chemical, and thermal membrane degradation. The above strategies aim to improve membrane durability, resulting in prolonging the lifetime of the membrane and the fuel cell. In addition, some recommendations, such as tracking the transition of the combustion process in the PEMFCs embedding reinforced membranes, are also proposed for expanding the current study.

5.1 Overall conclusions

The use of low-temperature polymer electrolyte membrane fuel cells (PEMFCs) as the powertrain fueling green hydrogen is a viable solution for addressing today's pressing issues, such as the depletion of fossil fuels and environmental concerns caused by the direct combustion of gasoline and diesel in internal combustion engine vehicles. However, fuel cell stack durability in general and the durability of the membrane in particular in the PEMFC is the bottleneck for the widespread commercialization of FCVs on the market. Therefore, improving membrane durability in fuel cell vehicles is one of the top priorities, especially in heavy duty vehicles where the membrane must experience much harsher operating conditions than that in light duty vehicles. Understanding the mechanisms that accelerate membrane deterioration (mechanical, chemical and thermal membrane degradation) is crucial for developing mitigation strategies that will prolong membrane lifetime and help achieve the ultimate lifetime targets of 8,000 h for light-duty vehicles and 30,000 h for heavy-duty vehicles [1]. Besides, developing practical and reliable diagnosis methods is also crucial for shortening the maintenance duration, reducing the maintenance cost, and increasing the reliability of the FCVs.

Chapter 2 of this dissertation elucidated purely mechanical degradation on membrane. Membrane Nafion NRE211 experienced a mechanical stress induced by the relative humidity (RH) cycling test using nitrogen gas on both sides of the cell at 80 °C and at atmospheric pressure.

- The author has succeeded in calculating the in-plane stresses formed in the membrane in the current testing condition based on the membrane resistance data. The alternation of the compressive and tensile stresses with an amplitude of approximately 2 MPa during the RH cycling test accelerates membrane degradation.
- The fluctuation of the LSV curves during hydrogen crossover rate measurement due to water blockage in the flow channel and its drainage after 10,500 RH cycles indicates the appearance of small through-membrane cracks under mechanical stress.

- Afterwards, membrane completely failed after the membrane experienced 12,500 RH cycles that can be indicated by two indicators, including the hydrogen crossover rate and open-circuit voltage (OCV).
- This decreasing the OCV comes from mixed potentials. The leaking of reactant gases through the membrane leads to the oxygen reduction reaction at the anode and hydrogen oxidation reaction at the cathode, yielding the mixed potentials at the electrodes.
- The membrane durability is the primary target of the RH cycling test using N_2 at both the cathode and anode compartments; therefore, the catalyst layer's deterioration is negligible. As a result, the rise in hydrogen crossing rate through the degraded membrane is what accounted primarily to the decrease in OCV during the durability test. Namely, the negligible deterioration at catalyst layer does not responds to the decrease in OCV.
- A novel diagnostic method has been developed based on an existing model for converting OCV decay to anticipate the change in hydrogen crossover rate during the durability test. This idea was proved through a quantitative agreement between the measured crossover rate and crossover rate estimated through the OCV. Although the hydrogen crossover rate is the most reliable indicator for checking the integrity of membrane, directly measuring the hydrogen crossover rate requires Nitrogen gas (and so its cylinder) and electrochemical apparatus, resulting in larger cost. Thus, direct measurement of hydrogen crossover rate, such as on a light-duty fuel cell vehicle (around 400 cells in the stack of the Toyota Mirai 2022 version [1]), is unrealistic to diagnose membrane integrity. Meanwhile, it is practical and easy to scan OCV of each cell in the stack of a FCV. Therefore, this method could be very helpful in diagnosing the membrane integrity via scanning OCV, thus saving time and reducing cost for the maintenance.

Chapter 3 aims to investigate the combined effects of chemical and mechanical mechanisms on membrane durability. Under actual operating conditions of the FCVs, the membrane experiences both chemical and mechanical processes of deterioration. Thus, the chapter 3 supposes a more practical situation. Additionally, because hydrogen and air were used in this durability test, catalytic combustion of the hydrogen that leaked through the membrane and the air on the cathode side occurs and was investigated in-situ manner by using the IR imaging method. A high IR transmittance glass window (ZnS-glass) installed on the cathode side makes it possible to precisely measure a temperature rise at the surface of cathode's gas diffusion layer (GDL) brought by the catalytic combustion. The ZnS-glass is weak to water, thus the hydrogen stream's RH was only alternated between wet and dry states at the OCV condition. During the durability test and the electrochemical measurements, meanwhile, all supplied gases were maintained in a dry state at 80 °C and at atmospheric pressure. The effects of the chemical and mechanical stresses on the membrane were evaluated quantitatively based on the calculation of the in-plane stresses (tensile and

compressive stresses) formed in the membrane and the H_2O_2 formation rate at the anode-membrane interface under the OCV condition, respectively.

- At low RH and OCV mode, the tensile stress reaches its peak and the rate of H_2O_2 is higher than other conditions. In other words, both mechanisms have the most severe impact on the membrane when the cell operates at low RH and at the OCV mode. The current finding calls into question the tendency of PEM fuel cell vehicles to operate in low RH conditions.
- Under the synergetic impact of the chemical and mechanical stresses, the membrane failed quickly after enduring 1,600 RH cycles. This was suggested by the abrupt rise of the hydrogen crossover rate and drop of OCV, around 7.8 times earlier than purely mechanical stress test after 12,500 cycles that has been reported in Chapter 2. Because the free radicals can attack on both the main chain and the side of the PFSA membrane structure, membranes change their mechanical properties from ductile to more brittle, resulting in a reduction in crack propagation resistance. In the meantime, the increase of reactant gases through the cracks induced by the mechanical stress accelerates the formation of H_2O_2, eventually forming free radicals. In sum up, chemical stress enhances the mechanical membrane degradation and vice versa, so that the membrane in the combined stress test deteriorates quickly in comparison with the purely mechanical stress test.
- The appearance of a hotspot after 1,600 RH cycles on the IR image successfully indicates the transition of the combustion process. The emergence of a hotspot is consistent with membrane failure, which is indicated by the abrupt increase in the hydrogen crossover rate and drop in OCV. In other words, the IR imaging technique is indeed able to track in-situ the transition of the combustion process in the PEMFCs.
- Furthermore, the maximum temperature rise of GDL at hotspots was under 100 °C, even though the hydrogen crossover rate was extremely high, for example, approximately 0.41 Acm^{-2} at the end of the durability test. The self-cooling capability of the cell helped to transfer the combustion heat from the catalyst to the environment.
- When the combustion heat flux exceeds the maximum dissipated heat flux, combustion process transitions from the moderate to accidental scale, then burning the membrane and eventually pinhole formation. The maximum dissipated heat flux of the cell was calculated corresponding to the auto-ignition temperature of the Nafion membrane approximately at 2.0 Wcm^{-2}. During the post-mortem analysis, three pinholes discovered in SEM images provided unequivocal proof that accidental combustion occurred instantly and temporarily during the durability test.
- The development of these pinholes was the primary factor in the membrane's abrupt failure during the durability test. The current discovery raises another question about how to ensure the reliability of FCVs with the probability of accidental combustion. Furthermore, when the

hotspots appeared, the membrane in the durability test experienced not only the combined chemical and mechanical stress but also the thermal stress, resulting in faster membrane degradation. This is due to the fact that Nafion membranes would creep and reduce thickness under mechanical stress at temperatures close to their glass transition temperature (100-150 °C), particularly in dry conditions [2].

Chapter 4 investigates the effect of current density on membrane durability. In the operation of fuel cell vehicles, the membrane in the stack experiences different modes, including braking, idling, low speed coasting, cruise/acceleration, and moderate speed coasting. Power demand or the applied current density on the stack will change to cope with these corresponding operation modes, leading to the changes in the membrane temperature and water content. This harsh change in cell suggests a thermal-hygral dimensional fluctuation of the constrained membrane and leads to the formation of residual stress, which then deteriorates mechanically the membrane with time. Furthermore, the concentration of reactant gases is also different at different applied current densities. Thus, the formation rate of H_2O_2, which is a precursor of the hydroxyl radicals, is not the same at different current densities. Thus, the effect of current density on membrane durability should be addressed. The membrane NRE211 was subjected to a RH cycling test where the hydrogen stream was changed repeatedly between the dry and wet conditions at the OCV condition, and at applied current densities of 0.05 and 0.3 Acm^{-2} in a visualization cell. These testing conditions were expected to partially mimic the operating modes in FC vehicles. Electrochemical indicators and IR thermal imaging were used to evaluate membrane integrity and combustion of the combustible mixture of leaked hydrogen and air in the presence of Pt at the cathode side. Similar to the previous chapter 4, effects of the chemical and mechanical stresses at three current densities were considered through the residual stress on the membrane and the formation rate of H_2O_2. Furthermore, thermal stress induced by combustion was also clarified based on the IR imaging analysis.

- The hydrogen crossover rate and OCV suggest that membrane failed quickly after 1,600, 1800 and 2,200 RH cycles in the durability tests at OCV, 0.05 and 0.3 Acm^{-2}, respectively, which is much earlier than purely mechanical stress test after 12,500 cycles in Chapter 2. It is apparent that membrane experiences higher mechanical stress and H_2O_2 is generated at higher rate with the lower applied current density. Meanwhile, higher applied current densities narrow the change in membrane water content during the RH cycling test, resulting in a lower stress range (or stress amplitude). Therefore, the membrane is hydrated sufficiently at a higher applied current density, which mitigates the effect of mechanical stress on the membrane. On the other words, OCV and closed to OCV are not desired operating conditions in the fuel cell vehicles.
- In three durability tests with the different current densities, hotspots were observed on the IR images, which was consistent with the points at which the membrane failed, as indicated by a

dramatic rise in the hydrogen crossover rate and a sharp decline in OCV at 20-kPa anode backpressure.

- Through-membrane cracks and pinholes have been found on the degraded catalyst coated membranes (CCMs) in the SEM images at the same locations where hotspots were observed.
- The maximum GDL temperature at hotspots observed under 100 °C at the end of the durability tests, despite the hydrogen crossover rates being much higher than the membrane failure threshold of 15 $mAcm^{-2}$ [3]. Through the fatal defects in the failed membrane, the hydrogen crossover rate increased appreciably, and combustion heat was released at a high rate, but it is considered to be under the maximum dissipated heat flux of the cell structure of around 2.0 Wcm^{-2}. That explains why the GDL temperature rise is induced by combustion being under 100 °C, which is much lower than the membrane's auto-ignition temperature. Therefore, the membrane won't be destroyed instantly but instead will be subjected to thermal stress, which can accelerate membrane deterioration.
- The rise in GDL temperature induced by combustion has been predicted using a one-dimensional heat transfer model. The model can track the transition of the combustion process from a moderate to accidental scale based on the hydrogen crossover rate data. Besides, combustion heat is transferred predominantly from the cathode's catalyst to the hydrogen stream. Despite the high dissipated heat flux of the cell, approximately 2.0 Wcm^{-2}, the formation of pinholes in the OCV condition implied that the local combustion heat flux exceeded this maximum dissipated heat flux during the durability test when the IR imaging did not perform, resulting in the thermal decomposition of the membrane.
- The IR imaging technique using in the visualization cell can provide more useful information than post-mortem techniques and can provide information on how the membrane fails. The advantages of the IR technique, indeed, in-situ IR technique, are summarized as follows: (i) The in situ IR technique detects when and where a pinhole (or through-membrane crack) forms; (ii) The recorded temperature (distribution) obtained through the in-situ IR technique clearly suggests that catalytic combustion occurs at the pinhole formed; (iii) The severity of the temperature increase triggered by combustion can be determined. It can be determined whether the temperature increase owing to combustion causes fatal damage or understood that the combustion does not cause fatal damage owing to the self-heat dissipation capability of the cell. In other words, IR imaging is a powerful and in-situ diagnostic tool for capturing the transient change of the combustion process from moderate when the membrane is intact to transition and accidental scaling when the membrane is degraded and fatal defects appear.

5.2. Mitigation strategies and future prospects

5.2.1. Mitigation strategies

5.2.1.1. Mitigation strategies for the mechanical membrane degradation

The constrained membrane in the PEMFC shrinks when it is dry and expands when it is hydrated, inducing compressive stress and tensile stress, respectively. These stresses impact on the membrane in two directions: the through-plane and the in-plane. The latter direction was confirmed to have the dominant influence. The membrane is deteriorated mechanically depending on the stress amplitude ($\Delta\sigma/2$) and frequency of the water content change ($\Delta\lambda/\Delta t$) or the RH swing. Mechanical defects such cracks tend to appear in the locations having high stress amplitude. In the current study, cracks were found in the channel regions and the edge between land/channel in the CCM. Therefore, the possible strategies for mitigating mechanical membrane degradation should be based on the principle of reducing the stress amplitude and the stress frequency. There are two general strategies focusing on modification membrane and operation of the fuel cell vehicles.

The membranes with low hygral expansion coefficient will reduce the residual stress formed in the membranes when there are variations in water content and temperature. Nafion® N111-IP is an extruded PFSA membrane that has an EW of 1100 and is likely to be NRE211, a solution-cast membrane. N111-IP is fabricated using melt processes, which aim to reduce the in-plane expansion coefficient. It was proved that N111-IP has no degradation after enduring 20,000 RH cycles using air as the testing gas [4]. Besides, reinforced membranes, in which a porous PTFE layer is fabricated in the middle of the membrane, are another alternative solution for improving the membrane's mechanical durability. The Gore™ Primea® and Nafion XL (Dupont) are two typical reinforced membranes. Even though N111-IP and Gore™ Primea® showed excellent mechanical durability, both membranes were degraded quickly after experiencing the chemical stress test and/or the combined chemical and mechanical stress tests [4]. Noticeably, Nafion XL has been reinforced with e-PTFE in the middle of the membrane and also chemically stabilized with cerium. Thus, Nafion XL membrane showed the good mechanical and chemical durability when it experienced the OCV holding test and the combined chemical and mechanical stress test (RH cycling at the OCV condition) [5]. To sum up, it is evident that the chemical degradation process is more constrained than the mechanical degradation process. The membrane's mechanical strength was significantly reduced by chemical deterioration, particularly via the increased crystallinity and hydrophilic domain spacing of the ionomer. Therefore, it is necessary to employ both mechanical and chemical mitigation techniques at the same time.

Flattening the load demand imposed on the cell is another operational strategy to reduce the mechanical stress on the membrane. The variation of load is inevitable in during operation of the FCVs which can cause changes in the temperature and water content, leading to dimensional oscillation of the membrane eventually resulting in the formation of stress. According to reports, load changing cycles account for 56% of all fuel cell deterioration in the actual operation of the FCVs [6]. Furthermore,

increasing the length of the loading change and decreasing the load changing speed are the desired actions. But, stable operation as for a countermeasure against the mechanical degradation seems not to be feasible and practical in the actual operation of a FCV if the cell stack is the only powertrain. Therefore, an assisted battery system, which is an axillary power system, works together with the main fuel cell stack. This combination has been applied to the commercialized FCVs on the market. With the support from an additional battery, the load range can be smaller, resulting in a smaller hydro-thermal dimensional change of the membrane. However, there are two drawbacks from this solution: shortening the lifetime of the battery due to burden of load variation given on the battery and the increase in FCV's cost.

5.2.2.2. Mitigation strategies for the chemical membrane degradation

Hydroxyl radicals (•OH, •OOH) are responsible for the chemical decomposition of the membrane. The appearance of these radicals relies mainly on the appearance of H_2O_2 and the metal ions impurities (Fe^{2+}, Fe^{3+}, Cu^{2+}). These cations impurities can derive from the water in bubblers, supplied gases, corrosion materials, during MEA preparation and other sources. They accumulate in the membrane, resulting in initiation of free radicals. H_2O_2 has a negligible effect on membrane degradation, however, it triggers the formation of free radicals. As mentioned in Chapter 4 of this dissertation, the formation rate of H_2O_2 tends to be high when the fuel cell operates at low current density and low RH. Therefore, all chemical mitigation strategies must be developed based on the above considerations. In the current study, the author will select and propose some typical MEA modifications and operational solutions for suppressing chemical membrane degradation, as listed in (1) and (2) below

(1) Modification MEA

In the case of heavy-duty fuel cell vehicles, a scavenger that is more durable and does not degrade fuel cell performance is required to suppress chemical degradation. The free radical scavengers, which are usually dispersed into the membrane matrix in the form of nanocrystals or in the form of additives, will react with the free radicals, thus protecting the membrane from chemical decomposition. The free radical scavengers introduced into the membrane must be long-lasting, difficult to wash away by the produced water, and do not degrade fuel cell performance. Ceria, with two common valence states: Ce^{3+} and Ce^{4+}, are notable free radical scavengers that are successfully used to mitigate chemical degradation. Ce^{3+} ion decomposes •OH to Ce^{4+} ion ($Ce^{3+} + \cdot OH + H^+ \rightarrow Ce^{4+} + H_2O$), in turn, Ce^{4+} ion is reduced to Ce^{3+} ion ($Ce^{4+} + 1/2H_2 \rightarrow Ce^{3+} + H^+$). Nafion/$CeO_2$ composite membranes have been confirmed to mitigate chemical degradation in the real operation of the PEMFCs [6]. The efficacy of the cerium scavengers relies on the amount of them in the membrane, so at a higher concentration of Ce^{3+} and Ce^{4+}, the membrane is protected better from chemical degradation [7]. However, the appearance of cations in the membrane decreases the proton conductivity, thus increasing performance loss. Furthermore, ceria free radical scavengers migrated from the membrane to the cathode and then to drain water at the outlet of the

cell, especially at low cell voltage [8]. The necessary actions are to reduce the content of ceria in the membrane but still satisfy the high surface area; then secure a high scavenging efficiency; and stop the scavengers from leaching out the membrane. A possible solution is N-doped ceria, which can reduce the amount of cerium while still securing the active surface area of cerium in the reaction with radicals. Another solution is to add ceria to both the cathode and anode catalyst layers. Cerium ions tend to move from catalyst layers into the membrane. Thus, this can be a ceria make-up source for scavenging free radicals formed in the membrane. Besides, organic free radical scavengers like terephthalic acid is another approach to decompose •OH radical, mitigating the chemical degradation [9].

As mentioned in the previous chapters, H_2O_2 is formed at the electrode-membrane interfaces and then immigrate into the membrane where it will trigger to formation of hydroxyl free radicals in the presence of metal cations. Therefore, suppression formation of H_2O_2 is a second strategy to suppress the formation •OH radical. The hybrid catalyst Pt/C/MnO_2 was applied in both electrodes to decompose the H_2O_2 [10]. With the presence of MnO_2 in the catalyst layer, the activation energy of the decomposition reaction of H_2O_2 into water and oxygen ($H_2O_2 \rightarrow H_2O + 1/2O_2$) is reduced approximately from 75 $kJmol^{-1}$ to around 58 $kJmol^{-1}$, resulting in a reduction of H_2O_2 formation. Besides, Shi Guoyu et al. proposed a hybrid anode catalyst, called Pt_{skin}-PtCo [11]. This hybrid catalyst has suppressed the formation rate of H_2O_2 at the anode electrode by 50% compared with the conventional Pt/C catalyst. As a result, the cell with the hybrid catalyst Pt_{skin}-PtCo showed much greater chemical durability than the cell with the Pt/C catalyst in the OCV holding test.

Thirdly, dispersing Nano Pt particles into the membrane is another approach to mitigate the chemical degradation. The effect of Pt band is still a controversial topic among researchers. In the positive aspect, Pt band has been reported to mitigate the chemical degradation on the PFSA membranes. In particular, Pt ions after detaching from the cathode's catalyst will migrate into the membrane. Under operation, hydrogen diffuses into the membrane and is oxidized on the surface of Pt particles in the membrane, proton will then react oxygen diffusing from the cathode side, generating water [12]. In the other words, Pt particles in the membrane prevents the formation of H_2O_2 in the electrodes by consuming hydrogen and oxygen. Macauley et al. reported that the Pt band suppressed membrane degradation under the synergetic impact of chemical and mechanical degradation processes [13]. However, this method also has drawbacks in decreasing proton conductivity with the presence of Pt ion and increasing amount of Pt in the fuel cell.

The last but not least, minimizing the accumulation of cations impurities in the membrane can suppress the formation of free radicals. In the PEMFC, the metal-based flow field plates must work under the hot, humid and acidic environment, so that corrosion is an apparent issue, leading to the release of metal cations. The foreign metal cations may, also, intrude to the membrane from MEA preparation processes. The graphite flow filed plate is a good conductor, corrosion resistance and low density. However, the total price is high due to difficulty in machinery and increase the weight of the cell due to its thickness. The

composite flow field plates (for instance, polymer/carbon flow field plates) and the metal-based flow field plates with improved coating methods are the most promising ways to minimize the release of metal cations. Meanwhile, establishing high quality control in the manufacture processes of the FCVs will curtail the infiltration of cations into the membrane.

(2) Optimizing FCV operation

OCV and closed OCV are two states that can accelerate the formation of H_2O_2, and thus free radicals. These dangerous states of the cell can appear when the FCVs work in the idling and braking modes. One possible solution is fuel cell hybrid vehicles. In particular, a (lithium) battery, as an auxiliary power source, is installed and works in tandem with the stack to power the vehicle's powertrain. Electricity generated from the stack during braking by the FCVs will be stored in a battery and supplied to the motor again during acceleration. In fact, this solution has been applying in the commercialized FCVs like Mirai, Toyota. However, the drawbacks of using an auxiliary battery are its durability and price.

5.2.1.3. Mitigation strategies for the thermal decomposition

Thermal stress caused by combustion can be considered secondary membrane degradation after mechanical and chemical degradation. In a fresh membrane, the rising temperature of the membrane induced by combustion is marginal due to the low crossover rate. In the deteriorated membrane, defects such as cracks and membrane thinning induced by mechanical and chemical stress, respectively, lead to an increase in the hydrogen crossover rate, resulting in direct combustion of hydrogen and air at the catalyst-GDL interface. Depending on the correlation between the combustion heat and the self-cooling capability of the cell, represented by the self-dissipated heat flux, the membrane temperature goes up more or less. On the accidental scale, the membrane can be decomposed thermally when the combustion heat flux locally and temporary exceeds the self-dissipated heat flux, leading to the formation of pinholes. The appearance of pinholes is apparently responsible for the instant collapse of the fuel cell.

According to the aforementioned perspective, there are two solutions to prevent accidental combustion in the PEMFC: (i) lowering the crossover rate of the reactant gases and (ii) increasing the self-dissipated heat flux of the cell. With the former solution, this can be accomplished by combining all strategies for mitigating the chemical and mechanical degradation on the membrane, as indicated in the previous sections. The crossing rate through the membrane is reduced because the membrane is less degraded, which reduces the heat flux from combustion. With the latter solution, the cell must be designed and fabricated so that the GDLs cover or overlap the CCM. Because the GDL is primarily made of carbon, a good thermal conductor, it aids in the transfer of combustion heat to the cooling water in the fuel cell stack [14]. Furthermore, the cooling system must operate efficiently, preventing local temperature rise because higher cell temperature decreases the dissipated heat flux.

Kreitmeier Stefan et al. [15] have researched the combustion in the artificially degraded membrane under OCV condition. They found that accidental combustion occurs on the cathode side with a small anode

backpressure, eventually leading to the sudden expansion of the artificial pinholes on the membrane. Whereas, the artificial pinhole size didn't change much when there was a small cathode backpressure, proving that accidental combustion had not occurred in this condition. This is because oxygen crossing through the membrane was consumed predominantly in the reaction to form H_2O_2 at the anode side (with low potential). This formation mechanism of H_2O_2 has been described in detail in Chapters 3 and 4 of this dissertation. As a result, the hydrogen concentration in the combustible mixture with air may be too high (> 75 vol%) and thus may not initiate combustion. Besides, based on the heat transfer calculation, the combustion heat is mostly dissipated through the anode side to the hydrogen stream due to the high heat transfer of coefficient (from 5 to 7 times higher than the air side). Thus, the combustion heat of the leaking air with hydrogen at the anode is quickly transferred to the hydrogen stream, resulting in marginal membrane temperature rise. When the FCVs are in breaking and idling modes, the hydrogen concentration at the anode compartment is highest among the operational conditions due to the low load demand, leading to the large crossover rate of hydrogen through the membrane. In addition, anode pressure is generally higher than that of the cathode compartments in the FCVs. All of the aforementioned factors demonstrate the high possibility of accidental combustion at the cathode of the fuel cell in FCVs. Therefore, in order to prevent the occurrence of accidental combustion in the FCVs, the hydrogen gas pressure must be reduced to equal the air pressure at the cathode side during the breaking and idling modes, resulting in decrease of the hydrogen crossover rate, lowering the risk of accidental combustion occurrence.

It is apparent that there will be not a single mitigating solution for all membrane degradation mechanisms. In the scope of the current study, the author proposed some fundamental strategies based on important findings from the membrane degradation investigation. However, these strategies obviously should work together to achieve desire target of prolonging membrane durability and reliability under actual operation conditions of FC vehicles.

5.2.2. Future prospects

The model that can convert the OCV decay into the rate of hydrogen crossing through the membrane is described in Chapter 2 as a promising and practical diagnostic tool for membrane degradation. In this study, because the RH cycling test using nitrogen gas at both sides of the cell was conducted in 20,000 RH cycles (around 69 days continuously), the author just conducted one RH cycling test in the limited time of the doctoral program. Therefore, the validation of the current model should be confirmed by further tests.

IR imaging and SEM images confirmed that the combustion process was transitioning from a moderate to an accidental scale with the formation of pinholes. These pinholes are responsible for the sudden failure of the PFSA membrane, reducing the reliability of PEMFCs in their applications. The current durability tests were applied to the commercial, non-reinforced membrane (Nafion NRE211). Recently, modified membranes with high chemical and mechanical stability have been applied in the FCVs. Thus,

the transition of the combustion process should be checked on the PEMFC using state-of-the-art membranes like Nafion XL and Gore.

The RH cycling tests conducted at the OCV, 0.05 and 0.3 Acm^{-2} just partially mimic the operating conditions of the FCVs. Apparently, these testing conditions are too harsh compared with the real operation of the FCVs. Meanwhile, the demanding load variation was reported as having a dominant impact, leading to fuel cell failure in the FCVs. Therefore, load cycle testing combined with the IR imaging method using state-of-the-art membranes will be more practical to conduct.

A visualization cell embedded in ZnS glass was used to track the transition of the combustion process in this study. Even though ZnS has a high IR emissivity, its drawback is that the air stream must be kept dry to prevent the impact of water on the ZnS glass. Thus, during the chemical and combined chemical and mechanical stress tests and checking of the OCV, the dry air feeding to the cathode side was not close to the real operating conditions of the fuel cell. Infrared-transparent insulation protection cover (GAT) is also a high transmitting emissivity, and neutral with the condensate. However, GAT deforms when the cell temperature exceeds 80 °C. Therefore, durability tests using GAT at lower cell temperatures will be appropriate.

5.3 References

1. Cullen, David A., et al. “New Roads and Challenges for Fuel Cells in Heavy-Duty Transportation.” Nature Energy, vol. 6, no. 5, 25 Mar. 2021, pp. 462–474, 10.1038/s41560-021-00775-z.

2. Kundu, Sumit, et al. “Mechanical Properties of NafionTM Electrolyte Membranes under Hydrated Conditions.” Polymer, vol. 46, no. 25, 28 Nov. 2005, pp. 11707–11715, www.sciencedirect.com/science/article/abs/pii/S0032386105013674, 10.1016/j.polymer.2005.09.059.

3. A.B. LaConti, M. Hamdan, and R.C. McDonald, Handbook of Fuel Cells: Fundamentals, Technology, and Applications, Vol. 3, W. Vielstich, A. Lamm, and H. A. Gasteiger, Editors, Wiley, New York (2003).

4. Gittleman, Craig & Lai, Yeh-Hung & Miller, Daniel. (2005). Durability of Perfluorosulfonic Acid Membranes for PEM Fuel Cells.

5. Mukundan, Rangachary, et al. “Membrane Accelerated Stress Test Development for Polymer Electrolyte Fuel Cell Durability Validated Using Field and Drive Cycle Testing.” Journal of the Electrochemical Society, vol. 165, no. 6, 2018, pp. F3085–F3093, 10.1149/2.0101806jes.

6. Matulić, N., et al. "Commercial Vehicle Auxiliary Loads Powered by PEM Fuel Cell." International Journal of Hydrogen Energy, vol. 44, no. 20, Apr. 2019, pp. 10082–10090, 10.1016/j.ijhydene.2018.12.121.

7. Wang, Zhao, et al. "Synthesis of Nafion/CeO2 Hybrid for Chemically Durable Proton Exchange Membrane of Fuel Cell." Journal of Membrane Science, vol. 421-422, Dec. 2012, pp. 201–210, 10.1016/j.memsci.2012.07.014

8. Wong, Ka Hung, and Erik Kjeang. "In-Situ Modeling of Chemical Membrane Degradation and Mitigation in Ceria-Supported Fuel Cells." Journal of the Electrochemical Society, vol. 164, no. 12, 2017, pp. F1179–F1186, 10.1149/2.1201712jes

9. Zhu, Yan, et al. "Enhanced Chemical Durability of Perfluorosulfonic Acid Membranes through Incorporation of Terephthalic Acid as Radical Scavenger." Journal of Membrane Science, vol. 432, Apr. 2013, pp. 66–72, 10.1016/j.memsci.2012.12.050

10. Trogadas, Panagiotis, and Vijay Ramani. "Pt/C/MnO_2 Hybrid Electrocatalysts for Degradation Mitigation in Polymer Electrolyte Fuel Cells." Journal of Power Sources, vol. 174, no. 1, Nov. 2007, pp. 159–163, 10.1016/j.jpowsour.2007.08.088

11. Shi, Guoyu, et al. "Unparalleled Mitigation of Membrane Degradation in Fuel Cells Via a Counter-Intuitive Approach: Suppression of H_2O_2 Production at the Hydrogen Anode Using a Ptskin–PtCo Catalyst." Journal of Materials Chemistry A, vol. 8, no. 3, 2020, pp. 1091–1094, 10.1039/c9ta12023h

12. Watanabe, Masahiro, et al. "Self-Humidifying Polymer Electrolyte Membranes for Fuel Cells." Journal of the Electrochemical Society, vol. 143, no. 12, 1 Dec. 1996, pp. 3847–3852, 10.1149/1.1837307

13. Macauley, N., et al. "Pt Band Formation Enhances the Stability of Fuel Cell Membranes." ECS Electrochemistry Letters, vol. 2, no. 4, 5 Feb. 2013, pp. F33–F35, 10.1149/2.007304eel

14. Gunji, Hiroyuki, et al. "Gas-Leak-Induced Pinhole Formation at Polymer Electrolyte Membrane Fuel Cell Electrode Edges." International Journal of Hydrogen Energy, vol. 42, no. 1, Jan. 2017, pp. 562–574, 10.1016/j.ijhydene.2016.11.038

15. Kreitmeier, Stefan, et al. “Local Degradation at Membrane Defects in Polymer Electrolyte Fuel Cells.” Journal of the Electrochemical Society, vol. 160, no. 4, 2013, pp. F456–F463, 10.1149/1.023306jes

Appendix A

One-dimensional heat transfer model

A one-dimensional heat transfer model was proposed to predict the cathode's GDL surface induced by combustion, which is based on the hydrogen crossover rate data with 20-kPa anode backpressure. The heat released from combustion of q''_{com} will be transferred in two directions: anode ($q''_{An,\ H_2}$) and cathode ($q''_{Ca,\ air}$) sides, as described in Fig.A.1. This calculation has some assumptions as follows: (i) Combustion of the gas mixture (H_2 and air) occurs on the cathode's catalyst layer; (ii) A stable heat transfer progress in the through-plane direction; (iii) Thermal radiation heat from the anode GDL to the hydrogen stream is negligible; (iv) The emissivity (ε) of the cathode's GDL is 1; (v) the thermal contact resistances between cell components are negligible. The calculation procedure is shown in Fig.A.2.

Assuming that the crossover hydrogen gas burns completely, the maximum heat formation (q''_{Com}) can be calculated as follows.

$$q''_{Com} = \frac{i_{cross} \times \Delta H_f}{2F} \quad (Wcm^{-2}) \qquad (A.1)$$

where $\Delta H_f = 241$ kJmol^{-1} is the heat of hydrogen combustion at 25 °C (water vapor); F = 96,485 Cmol^{-1} is Faraday's constant; and i_{cross} (Acm^{-2}) is the hydrogen crossover current density.

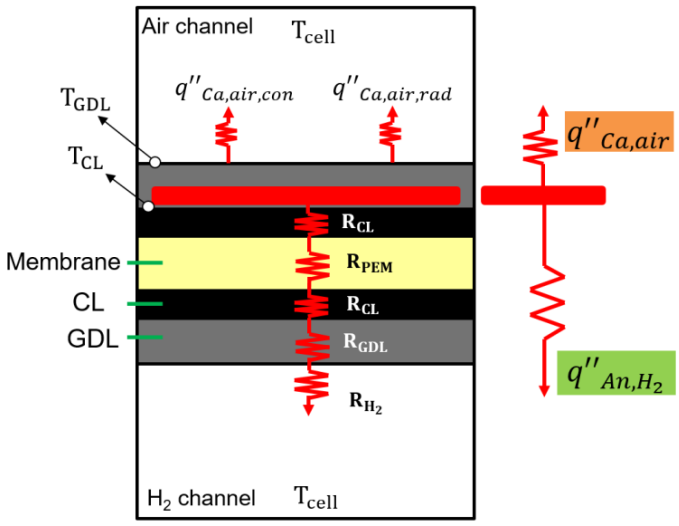

Fig.A. 1. Combustion heat is dissipated via anode and cathode sides.

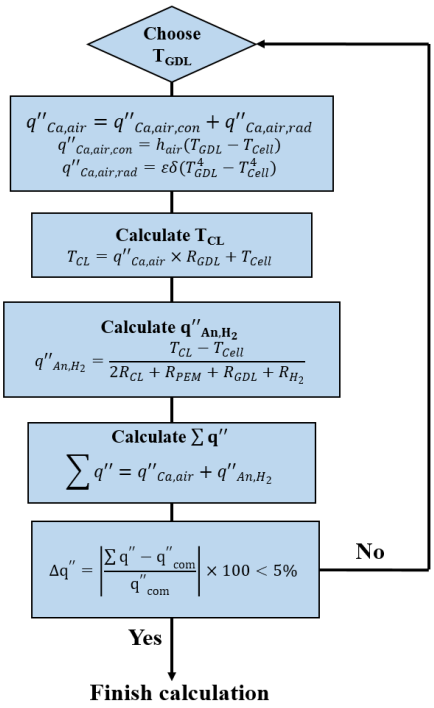

Fig.A. 2. Calculation procedure for prediction the GDL temperature rise due to combustion.

(1) Choose the GDL temperature.

(2) Calculating the heat transfer coefficient at the air side (h_{air}) and the thermal radiation heat flux from the GDL surface to the air stream ($q''_{Ca,\,air,\,rad}$).

♦ The convection heat transfer coefficient of the air side h_{air}

- Reynold number of the air stream:

$$Re = \frac{V_{air} \times D}{\nu_{air}} = \frac{4 \times \dot{Q}_{air}}{\pi \times D \times \nu_{air}} \qquad (A.2)$$

where ν_{air} is the kinematic viscosity of the air at the mean temperature ($T_m = \frac{T_{GDL}+T_{Cell}}{2}$); $\dot{Q}_{air}$ = 200 Nccm is the air flow rate; D = 0.267 cm is the equivalent diameter of the channel (a×b = 0.4×0.2 cm).

- Nusselt number:

❖ Re < 3000: Laminar flow

$$Nu = \frac{h_{air} \times D}{k_{air}} = 3.61 \qquad (A.3)$$

where k_{air} is the thermal conductivity of the air at the mean temperature (T_m).

❖ Re > 10000: Fully developed turbulent flow [1]

$$Nu=\frac{h_{air}\times D}{k_{air}}=0.023Re^{0.8}Pr^{0.4} \quad (A.4)$$

- Heat transfer coefficient of the air side h_{air}

$$h_{air}=\frac{Nu\times k_{air}}{D} \quad (A.5)$$

♦ The thermal radiation heat flux from the GDL surface to the air stream is calculated via below equation

$$q''_{Ca,\,air,\,rad}=\varepsilon\delta(T^4_{GDL}-T^4_{Cell}) \quad (A.6)$$

(3) Calculate the heat flux from GDL to the cell, $q''_{Ca,\ air}$

$$q''_{Ca,\,air}=q''_{Ca,\,air,\,con}+q''_{Ca,\,air,\,rad}=h_{air}(T_{GDL}-T_{cell})+\delta\varepsilon(T^4_{GDL}-T^4_{Cell}) \quad (A.7)$$

$$q''_{Ca,\,air}=\frac{T_{GDL}-T_{cell}}{\frac{\mathbf{1}}{\boldsymbol{h_{air}+\varepsilon\delta(T_{GDL}+T_{Cell})(T^2_{GDL}+T^2_{Cell})}}}=\frac{T_{GDL}-T_{cell}}{\frac{\mathbf{1}}{\boldsymbol{h_{air}+h_{rad}}}}$$

$$=\frac{T_{GDL}-T_{cell}}{R_{air}}$$

where R_{air} (cm^2KW^{-1}) is the heat resistance from the cathode's GDL to the air stream.

(4) Calculate the catalyst temperature, T_{CL}

$$T_{CL}=q''_{Ca,\,air}\times R_{GDL}+T_{GDL} \quad (A.8)$$

(5) Calculating the heat flux dissipated via the anode side, $q''_{An,\,H_2}$.

$$q''_{An,\,H_2}=\frac{T_{CL}-T_{Cell}}{2R_{CL}+R_{PEM}+R_{GDL}+R_{H_2}} \quad (A.9)$$

where R_{CL},R_{PEM}, $R_{GDL}$and R_{H_2} are thermal conduction resistance of the CL, the membrane, the anode's GDL and the convection heat resistance from the GDL to the hydrogen stream, respectively.

The convection heat resistance from the GDL to the hydrogen stream R_{H_2}

$$R_{H_2}=\frac{1}{h_{H_2}} \quad (A.10)$$

- Reynold number of the H_2 stream:

$$Re=\frac{V_{H_2}\times D}{\nu_{H_2}}=\frac{4\times\dot{Q}_{H_2}}{\pi\times D\times\nu_{H_2}} \quad (A.11)$$

where ν_{H_2} is the kinematic viscosity of the H_2 at the cell temperature; $\dot{Q}_{H_2}$ = 100 Nccm is the hydrogen flow rate.

- Nusselt number:
  - ❖ Re < 3000: Laminar flow

$$Nu=\frac{h_{H_2}\times D}{k_{H_2}}=3.61$$

where k_{H_2} is the thermal conductivity of H_2 at the cell temperature.

  - ❖ Re > 10000: Fully developed turbulent flow [1]

$$Nu=\frac{h_{H_2}\times D}{k_{H_2}}=0.023Re^{0.8}Pr^{0.4}$$

(6) Calculating the total heat flux, $\sum q''$

$$\sum q'' = q''_{An,\,H_2} + q''_{Ca,\,air} \quad (A.12)$$

(7) If the deviation ($\Delta q''$) between $\sum q''$ and the combustion heat flux (q''_{com}) is less than 5%, the iteration is stopped.

$$\Delta q'' = \frac{\left|q''_{com} - \sum q''\right|}{q''_{com}}\times 100 < 5 \quad (A.13)$$

Table A. 1. Summary of all the related heat transfer resistances

Components	Equation	Value	Unit
Thermal conduction resistance of the GDL	$R_{GDL}=\frac{L_{GDL}}{k_{GDL}}$ (A.14) where L_{GDL} = 0.031 cm is the GDL thickness, and k_{GDL} = 0.0031 $Wcm^{-1}K^{-1}$ is the thermal conductivity of the GDL [2].	10.16	cm^2KW^{-1}
Thermal conduction resistance of the CL	$R_{CL}=\frac{L_{CL}}{k_{CL}}$ (A.15) where L_{CL} = 0.0012 cm is the CL thickness (obtained from the SEM image in chapter 2) and k_{CL} = 0.0027 $Wcm^{-1}K^{-1}$ is the thermal conductivity of the CL [2].	0.444	cm^2KW^{-1}

Thermal conduction resistance of the membrane	$R_{PEM} = \frac{L_{PEM}}{k_{PEM}}$ (A.16) where $L_{PEM} = 0.0025$ cm is the membrane thickness, and $k_{PEM} = 0.0016$ $Wcm^{-1}K^{-1}$ is the thermal conductivity of the membrane [2].	1.563	cm^2KW^{-1}

Reference

A.1 Incropera, Frank P, and David P DeWitt. Fundamentals of Heat and Mass Transfer. 3rd ed., Wiley, New York, 1990.

A.2 Khandelwal, Manish, and M.M. Mench. "Direct Measurement of Through-Plane Thermal Conductivity and Contact Resistance in Fuel Cell Materials." Journal of Power Sources, vol. 161, no. 2, Oct. 2006, pp. 1106–1115, 10.1016/j.jpowsour.2006.06.092

Appendix B

Investigation of chemical durability of the membrane in PEMFCs

Abstract

The aim of this appendix is to investigate membrane durability under purely chemical degradation in polymer electrolyte membrane fuel cells. The catalyst-coated membrane using NRE211 membrane is subjected to the holding Open-Circuit voltage (OCV) test at the cell temperature of 80 °C and at atmospheric pressure in the visualization cell. Membrane integrity is evaluated during the test by two indicators, including the hydrogen crossover rate and the OCV. Furthermore, the infrared (IR) imaging method is applied to capture in-situ the rise in gas diffusion layer temperature induced by catalytic combustion of the leaking hydrogen at the cathode side. The membrane failed after only 25 hours of testing (or 300 equivalent 5-min relative humidity cycles), as indicated by a significant increase in the hydrogen crossover rate and a sudden drop in the OCV. The formation of pinholes induced by accidental combustion could be largely responsible for the early failure of the membrane. The emergence of hotspots in IR images reveals that pinholes have formed at the entrance of the air stream. To overcome the pressure loss in the serpentine flow field, the pressure of the air stream at the entrance of the cell is slightly higher than in the outlet. Thus, the oxygen crossover rate is highest at the entrance of the cathode, resulting in the faster formation of H_2O_2. Therefore, membrane chemical decomposition induced by free radicals is more severe at entrance of the airstream during the holding OCV test, leading to membrane thinning. The rate of hydrogen crossover through the locally thin membrane will be high enough to cause combustion with a heat flux greater than the maximum heat dissipated flux, eventually resulting in the formation of pinholes.

B.1 Experimental

B1.1. Experimental apparatus and the cell characteristics

In order to carry out the current test, the experimental apparatus, which has been described in chapters 3 and 4 (see Fig. B1a), was utilized. Furthermore, CCM fabrication, the cell assembly procedure, and the cell characteristics have been indicated in chapters 3 and 4 (see Fig. B1b).

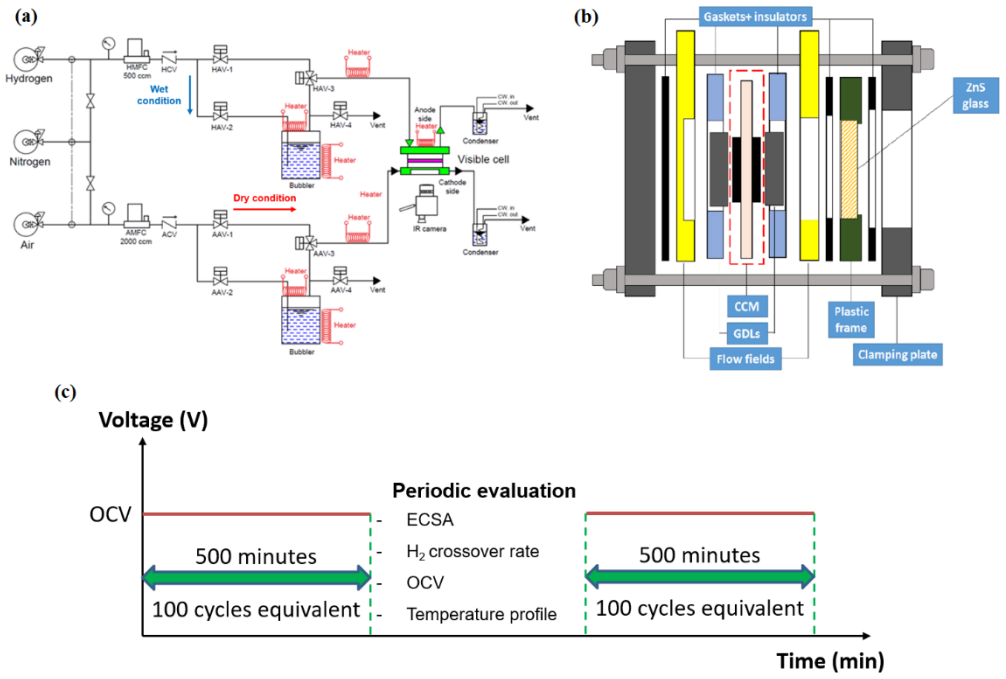

Fig. B. 1. (a) Experimental apparatus, (b) schematic cross-sectional cell structure, and (c) experimental procedure.

Fig. B1c illustrates the durability testing procedure. Prior to the durability test, the cell was incubated with 100% RH nitrogen gas (only on the anode side) for 24 h at a cell temperature (T_{cell}) of 80 °C to ensure that the membrane could be hydrated completely. During the durability test, the cell was maintained under OCV conditions at T_{cell} = 80 °C and at atmospheric pressure. For the anode compartment, fully-humidified hydrogen gas was fed at a flow rate of 100-Nccm (normal cm^3 min^{-1}). Meanwhile, dry air at a flow rate of 200-Nccm was continuously fed into the cathode compartment. The dry air helps prevent water droplets from attaching to the ZnS glass. Because water absorbs IR rays, the temperature measurement would thus be inaccurate. The membrane resistance and OCV were measured using a high-frequency resistance device (Tsuruga, 3566) and then recorded using a data logger (Graphtec Corporation, GL840) every 1 s during the durability test. Electrochemical measurements (crossover rate and OCV) were conducted every 100 equivalent RH cycles (or 500 min). The IR camera captured the temperature distribution on the surface of the GDL through the ZnS-glass window during OCV measurements.

B.1.2 Details of thermal imaging and electrochemical measurements

In the evaluation period presented in Fig. B1c, thermographs (IR images) of the GDL surface are captured via an IR camera (NEC Avio, R300) through a high-transmittance glass (ZnS) window embedded at the cathode under the OCV state at T_{cell} = 80 °C. In order to accurately measure the GDL surface temperature, we calibrated the camera emissivity according to the cell temperature on the cathode side. As a result, a substantial emissivity was determined to be 0.63 under the condition that the cell temperature is 80 °C while N_2 was fed to both the cathode and anode sides.

The operation conditions at the OCV state are as follows. Fully-humidified H_2 at a flow rate of 100-Nccm and dry air at a flow rate of 200-Nccm are fed into the anode and cathode compartments, respectively. The cell temperature is maintained at 80 °C. The OCV is checked under two pressure conditions:

(a) Atmospheric pressure for both anode and cathode compartments, and

(b) Application of 20-kPa backpressure only in the anode compartment.

In the following, conditions (a) and (b) are denoted as "atmospheric pressure" and "20-kPa anode backpressure," respectively.

Linear sweep voltammetry (LSV) and cyclic voltammetry (CV) are performed to measure the hydrogen crossover rate through the membrane and the ECSA of the cathode catalyst using a voltammetry system (SP300, BioLogic Science Instruments). A flow rate of 100-Nccm of fully humidified hydrogen is fed into the anode side, which serves as both the counter and reference electrode, whereas 200-Nccm of dry nitrogen gas is fed into the cathode side, which is operated as the working electrode. The cell temperature is maintained at 80°C, and nitrogen gas is stopped immediately before starting the CV measurements. The hydrogen desorption area at the cathode electrode is a measure of the ECSA. The applied potential ranges from 0.05 V to 0.9 V vs. NHE (Normal hydrogen electrode) with a scan rate of 50 mVs^{-1}.

The LSV technique can reveal the hydrogen crossover rate, which is represented in the units of current density. The applied potential is swept from 0.05 to 0.5 V versus NHE, with a scan rate of 0.5 mV s^{-1}. The crossover current density is then obtained at an applied potential of 0.4 V versus NHE, at which the leaked hydrogen gas from the anode is oxidized completely on the cathode's catalyst. When the fatal defects appear in the membrane, the hydrogen crossover rate increases and fluctuates vigorously as confirmed in Chapter 2, and the current density saturation in the potential from 0.4 to 0.5 V corresponds to the crossover current density. As in the case of the OCV, the hydrogen crossover rate is measured under the same and differential pressure conditions. Although the differential pressure condition, as noted above, comprises a differential pressure of only 20-kPa, it helps to highlight the existence of severe defects in the membrane, such as pinholes or through-thickness cracks.

B.2 Results and discussion

B.2.1. Membrane degradation investigation

The evolution of OCV during the durability test is shown in Fig. B2, with an average decay rate of approximately 1.1 mVh^{-1}. This OCV decay rate is slightly smaller than 1.43 mVh^{-1} in the RH cycling test at the OCV condition, as indicated in Chapter 3. The reduction of OCV comes from two reasons: catalyst degradation (or the decrease of ECSA) and membrane degradation. The fluctuation of the cell voltage initiates carbon-support oxidation and Pt dissolution, leading to the decrease of ECSA. However, there is a slight reduction of the ECSA, as seen in Fig. B3. Catalyst degradation should be severe when the cell

experiences a large voltage fluctuation. In the OCV holding test, the OCV oscillated in a narrow range, so that ECSA decreased marginally. As mentioned clearly in Chapter 3, the formation of H_2O_2 at the interface between the anode electrode and membrane under OCV conditions is responsible for the production of hydroxyl radicals. The membrane structure is then decomposed chemically by these radicals, resulting in a locally thin membrane. The rise in hydrogen crossover rate through the thin membrane will eventually reduce the OCV.

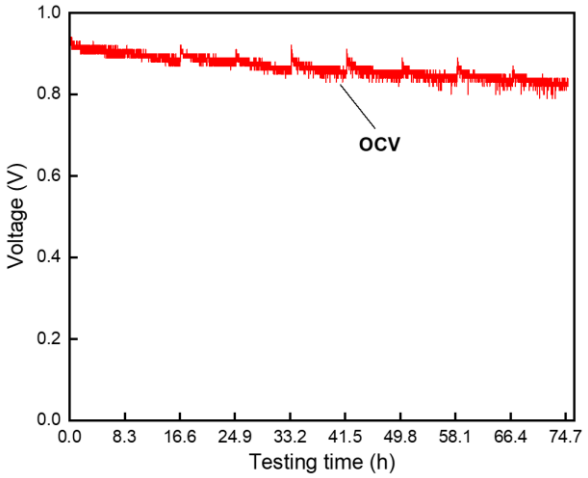

Fig. B. 2. Evolution of OCV during the durability test.

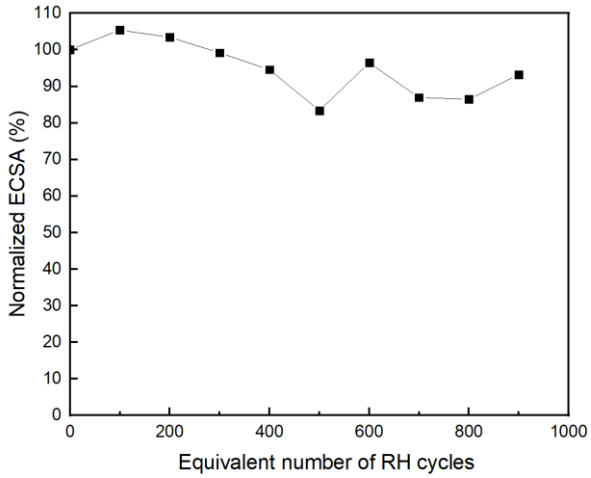

Fig. B. 3. Variation of the ECSA during the durability test.

Based on the data in Fig. B4, the membrane apparently failed after enduring 300 equivalent RH cycles (or 25 h of testing) when the hydrogen crossover rate was 15.4 $mAcm^{-2}$, exceeding the failure criterion of 15 $mAcm^{-2}$ with 20-kPa anode backpressure. The hydrogen crossover rate at atmospheric pressure only slightly rose throughout the test while the hydrogen crossover rate with a 20-kPa anode backpressure rapidly increased after membrane failure. Without mechanical stress, only the pinhole could be created by accidental combustion in the current durability test. When a 20-kPa anode backpressure is

used during hydrogen crossover rate measurements, the development of pinholes on the membrane will significantly enhance the rate of hydrogen crossover. The exponential increase of hydrogen crossover rate after 300 RH cycles to the end of the durability test clarifies the expansion of pinholes or the increase in number of pinholes due to the thermal decomposition.

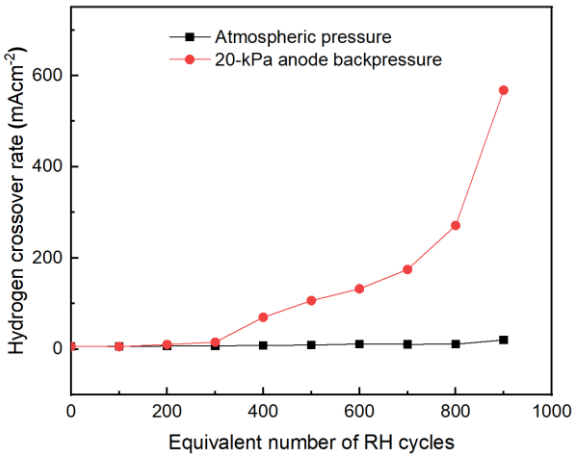

Fig. B. 4. The change of hydrogen crossover rate during the durability test.

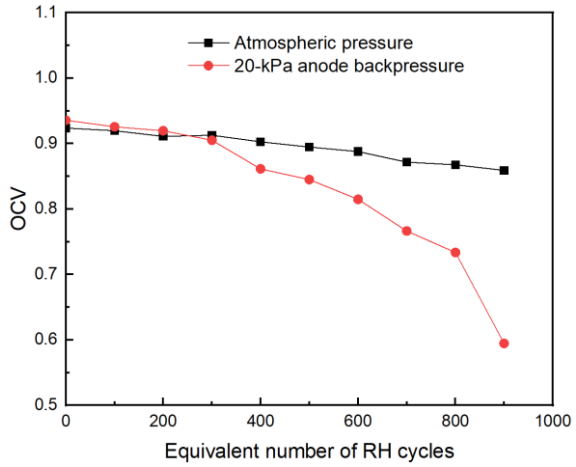

Fig. B. 5. The variation of OCV during the durability test.

The data on Fig.B5 shows the possibility of the OCV in diagnosing membrane failure. In particular, the OCV at 20-kPa anode backpressure started to drop under the OCV at the atmospheric pressure after 300 equivalent RH cycles. This result is consistent with the abrupt increase in the hydrogen crossover rate as shown in Fig. B4. Because the ECSA decreases marginally during the durability test as shown in Fig.B3, the appreciable increase of hydrogen crossover rate through pinholes once again could be the main reason for the sudden drop of OCV. At atmospheric pressure, OCV decreases slightly and linearly during the durability test, with a decay rate of 0.86 mVh^{-1}. Whereas, with 20-kPa anode backpressure, the decline of OCV can be divided into 2 regions. Prior to membrane failure (from BOL to after 300 RH cycles), OCV decreases at a rate of 1.22 mVh^{-1}. After 400 RH cycles to the end of the durability test, OCV dropped gradually at a decay rate of 6.4 mVh^{-1} which is over 5.2 times faster than prior to membrane failure.

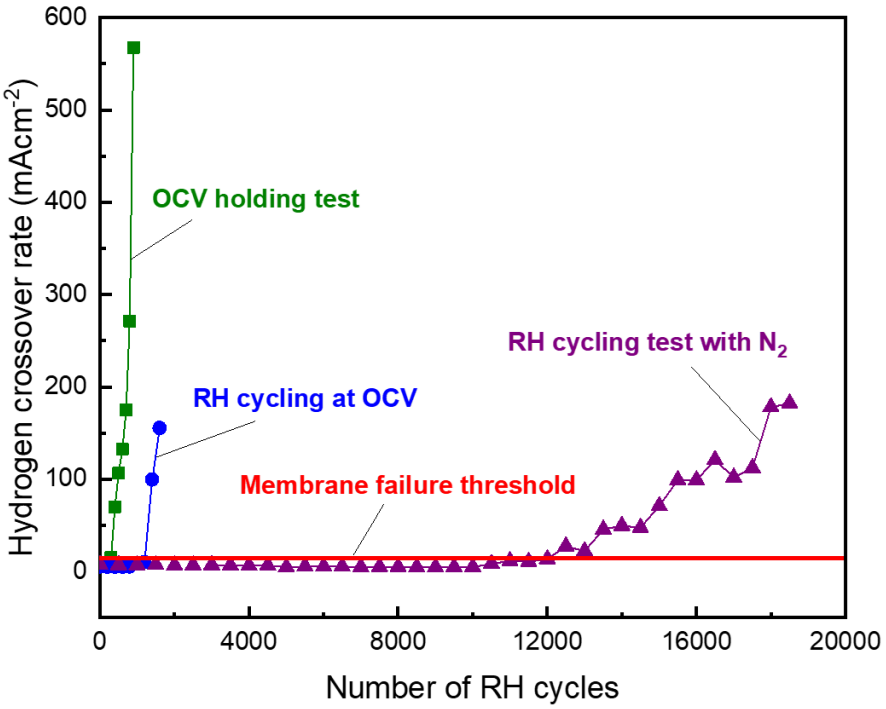

Fig. B. 6. The hydrogen crossover rate vs. number of RH cycles under purely mechanical stress (data from Chapter 2), in the RH cycling test at the OCV condition (data from Chapter 3), and in the OCV holding test. The red, horizontal line represents the hydrogen crossover rate of 15 $mAcm^{-2}$, which is defined as the membrane failure threshold.

In comparison with results from the purely mechanical membrane degradation test and the combined stress test, the membrane failed very early in the OCV holding test, as shown in Fig. B6. As predicted, the membrane would be degraded faster under the synergetic effects of the combined chemical and mechanical mechanisms in the RH cycling test at the OCV condition; however, the membrane subjected to the OCV holding test failed four times faster. The plausible reason for this unexpected sequence is the formation of pinholes during the durability test owing to the utilization of H_2 and air at the anode and cathode compartments. Because of the appearance of pinholes in the membrane, the hydrogen crossover rate will abruptly increase, especially with an anode backpressure.

A.2.2. The change of GDL temperature induced by the catalytic combustion

In Fig. B7, a hotspot at 92.3 °C (or a temperature increase of 12.3 °C) appeared at the inlet of the air stream after 400 equivalent RH cycles (or 33.3 h of testing). This emergence was later than the time when the hydrogen crossover rate exceeded the failure threshold of 15 $mAcm^{-2}$ after 300 equivalent RH cycles, as indicated by the sudden increase in Fig. B4. The cause is that the heat generated by combusting the rate of hydrogen ($q''_{com} = 1.23 \times i_{H_2}$) after 300 equivalent RH cycles was small, at 0.0189 Wcm^{-2}, and sufficiently transferred to the environment. After 400 equivalent RH cycles, the combustion heat was approximately 4.7 times higher than after 300 equivalent RH cycles, resulting in the formation of a hotspot at channel 7. Afterward, the hotspot temperature increased with the rise of the hydrogen crossover rate through the

degraded membrane and eventually reached 97 °C (a 17 °C increase) at the end of the durability test (after 900 equivalent RH cycles).

The entrance the air stream is a predictable location to form H_2O_2 during the OCV holding test. Because the flow field plate has a serpentine pattern, the pressure of the air stream at the inlet is slightly higher than at other locations in the cell. Thus, the oxygen leakage flux is highest at the inlet of the air stream. Besides, H_2O_2 formation at the anode under the OCV condition depends mainly on the flux of oxygen through the membrane. Therefore, the membrane at the inlet of the cathode can be highly attacked by the hydroxyl radicals, resulting in thinning the membrane. The significant increase in the hydrogen crossover rate through the thinning membrane can cause the transition of the combustion process to the accidental scale, resulting in the membrane being burned and the formation of pinholes.

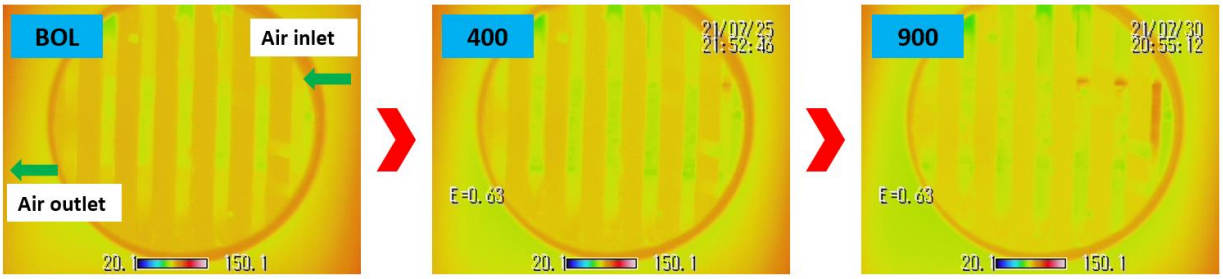

Fig. B. 7. IR images of the cathode side recorded under 20-kPa anode backpressure case during periodic OCV measurements in the RH cycling test. 100 Nccm of fully humidified hydrogen gas and 200 Nccm of dry air were fed into the anode and cathode sides, respectively, at a cell temperature of 80 °C.

B.3 Conclusion

Even though the membrane NRE211 was found fairly durable under mechanical degradation when it can last 12,500 RH cycles (or over 1,042 h of testing) as indicated in Chapter 2, it quickly failed after only 300 equivalent RH cycles (or 25 h of testing) under chemical degradation in the OCV holding test. Similarly, in Chapter 3, the membrane exposed to the RH cycling test under the OCV condition showed failure after 1,600 RH cycles (133 h of testing), which is over five times longer than the result in the current study. Apparently, chemical degradation remains a critical barrier to extending the lifetime of PEMFCs in general and FCVs in particular. In addition, under the OCV holding test and the RH cycling test under the OCV condition, the formation of pinholes induced by accidental combustion can be predominantly responsible for the early failure of the membrane instead of the chemical and mechanical impacts.

IR imaging technique gave information when, where and how much temperature rise of the GDL induced by combustion during the durability test. Under the OCV condition, the entrance of the cell is the riskiest location for the formation of pinholes when the combustion transitions to accidental scale.